Progress in Materials Science 115 (2021) 100706

Contents lists available at ScienceDirect

Progress in Materials Science

journal homepage: www.elsevier.com/locate/pmatsci

Recent progress on control strategies for inherent issues in friction stir welding

Xiangchen Meng[a], Yongxian Huang[a,*], Jian Cao[a,*], Junjun Shen[b], Jorge F. dos Santos[b]

[a] State Key Laboratory of Advanced Welding and Joining, Harbin Institute of Technology, Harbin 150001, China
[b] Helmholtz-Zentrum Geesthacht, Institute of Materials Research, Materials Mechanics, Solid-State Joining Processes, Geesthacht 21502, Germany

ARTICLE INFO

Keywords:
Friction stir welding
Issues and strategies
Self-support
Non-weld-thinning
Green remanufacturing

ABSTRACT

Friction stir welding (FSW), a mature solid-state joining method, has become a revolutionary welding technique over the past two decades because of its energy efficiency, environmental friendliness and high-quality joints. FSW is highly efficient in the joining of Al alloys, Mg alloys, Ti alloys, polymers and other dissimilar materials. Recently, FSW has gained considerable scientific and technological attention in several fields, including aerospace, railway, renewable energy and automobile. To broaden the adoption of FSW in manufacturing fields, three inherent issues—back support, weld thinning and keyhole defects—must be addressed to ensure the structural integrity, safety and service life of the manufactured products. This review covers the recent progress on the control strategies for these inherent issues, which are basically divided into self-supported FSW, non-weld-thinning FSW and friction stir-based remanufacturing. Herein, the aim is to focus on the corresponding technical development, process parameters, metallurgical features and mechanical properties. Additionally, the challenges and future outlooks are emphasized systematically.

1. Introduction

Friction stir welding (FSW), a mature solid-state welding technique, involves temperature, mechanics, metallurgy and interactions. FSW has been widely applied in many fields, including aerospace, defence, railway, renewable energy and automobile, as shown in Fig. 1 [1]. Invented by The Welding Institute (TWI) of the UK in 1991, FSW is thought to be the most revolutionary welding technique due to its advantages of low processing time, low machine/tool consumable costs, low peak temperature, severe plastic deformation and high-quality joints [2–4]. Within the past 29 years of invention and rapid development, FSW has been successfully used to join different series of Al alloys in the automobile and aerospace sectors (2xxx [5–7], 5xxx [8–10], 6xxx [11,12] and 7xxx [13–16]) and Mg alloys [17–19] that are hard to be welded by conventional fusion welding techniques [20]. FSW has also achieved partial successes in the joining of other metallic materials (Ti alloys [21,22], Cu alloys [23–25] and steels [26–29]) and non-metallic thermoplastic polymers [30–32]. Moreover, FSW can improve the mechanical interlocking of the welded materials due to severe plastic deformation. Hence, FSW has been used to join many kinds of dissimilar materials according to interfacial reaction systems, as listed in Table 1.

FSW has achieved satisfactory results for joining similar and dissimilar materials. With further intensive research and applications, the inherent issues of FSW, which mainly consist of back support, weld thinning and keyhole defects, have attracted substantial attention. These issues are detrimental to the formation and integrity of joints. Currently, corresponding control strategies for the

* Corresponding authors.
E-mail addresses: yxhuang@hit.edu.cn (Y. Huang), cao_jian@hit.edu.cn (J. Cao).

https://doi.org/10.1016/j.pmatsci.2020.100706
Received 19 December 2018; Received in revised form 25 April 2020; Accepted 8 June 2020
Available online 12 June 2020
0079-6425/ © 2020 Elsevier Ltd. All rights reserved.

Nomenclatures

FSW	Friction stir welding
FSP	Friction stir processing
FSR	Friction stir repairing
FSLW	Friction stir lap welding
BT-FSW	Bobbin tool friction stir welding
SRFSW	Self-reacting friction stir welding
SSBT-FSW	Stationary shoulder BT-FSW
SS_UBT-FSW	Stationary upper shoulder BT-FSW
SS_LBT-FSW	Stationary lower shoulder BT-FSW
DBT-FSW	Dual-rotation BTFSW
WBT-FSW	Water cooling BTFSW
PFSW	Penetrating FSW
$SSFSW_1$	Self-support FSW
NRSA-FSW	Non-rotating shoulder assisted FSW
$SSFSW_2$	Stationary shoulder FSW
NWT-FSW	Non-weld-thinning FSW
MPD-FSW	Micro plunge depth FSW
HYB	Hybrid metal extrusion and bonding
SCFSW	Surface compensation FSW
VCFSW	Vertical compensation FSW
FPW	Friction plug welding
FTPW	Friction taper plug welding
FFSW	Filling FSW
DFFSR	Drilling-filling FSR
SRFSW	Self-refilling FSW
A-PFFSR	Active-passive filling FSR
FFSJ	Friction filling staking joining
RFSSW	Refill friction stir spot welding
GTAW	Gas tungsten arc welding
CFD	Computational fluid dynamics
PID	Proportional-integral-derivative
TWI	The Welding Institute
EADS	European aeronautic defence and space company
BM	Base material
AS	Advancing side
RS	Retreating side
TMAZ	Thermo-mechanically affected zone
HAZ	Heat affected zone
NZ	Nugget zone
UNZ	Upper NZ
LNZ	Lower NZ
SAZ	Shoulder affected zone
SDZ	Shoulder dominated zone
PSZ	Pin stirred zone
USDZ	Upper shoulder dominated zone
LSDZ	Lower shoulder dominated zone
USAZ	Upper shoulder affected zone
LSAZ	Lower shoulder affected zone
SSAZ	Stationary shoulder affected zone
PRZ	Plug recrystallized zone
HDP	Heat-dominated phase
HSTP	Heat-shear transition phase
SDP	Shear dominated phase
JLRs	Joint line remnants
PWHT	Post-weld heat treatment
DRX	Dynamic recrystallization
HAGBs	High-angle grain boundaries
LAGBs	Low-angle grain boundaries
IMCs	Intermetallic compounds
MMCs	Metal matrix composites
PP	Polypropylene
ABS	Acrylonitrile butadiene styrene
HDPE	High-density polyethylene
SCF/PEEK	Short carbon fiber reinforced poly ether ether ketone

three inherent issues have been proposed and developed. There is a strong need for an insightful review of all these aspects to advance FSW from laboratory research into industrial manufacturing fields. Herein, all aspects of the inherent issues and control strategies, including technical characteristics and development, microstructures, mechanical properties, limitations, and prospects, are reviewed. Moreover, future aims for scientific research and engineering applications are pointed out according to the presented information.

2. Inherent issues of friction stir welding

A schematic diagram of conventional FSW is shown in Fig. 2. During conventional FSW, the workpieces to be welded are placed on a backing plate made of harder materials that can hold a sufficient forging force. A rotating tool with a shoulder and a pin plunges to a certain depth in the top surface of the welding workpieces, causing frictional heat and material flow. With the rotation and advancement of the rotating tool, the welding workpieces behind the rotating tool are joined together. Upon completing FSW, the rotating tool is retracted, and then a keyhole defect is left at the end of the weld.

Based on the process characteristics, three inherent issues occur during conventional FSW.

(1) The necessity of strict assembly tools, rigid support and omnidirectional fixation results in welding difficulties and reduces mechanical properties. Moreover, the lack of root penetration defect easily occurs at the bottom of the joint.
(2) Weld thinning induced by a plunge depth of the shoulder is detrimental to joint integrity, which easily results in stress concentrations and fatigue damage.
(3) Keyholes left by the retraction of the pin and other welding defects induced by improper selections of welding tools and parameters appear in the weld, which causes the “bucket effect” due to the small joining area, diminishing mechanical properties.

FSW has been increasingly employed in the joining of large aerospace structures, such as fuel tanks of launch vehicles, space shuttles and space ships [42], as shown in Fig. 3a. In 2013, NASA established large-scale welding assembly tools for the rocket fuel tanks of its space launch system, which consisted of a circumferential dome welding tool, a gore welding tool and an enhanced



Fig. 1. Typical applications of FSW in industrial manufacturing fields.

Table 1
Classifications of dissimilar materials according to interfacial reaction systems.

Interfacial reaction system	Example
Severe interfacial reaction	Al-Mg [33,34]
Non-interfacial reaction	Mg-steel [35]
Medium-interfacial reaction	Al-steel [36,37], Al-Ti [38,39]
New dissimilar materials	Metal-polymer [40,41]

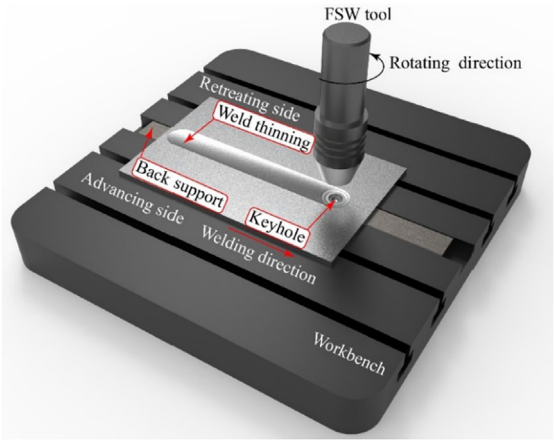


Fig. 2. Inherent issues in conventional FSW.

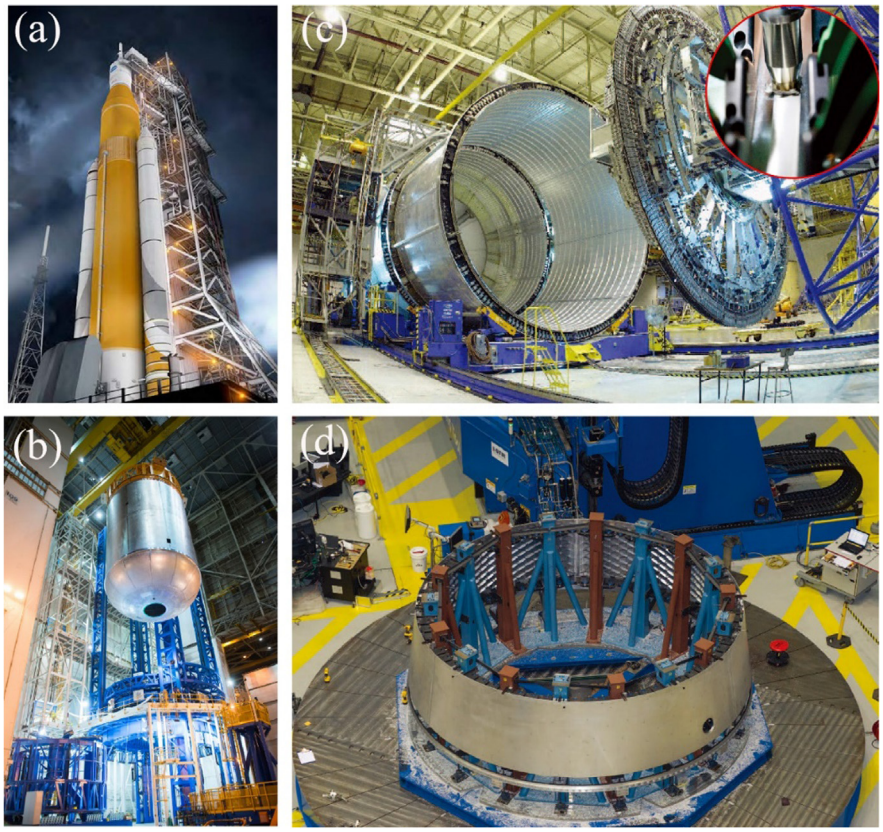


Fig. 3. Rocket fuel tanks of the SLS at NASA: (a) space launch system on its mobile launcher [44], (b) a liquid oxygen tank for a new rocket at Marshall Space Flight Center [45], (c) testing new FSW techniques before shuttle external tank production began on flight hardware [46] and (d) testing manufacturing processes and tools for the Orion structural test [46].

robotic welding tool [43]. The full-scale assembly tools are exceedingly complex. Moreover, the structural design is very large and the manufacturing cost is remarkably high, as shown in Fig. 3b–d. Additionally, these welded structural parts always experience complex internal/external pressure and structural torque during their service lifetime, which require highly reliable joints [42]. Conceivably, each of the residual inherent issues may lead to severe accidents during a space launch.

Therefore, there are three key issues that must be solved during conventional FSW: (1) reduce the complexity of the fixtures and

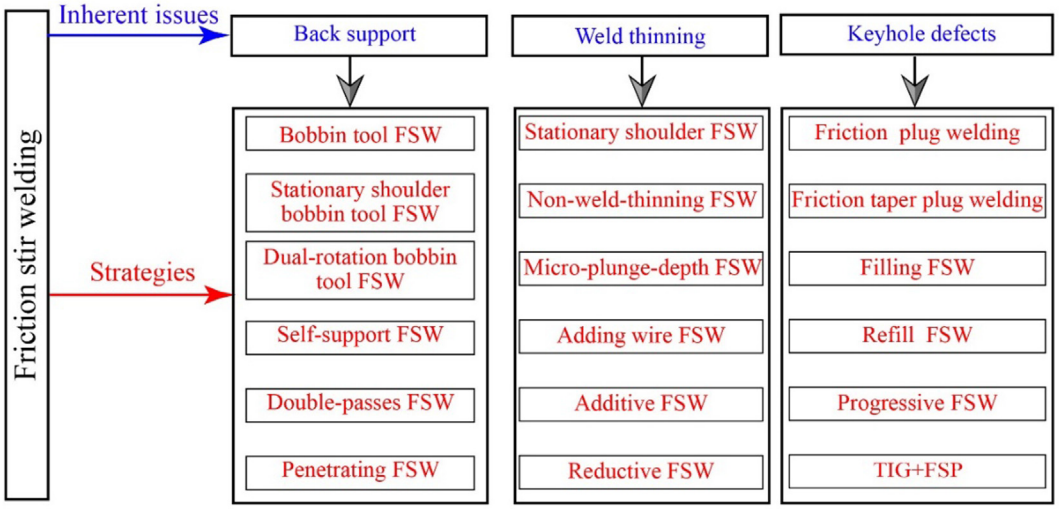


Fig. 4. Classifications of inherent issues and their control strategies in the FSW.

avoid the lack of root penetration defect, (2) increase the effective area of load bearing and eliminate stress concentrations, and (3) repair the keyholes and other defects and retain approximately equal strength after remanufacturing. New control strategies have prompted considerable scientific and technological interests due to the difficulties and challenges of ensuring the reliability and structural integrity during conventional FSW. According to causes and characteristics of the three inherent issues, novel FSW techniques have been developed and expanded, as shown in Fig. 4. The back support and lack of root penetration defect are solved by self-supported FSW concepts, comprising bobbin tool FSW (BT-FSW), self-support FSW ($SSFSW_1$) and penetrating FSW (PFSW). Weld thinning is eliminated by stationary shoulder FSW ($SSFSW_2$), micro-plunge-depth FSW (MPD-FSW) and additive FSW. Keyholes and other defects are addressed by friction stir-based remanufacturing technologies, such as friction plug welding (FPW), filling FSW (FFSW) and progressive FSW. In the next discussion, the main control strategies for solving three inherent issues are introduced and reviewed in terms of the corresponding concepts, technical developments, key factors, microstructures, mechanical properties, current limitations and prospects.

3. Self-supported friction stir welding

With the rapid development of industrial manufacturing fields, FSW has achieved satisfactory results and has been extensively applied in many domains, including aerospace and railway, wherein back support is provided by rigid backing plates. Gantry-type FSW equipment is used for hollow extrusions, tubes and enclosed structural parts, in which the welding workpieces need to be fixed and rigidly supported, increasing the manufacturing cost and welding difficulties. Moreover, the insufficient plunge depth of the rotating pin during conventional FSW results in the lack of root penetration defect, which subsequently diminished mechanical properties. As such, self-supported FSW techniques, including BT-FSW and $SSFSW_1$, were invented to solve these problems, which can decrease the structural rigidity and reduce the difficulties in design and manufacturing. Self-supported FSW can decrease the flexibility of a welding assembly and realize three-dimensional welding of single-curvature or double-curvature structural parts. Based on previous publications, the related technical developments, microstructures and mechanical properties are reviewed in the following chapters.

3.1. Bobbin tool friction stir welding

3.1.1. Principle

BT-FSW, also referred to as self-reacting friction stir welding (SRFSW), is a welding technique derived from conventional FSW that consists of an upper shoulder, a lower shoulder and a rotating pin, which has been widely used to join Al alloys [47,48], Mg alloys [49] and few ferrous alloys [50]. Fig. 5 shows a schematic of BT-FSW. The BT-FSW tool plunges into the preset hole or traverses along the butt interface between the welding workpieces. The upper and lower shoulders closely contact with the upper and lower surfaces of the welding workpieces, while the rotating pin stirs and blends the welding materials, generating frictional heat and material flow. Additionally, the lower shoulder can act as a backing plate, providing forging effects on the plasticized materials at the bottom of the joints. With the rotation and advancement of the welding tool, the plasticized materials flow in both welding workpieces under the action of the friction and extrusion induced by the shoulder and pin, realizing high-quality metallurgical bonding without the support of a backing plate.

Compared with conventional FSW, BT-FSW has many advantages, as detailed hereafter.

(1) The load along the vertical direction of the FSW equipment is reduced, and the rigidity requirements are also decreased.
(2) Rigid back support is avoided, which reduces the complexity of the welding fixtures.
(3) The adaptability of the working condition is broadened, which can realize a variety of welds, such as welds with a tailored thickness and three-dimensional welds.
(4) The lack of root penetration defect is eliminated.
(5) The heat input along the thickness direction is relatively uniform, decreasing the welding distortion and improving the mechanical property homogeneity.

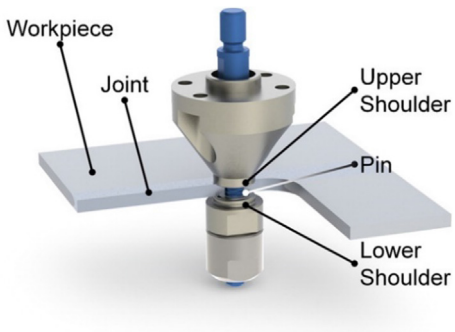


Fig. 5. Schematic of the BT-FSW technique [51].

3.1.2. Technical development

BT-FSW technique can be mainly divided into fixed-gap and adjustable or adaptive-gap BT-FSW. With the improvement of the welding equipment and the increase in control accuracy, other novel BT-FSW technologies have been proposed and optimized [49,52]. The fixed-gap welding tool is the most extensively used during BT-FSW process, for which the welding equipment requirements are relatively low. The design of the welding tool is simply integrated with the ability to adjust the lower shoulder. The main process parameters during BT-FSW are rotational velocity and welding speed, though other variables, such as dwelling time, tool gap, support/clamp settings and plate conditions, may also influence the joint strength. The process conditions also depend upon variations in several factors, such as tool geometry, features, and other process settings. The recommended parameters for BT-FSW of Al alloys are rotational velocities of 450–600 rpm and welding speeds of 75–100 mm/min for thin sheets (4–8 mm), while 170–300 rpm and 100–500 mm/min for thick plates (approximately 25 mm). Table 2 lists the functions and effects of different topological parameters of the BT-FSW tools, which can be adjusted according to the different welding requirements, such as the thickness and types of materials to be welded.

Sued et al. [53] stated that the best joint for thin Al alloy plates was produced by tool pins with four facets followed by threaded tool pins with three facets, as displayed in Fig. 6. Pirizadeh et al. [54] determined that a convex pin with 7% greater contact area with the welding workpieces resulted in a higher tensile strength efficiency (60.6%) than a simple pin (45.6%) due to higher frictional heat and better mixing of the materials during BT-FSW of thermoplastics. Additionally, the materials of the BT-FSW tools, particularly focusing on refractory alloys, have been further optimized. Thomas et al. [50] designed a bobbin tool consisting of a pin manufactured from refractory alloys with a high tungsten content and shoulders made of refractory alloys with a low tungsten content to weld 8-mm-thick 12% Cr alloyed steel, through which they produced excellent BT-FSW joints.

Fixed-gap BT-FSW has some shortcomings [49,56]. During BT-FSW, the frictional heat and advancing resistance easily lead to the distortion of the welding workpieces, causing the contact conditions between the welding workpieces and the welding tool cannot be adjusted. As a result, welding defects form at the welds or even lead to the fracture of the rotating pin. To achieve satisfactory results with fixed-gap BT-FSW, many preliminary experiments need to be performed to determine a suitable gap between the upper and lower shoulders.

TWI invented a novel welding mode called floating BT-FSW, in which the gap between the upper and lower shoulders was adjusted via displacement control or pressure control, as shown in Fig. 7 [57]. Floating BT-FSW has been successfully used to weld Al alloys [57] and steel [50]. There are few reports on floating BT-FSW due to the relatively complex welding control. Adjustable-gap BT-FSW is usually conducted under displacement control or pressure control modes. This technique can momentarily adjust the gap between the upper and lower shoulders to eliminate the thickness variations induced by thermal expansion. Hence, this control technique can realize BT-FSW of plates with unequal thickness. Fig. 8 shows a schematic of adjustable-gap BT-FSW, which was proposed by Marshall Space Flight Center and has been used to manufacture airplanes [58].

Counterrotating-shoulder BT-FSW was also proposed by NASA as an alternative to the mechanism and fixtures used in conventional BT-FSW [59], as shown in Fig. 9. The mechanism internally induces major or all the forces and torques exerted on the workpieces, simplifying massive external fixtures. By reducing or eliminating (relative to the use of a “self-reacting” tool) the torque that must be externally induced, the counterrotating-shoulder BT-FSW reduces the tendency towards distortion or slippage of the welded workpieces. In addition, dos Santos and Hilgert [60] invented stationary shoulder BT-FSW (SSBT-FSW), for which the aim was to complete the welding process at the lowest peak temperature via selective stationary upper and lower shoulders. The stationary conditions for the shoulder in SSBT-FSW mainly consist of stationary upper shoulder BT-FSW (SS_UBT-FSW) [61], stationary lower shoulder BT-FSW(SS_LBT-FSW) or synchronous stationary upper and lower shoulders BT-FSW. Goebel et al. [62] produced a high-quality surface finish on the stationary side and an ultimate tensile strength efficiency of 82% by SS_UBT-FSW of AA2198-T851.

The primary control methods for BT-FSW are displacement control and pressure control. For fixed-gap and adaptive-gap BT-FSW, the control modes present significant differences. Displacement control is primarily employed during fixed-gap BT-FSW. When the coincidence between the welding route and the rotating tool is confirmed, the fixed-gap BT-FSW can be started, which requires few welding parameters. Moreover, this welding procedure is relatively simple. Floating BT-FSW further simplifies the welding control,

Table 2
Functions and effects of different topological parameters of welding tools [55].

Topological parameter	Function	Dimensional effect
Shoulder morphology	Mixing and stirring of materials in the surface of joints.	The more suitably complex the morphology, the better the material flow.
Shoulder diameter	Heat generation, material transfer and plastic deformation.	The larger the shoulder diameter, the higher the heat generation.
Shoulder angle	Entrapment of materials.	A concave angle improves material accumulation, whereas a larger convex angle results in material overflow.
Pin morphology	Mixing and transferring of materials around the pin.	The more suitably complex the pin morphology, the better the heat generation and material flow.
Pin angle	Movement of materials along the thickness direction.	A large angle increases material flow.
Pin diameter	Heat generation and plastic flow.	A large diameter increases heat generation and decreases material flow.
Pin length	Material forging and stirring.	The longer the pin length, the stronger the material forging and stirring effects, and the better the defect elimination.

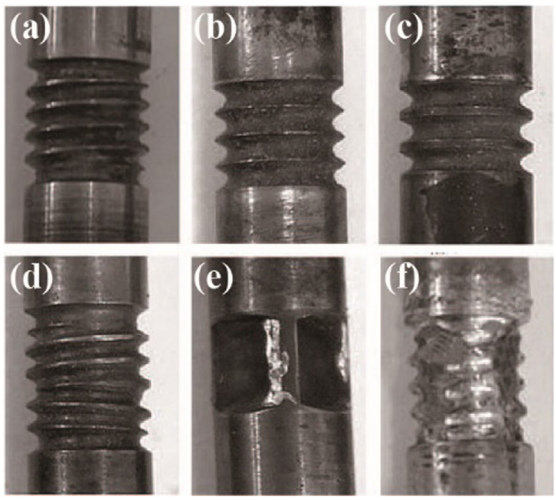


Fig. 6. BT-FSW tools: (a) threaded cylindrical pin, (b) cylindrical pin with 1.5-mm-pitch threads, (c) cylindrical pin with 2-mm-pitch threads, (d) cylindrical pin with left-hand and right-hand threads, (e) cylindrical pin with four facets and (f) threaded cylindrical pin with three facets [53].

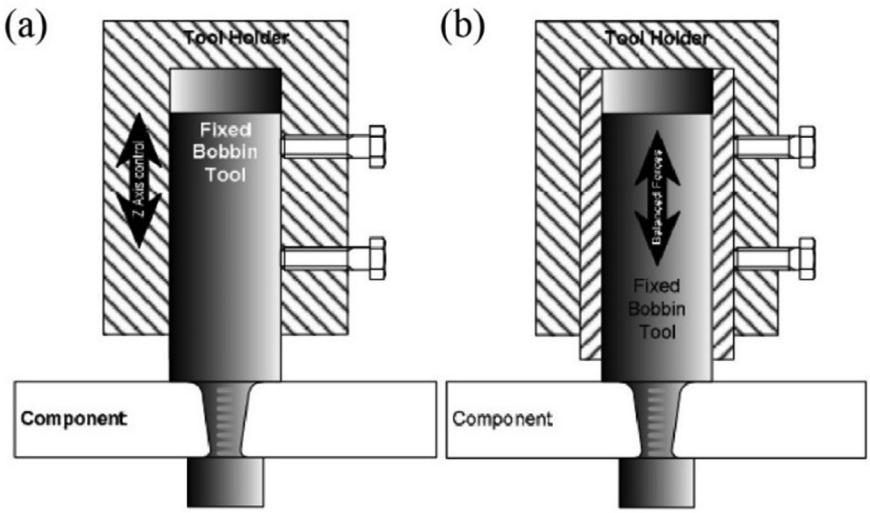


Fig. 7. Different kinds of bobbin tools: (a) fixed and (b) floating welding tools [57].

which can be realized by using the sensor responsible for balancing the axial mechanics of the rotating tool. This sensor is adapted for displacement control and pressure control modes. Both welding control modes require complex control devices, and the feedback information in the upper and lower shoulders as well as the rotating pin need to be precisely collected by the sensor system. Both of adaptive-gap BT-FSW and floating BT-FSW mainly depend on the configuration of the sensor system and its related selection. According to previously published papers, both of welding control modes have certain advantages, whereas deficiencies still exist in terms of welding adaptability. BT-FSW of plates greater than 4 mm in thickness has been widely reported. For BT-FSW of thin-walled structures, especially for sheets thinner than 2 mm, many problems must still be addressed, such as welding distortion that results in an incomplete weld. Therefore, further optimizing the welding control methods plays a significant role in promoting the welding stability of thin-walled structures. Moreover, there are still two challenges in BT-FSW that differ from conventional FSW [63]. One is the considerably increased load on the BT-FSW pin. In particular, the strength and lifetime of the pin is a major limiting factor for this process. The welding stability, especially in the BT-FSW of thin-walled sheets, is the other critical point. The transient temperature and material flow behaviour can lead to instabilities that cause defective welds and tool fracture, as shown in Fig. 10a. These instabilities are not observed in conventional FSW, as the transient temperature and dynamic flow are more constrained due to the presence of a backing plate. The unstable material flow easily results in welding defects, as shown in Fig. 10b. Moreover, there is notable tool wear, which results from two factors. One source for excessive wear is debris from a fractured upper shoulder ceramic inlay, in which the surface of the pin at the interface with the upper shoulder is considerably damaged (Fig. 10c). This phenomenon needs to be considered when using ceramic inlays. The torque transmitter for the lower shoulder also shows signs of wear and plastic deformation due to the overloading after a large number of welding experiments, as shown in Fig. 10d. Therefore, understanding the

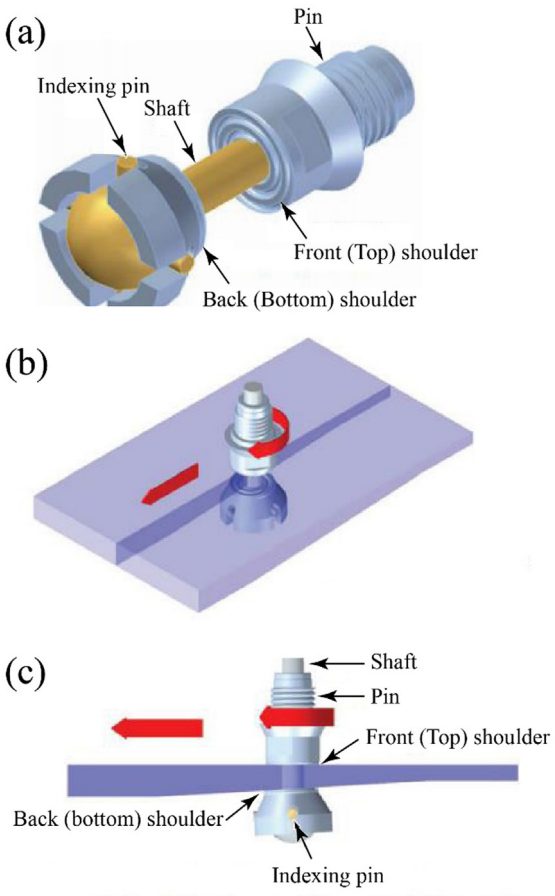


Fig. 8. Schematic view of adjustable-or adaptive-gap BT-FSW: (a) tool including a gimballed bottom shoulder, (b) tool in use on a tapered-thickness workpiece and (c) enlarged side view of tool in use on a tapered-thickness workpiece [58].

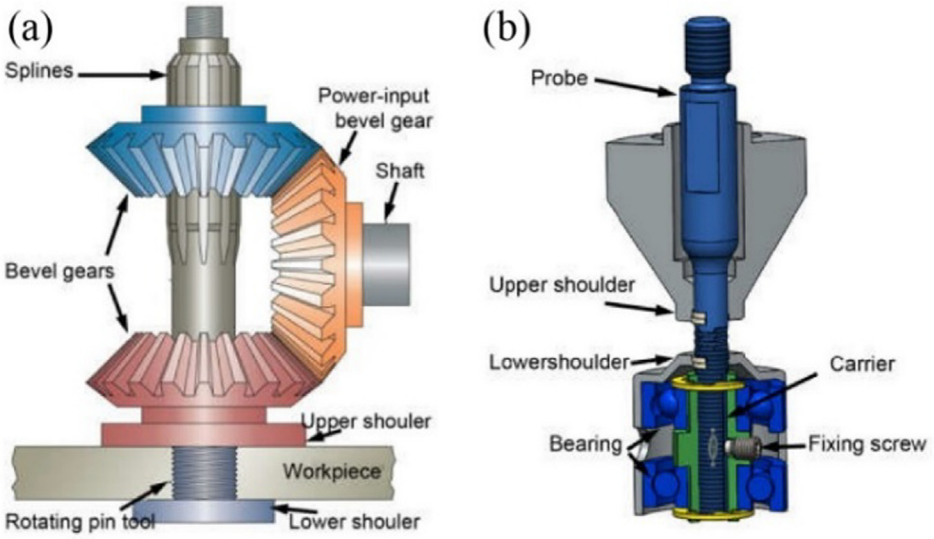


Fig. 9. Schematics of (a) counterrotating-shoulder BT-FSW [59] and (b) SSBT-FSW [61,62].

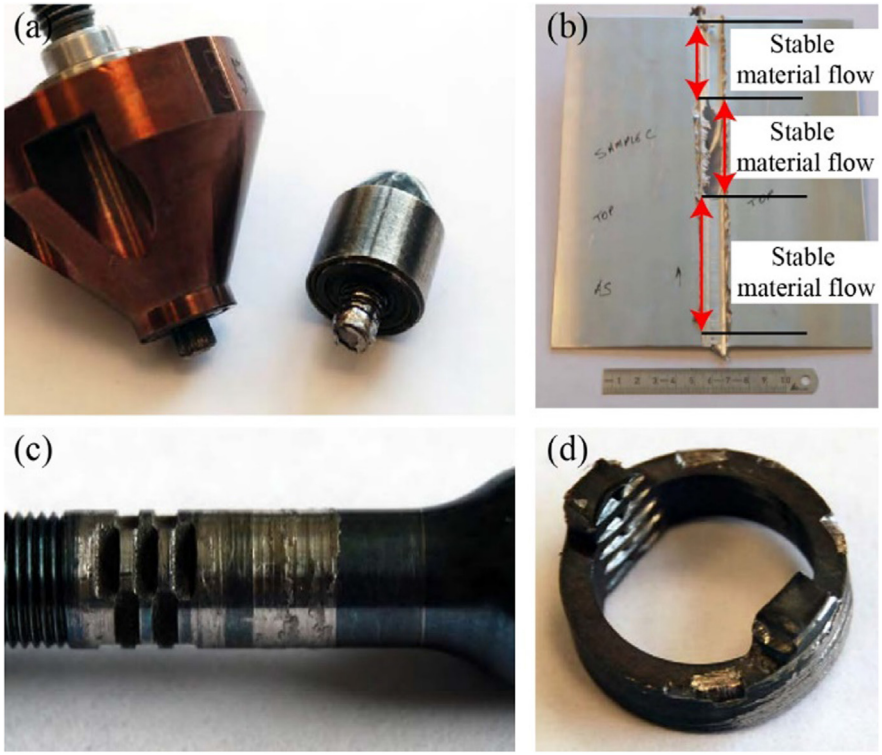


Fig. 10. Challenges in BT-FSW: (a) pin fracture, (b) spontaneous flow instability, (c) pin wear due to a fractured inlay and (d) wear of a lower shoulder holder [63].

joint formation mechanism is very important for high-quality BT-FSW welds.

3.1.3. Formation mechanism

The joint formation mechanism is the beginning of theoretical research for welding techniques. The intrinsic aspect of BT-FSW is that the original welding interfaces are changed into a new joining interface via plastic flow and transfer of the plasticized materials induced by thermo-mechanical behaviours, which are based on the friction between the rotating tool and the welding workpieces. The BT-FSW process involves complex heat generation and material flow behaviour, which are primarily governed by welding tool geometries, process parameters and properties (thermal and mechanical properties) of base materials (BMs). Determining the heat generation and material flow mechanism can provide valuable references for welding tool design, parameter selection and technical innovation. The heat generation and material flow behaviour are mainly investigated through experiments and numerical simulations.

Welding heat generation directly influences the interfacial material flow, microstructural evolution, welding defects and so on, thereby affecting the global mechanical properties and residual stress distribution [64]. The heat generation during BT-FSW is primarily influenced by the contact conditions between the rotating tool and the welding workpieces [65]. Trueba et al. [47] measured the spatial distribution of welding temperatures adjacent to the rotating tool. They found that the temperatures at the retreating side (RS) tended to be greater than those at the advancing side (AS), as shown in Fig. 11. The welding temperatures were also the highest at the beginning and ending of the weld due to the initial dwelling time and the exit from the workpieces, respectively. Chen et al. [52] developed a temperature measurement and control system, containing a closed-loop control system and the Smith predictive proportional-integral-derivative (PID) control method. In their study, the variations at the interface temperature within one rotation of the rotating tool were experimentally measured during BT-FSW for the first time. The characteristic parameters of the BT-FSW process were as followed: at 350 rpm, the steady-state temperature in the nugget zone (NZ) was maintained at 495 °C (the temperature was set to 480 °C). The temperature control error was approximately 15 °C, and the torque was maintained in the range of 48–50 N·m, which further improved the uniformity and stability of the BT-FSW process. The numerical simulation of heat generation during BT-FSW was based on conventional FSW, which simplified the boundary conditions to obtain a model of heat generation based on the constitutive relation of material mechanics.

In an experimental study of conventional FSW, the material tracer technique was used to investigate the material flow behaviour [66,67]. Guerra et al. [68] inserted a copper foil at the faying surface/joint line of butt-welded workpieces—overlapping both dissimilar materials—and examined the vertical flow pattern during welding. The transfer process of plasticized materials can be inferred by observing and analysing the spatial distribution of the tracing materials [66]. Schmidt et al. [69] employed conventional metallography, X-ray and computed tomography (CT) to investigate material flow by introducing a thin copper strip in the

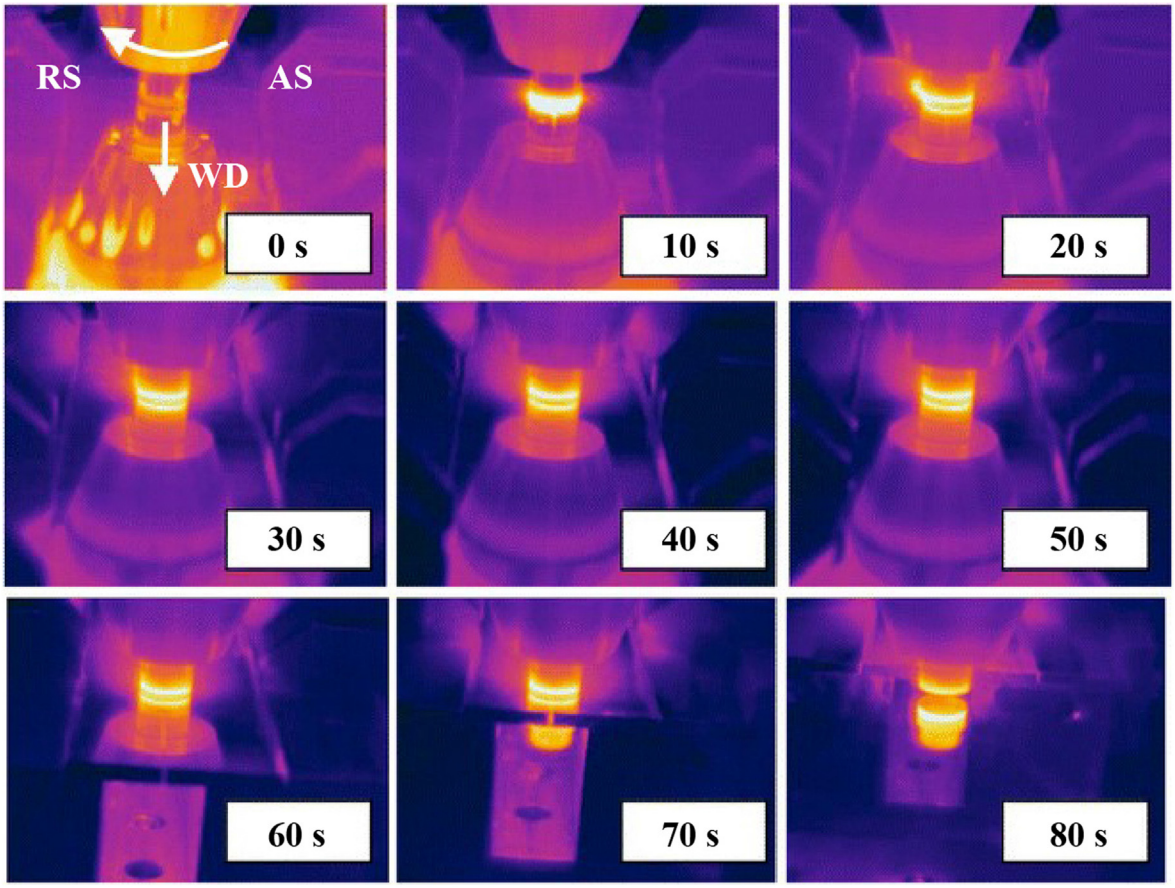


Fig. 11. Thermal infrared images during a trial weld [47].

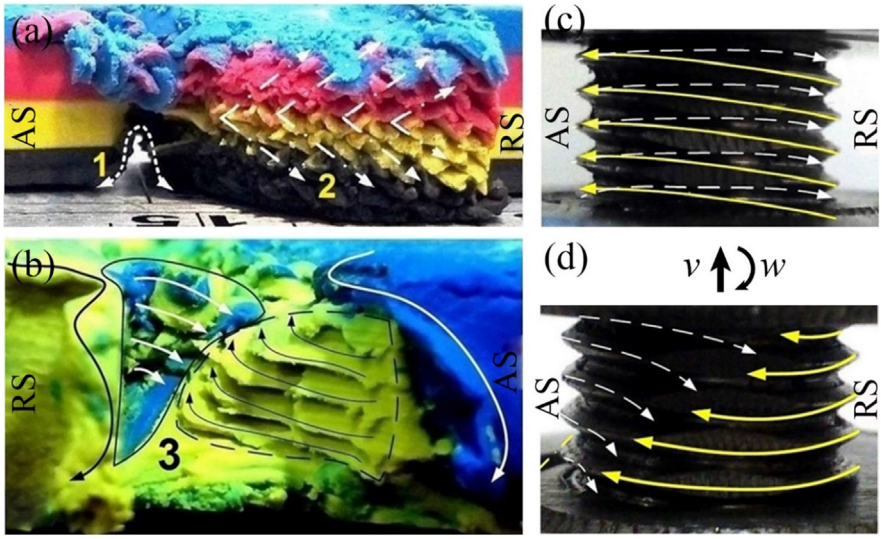


Fig. 12. Material flow behaviours: effect of threads (a) in the entry zone and (b) the exit zone replicated in the analogue model; (1) tunnel void, schematics of the shear bands in the (2) entry zone and (3) exit zone; schematics of the shear flow around the pin for the (c) entry zone and (d) exit zone, respectively [70].

workpieces as a marker material, and then estimated the flow velocity for the first time. Tamadon et al. [70] used stacked layers of multicolour plasticine as the tracer materials to investigate the material flow behaviour and formation mechanisms of the defects in the entry and exit, as shown in Fig. 12.

For the entry zone, as the bobbin tool enters the workpiece from the free edge of the butt line, the material flow from the RS to the AS is disrupted. The plasticized mass flow makes a spray zone outside of the workpiece at the RS along with a discontinuity line at the AS of the welding line. The multi-layered plasticine analogue model provided visualization of the plastic flow of the materials. This model accurately replicated the localized disruption for the positions of the severe plastic deformation. Although the material tracer technique has helped researchers comprehend the material flow, some limitations remain. Material transfer occurs in the NZ, which cannot be directly detected by common devices. The spatial distribution of the tracer materials during or after FSW is difficult to be quantized point by point to analyse the actual material flow around the rotating pin. There are differences between the tracer materials and the welding workpieces, including the BMs, dimensions and spatial distribution, which all inevitably result in differences between the tracer and actual experiments. Currently, there is still a lack of experimental studies on the joint formation mechanism of BT-FSW; related studies mainly focus on numerical simulations from the viewpoints of heat generation and material flow.

Schmidt and Hattel [71] proposed a new thermal pseudo-mechanical model in which the yield stress of the weld was the driver for heat generation. Hilgert et al. [72] presented a thermal 3D model that used a thermal pseudo-mechanical heat source and included tool rotation, an analytical shear layer model and ambient heat sinks, such as the machine and the atmosphere. The predictions of all models were in excellent agreement with each other and the experiment. Liu et al. [73] showed that the temperature field in the cross-section was symmetric about the mid-thickness of the welded workpieces. The high-temperature zones at the top and bottom surfaces near the shoulders were higher than those at the mid-thickness.

Compared with the numerical simulation of heat generation, the simulation of material flow behaviour is more mature. Hilgert et al. [51,74] proposed a computational fluid dynamics (CFD) model that treated the materials in the NZ as the highly viscous non-Newtonian shear thinning liquid. A customized parametric solver was used to solve the highly nonlinear Navier-Stokes equations. The contacts between the rotating tool and the welding workpieces were determined by coupling the torque within the CFD model to a thermal pseudo-mechanical model. An existing analytical shear layer model was calibrated using artificial neural networks trained with the predictions of the CFD model, as shown in Fig. 13. They also emphasized that the mixed approach was designed for fast predictions only. A deeper insight into the physics of the problem only could be gained through a 3D coupled thermomechanical model. Chen et al. [75] reported that a local “suction-filling” cycle appeared in front of the rotating pin ranging the shoulder radius. The flow field distribution presented a “butterfly” shape in the perpendicular section, while the distance between the butterfly region and surface was approximately 10–15% of the thickness between the upper and lower surfaces of the welding workpieces. Despite the process development, there are still unknown variables in the characterization of the process parameters that can cause uncontrolled welding defects. The entry zone and exit zone contain two discontinuity defects, and removing them is one of the current challenges for improving weld quality. Tamadon et al. [70] stated that numerical models showed that the entry zone and exit zone in BT-FSW were affected by the inhomogeneity of the material flow regime, which caused the ejection or disruption of the plastic flow in the gap between the bobbin shoulders. Fraser et al. [76] used smoothed particle hydrodynamics to simulate the BT-FSW process. This method allowed for easy tracking of the free surface for the welded workpieces, which permitted the visualization of welding defects. This method also showed the dispersion of the mixed materials in both workpieces. Predictions of the defects at the entry and exit regions were obtained via the numerical model (Fig. 14).

Based on a coupled Eulerian-Lagrangian model, Wen et al. [77] studied the formation mechanism of the band pattern zone during BT-FSW of AA2219-T87, where welding defects easily formed [78,79]. As shown in Figs. 15 and 16, the dynamic forming processes of the band pattern zone in the vertical and horizontal directions were calculated. First, the materials were heated and softened rapidly when the tool was in contact with the workpieces, and then the materials were pushed from the AS to the RS along the thickness direction. Second, two streams of material flow induced by the upper and lower shoulders were formed and mixed with each other during the movement of the rotating tool. Finally, the band pattern zone was formed when the two material streams were accumulated. The shoulder function was the main factor affecting this process. In the horizontal direction, plasticized materials adhering to the tool moved from the RS to the AS of the joint, as shown by the arrow, which had higher and lower velocities around the rotating tool, as illustrated in Fig. 16. Subsequently, the plasticized materials continued to move towards the AS and were released

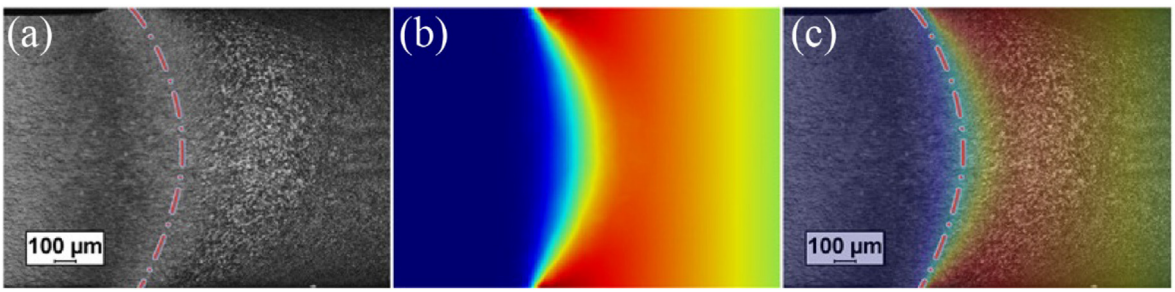


Fig. 13. Comparison between the predicted shear layer (red colour indicates high velocity) and microstructure: (a) microstructure at the RS, (b) velocity profile and (c) combination [51].

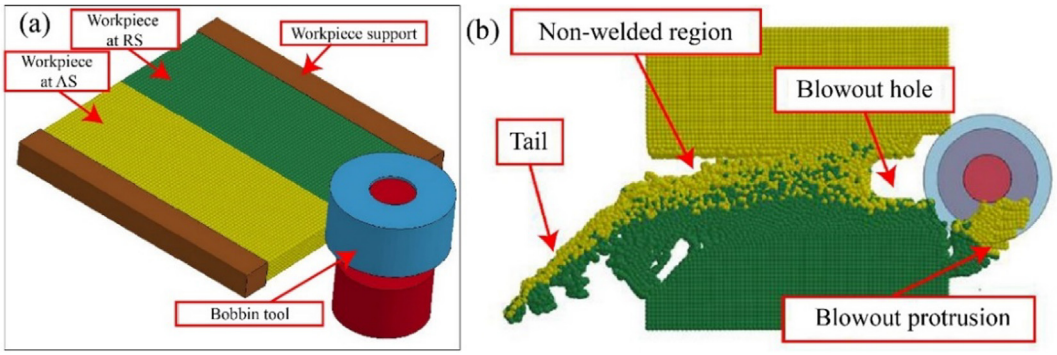


Fig. 14. Numerical simulation using smoothed particle hydrodynamics method: (a) model and (b) defect predictions at the entry and exit regions in BT-FSW [76].

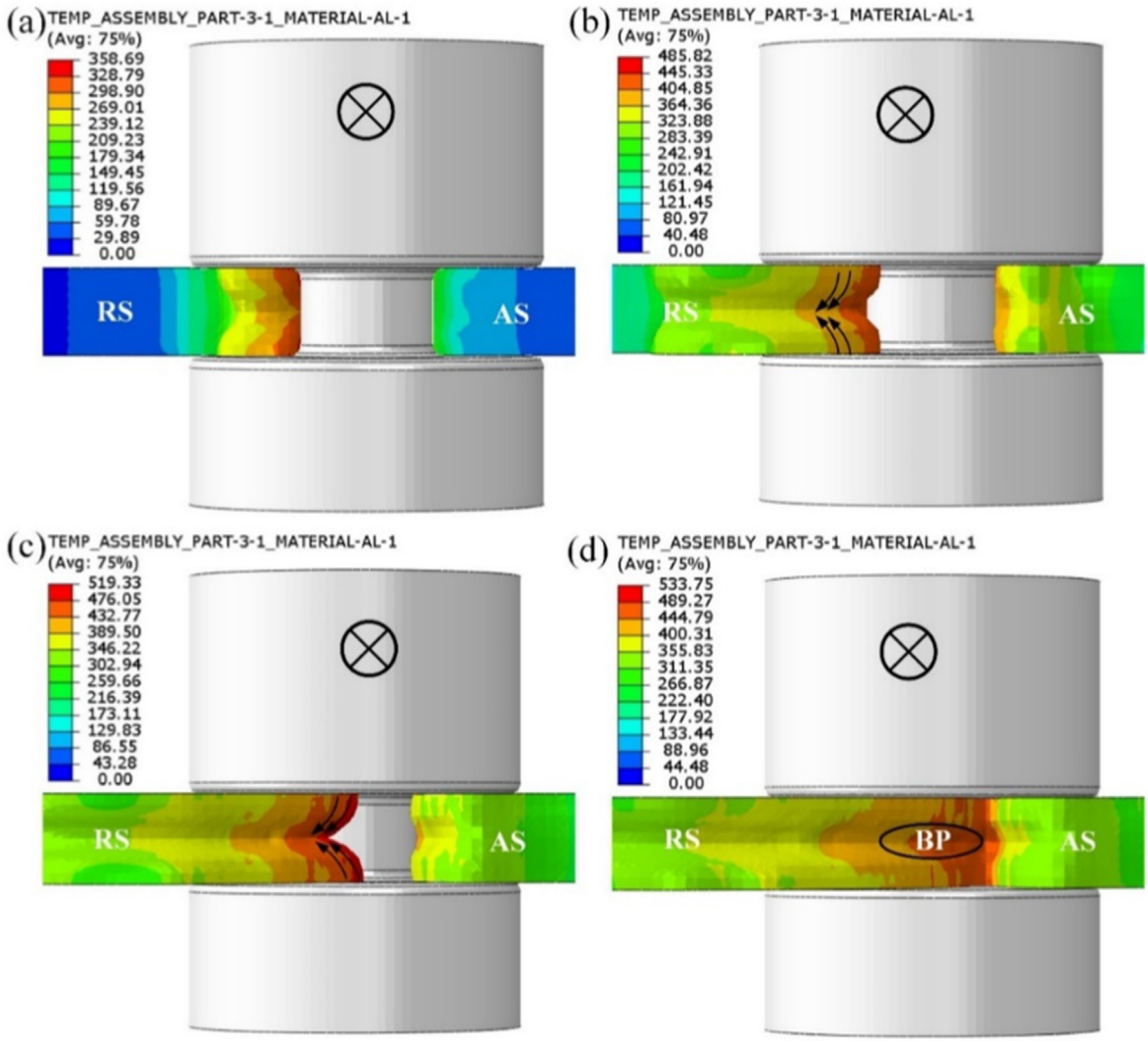


Fig. 15. Band pattern formations in the vertical direction at different times: (a) the tool only contacts the workpieces, (b) the tool plunges into the workpieces, (c) the tool moves away from the workpieces and (d) BT-FSW is completed [77].

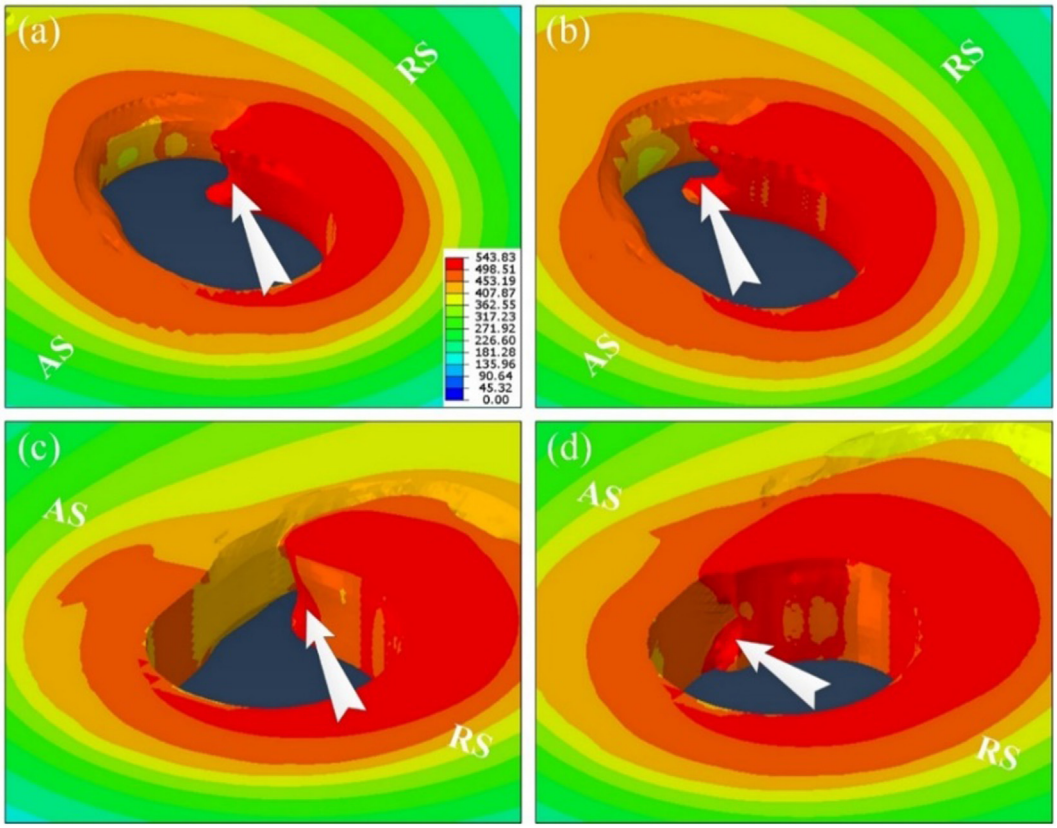


Fig. 16. Band pattern formation in the horizontal direction at different times: (a) the tool only contacts the workpieces, (b) the tool plunges into the workpieces, (c) the tool moves away from the workpieces and (d) BT-FSW is completed [77].

from the rotating tool to join the materials at the AS.

Numerical simulations of the heat generation, material flow, axial force and torque in BT-FSW are still in progress. Exploring an effective numerical simulation method is a hotspot for BT-FSW research, in which studies focus on the choice of numerical methods, the judgement of contact conditions, the selections of material constitutive relations and thermal conditions. This understanding is helpful for parameter optimization, avoiding defect formation and tool breakage.

3.1.4. Microstructural characteristics

During BT-FSW, severe thermo-mechanical behaviours are attributed to the microstructural evolution of the joint, which can be divided into four regions: NZ, thermo-mechanically affected zone (TMAZ), heat affected zone (HAZ) and BM, as shown in Fig. 17. The macrostructure in the cross-section presents a symmetrical deformed dumbbell shape, which is associated with thermo-mechanical effects. In contrast to conventional FSW, the central NZ of a BT-FSW joint presents a “finger” pattern resulting from the stacking of multiple “onion rings” induced by the complex metal flow [47].

Under a large strain rate and high peak temperature, dynamic recrystallization (DRX) occurs, which is attributed to fine and equiaxed grains [80,81]. The grain sizes in the upper shoulder affected zone (USAZ) and lower shoulder affected zone (LSAZ) are larger than those in the centre of the NZ. The reason for the coarser grains is that the heat generation near the shoulder affected zone (SAZ) is higher than that in the centre of the NZ. Padmanaban and Sundar [82] found that the grains in the NZ near the shoulders were coarser than the others in FSW joints of AZ31B Mg alloys. Moreover, it is difficult to dissipate heat from the welding tool because the lower shoulder also produces a lot of frictional heat and no heat sink is available during BT-FSW, similar to the backing plate in conventional FSW [83]. The grains in the TMAZ are deformed and elongated because of the plastic deformation caused by the interaction between the rotating tool and the welding workpieces, and the recrystallization of these grains generally does not occur for BT-FSW of Al alloys or conventional FSW of Al and Mg alloys [4].

DRX more easily occurs in Mg alloys than in Al alloys, which tends to equiaxed grains in the TMAZ of BT-FSWed Mg alloys [18,85,86]. Compared with conventional FSW, BT-FSW more easily generates DRX outside of the NZ due to the additional heat generation provided by the lower shoulder [49]. The HAZ is located between the TMAZ and the BM, wherein the materials only suffer from thermal effects without mechanical stirring, which results in grain coarsening. Esmaily et al. [87] indicated that the faster corrosion process in these regions could be linked to the progression of crevice corrosion. Threadgill et al. [88] found that a high-level substructure appeared in the TMAZ and a low-level substructure was observed in the NZ through electron back-scattered diffraction

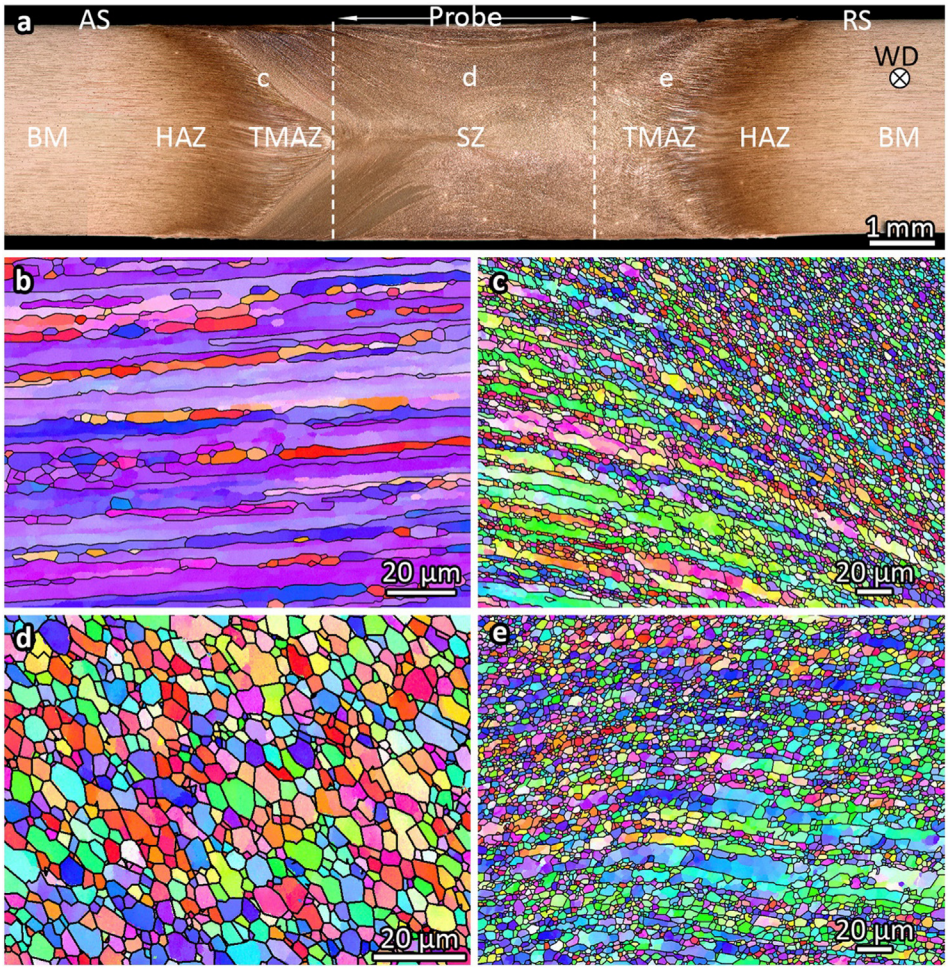


Fig. 17. Microstructures in a BT-FSW joint: (a) macrograph showing a typical BT-FSW joint; electron back-scattered diffraction micrographs showing the grain morphologies of (b) BM, (c) TMAZ at the AS, (d) NZ and (e) TMAZ at the RS [84].

analysis of AA6082-T6 joints produced by fixed-gap BT-FSW. Xu et al. [89] reported that more inhomogeneous refined grains, high-angle grain boundaries (HAGBs) in the NZ along the thickness direction and a larger percentage of low-angle grain boundaries (LAGBs) were achieved in conventional FSW joints than in BT-FSW joints of AA7085-T7452 due to the frictional heat and strain rate of plastic deformation combined with a certain degree of discontinuous DRX.

For precipitation-strengthened Al alloys, the dissolution, coarsening and reprecipitation of the precipitation phases occur during BT-FSW, which affect the mechanical properties. Fig. 18 shows bright-field transmission electron microscopy micrographs of the BM and NZ. High-density fine needle-shaped precipitates and low-density coarse block-shaped precipitates in the BM were composed of β'' and β' phases, which provided good mechanical properties. First, all metastable phases β'' and β' were diminished in the NZ, but some block-shaped equilibrium phases were randomly distributed in the NZ irrespective of the rotational velocity. This implied that the peak temperature in the NZ had surpassed the dissolution of β' (the dissolution of β' is higher than that of β''). Second, the dislocation densities increased with increasing rotational velocity [83]. The HAZ was characterized by the coarsening and transformation of the β' precipitates. Liu et al. [79] stated that the β'' and β' phases were diminished in the TMAZ of AA6061-T6 BT-FSW joints, which is different from the results reported by Sato et al. [90], who found that β' in the TMAZ region could remain in the matrix because the peak temperature was lower than the solvus temperature of β'. It is postulated that the thermal cycle in the BT-FSW process is more serious than that in conventional FSW. The combined effects were attributed to joint softening and reduced mechanical properties. Welding parameters also play significant role in the microstructural evolution and subsequent corrosion resistance. A fast BT-FSW process could improve the presence of the HAZ and lead to smaller intermetallic compounds (IMCs) particles in the NZ, effectively avoiding more pronounced intergranular corrosion attack caused by the formation of large Cu-rich IMCs in a slow BT-FSW process.

One of the most important characteristics in BT-FSW joints is joint line remnants (JLRs). Esmaily et al. [87,91] reported that JLRs resulted from the presence of oxide particles, which formed semi-continuous bands from the top to the bottom of the NZ, which were also known as kissing bonds or lazy S, as shown in Fig. 19. Kainuma et al. [92] and Zhou et al. [93] reported that the existence of

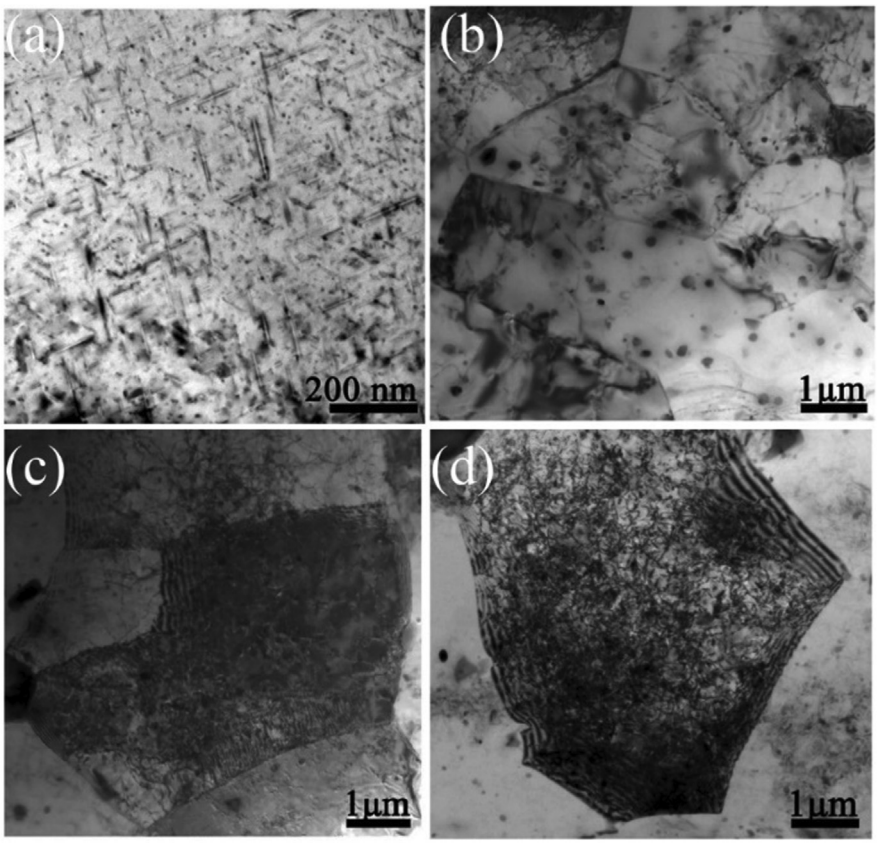


Fig. 18. Bright-field TEM micrographs: (a) BM; the NZ at rotational velocities of (b) 400 rpm, (b) 500 rpm and (b) 600 rpm [83].

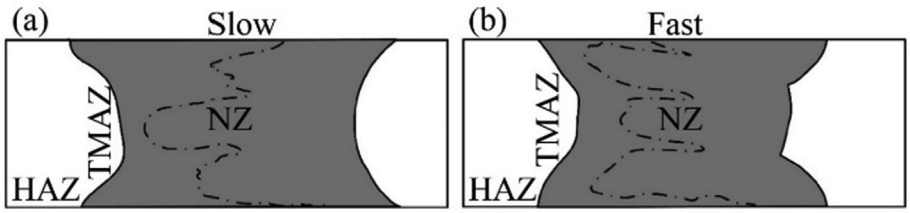


Fig. 19. Illustration showing the fraction of JLRs with respect to the area fraction of the NZs: (a) slow BT-FSW and (b) fast BT-FSW [87].

kissing bonds would seriously deteriorate the fatigue properties of joints in both low-cycle and high-cycle tests. Moreover, a severe corrosion attack at the location of joint line remnants was formed in the earlier stages of atmospheric corrosion ($\leq$200 h), and it was suggested that the faster corrosion could be related to the progression of crevice corrosion at the oxide particles/Al matrix and/or the presence of extrusion-induced contamination in these regions [87]. In fact, the formation of the JLRs is related to the local material flow induced by the shoulder-dominated zone (SDZ) and pin-stirred zone (PSZ) [84]. Increasing rotational velocity could evidently enhance the local material flow in the SDZ for thin sheets. However, the rotational velocity has a limited effect on the local material flow in the PSZ for thick sheets. In particular, a cylindrical pin with a small diameter and fewer features was less functional. To eliminate JLR defects, a reasonable design of welding tools that can improve the local material flow in the NZ is essential.

Wang et al. [94] stated that another typical feature of the BT-FSW joint was void defects formed at the triple junction of the TMAZ, upper shoulder dominated zone (USDZ) and lower shoulder dominated zone (LSDZ) of the AS, which reduced mechanical properties, as shown in Fig. 20. The formation of these voids was linked to the accumulation of the symmetrical material flow generated by the upper and lower shoulders at the AS, as shown in Fig. 20a and b. During BT-FSW, the layered structures of the USDZ and LSDZ had the same λ value, and the crests and troughs collided synchronously in the triple junction region (the periodic distance (λ) between each layer corresponded to the ratio of v/ω [95]). Apparently, some large voids were left between the troughs of the USDZ and LSDZ that were hard to be refilled, resulting in the void defects. They developed dual-rotation BT-FSW (DBT-FSW), in which the upper and lower shoulders rotated at certain rotational velocities, to avoid void defects by implementing a staggered layered structure and an unbalanced force between the upper and lower shoulders [94]. In DBT-FSW, the λ value was different for the

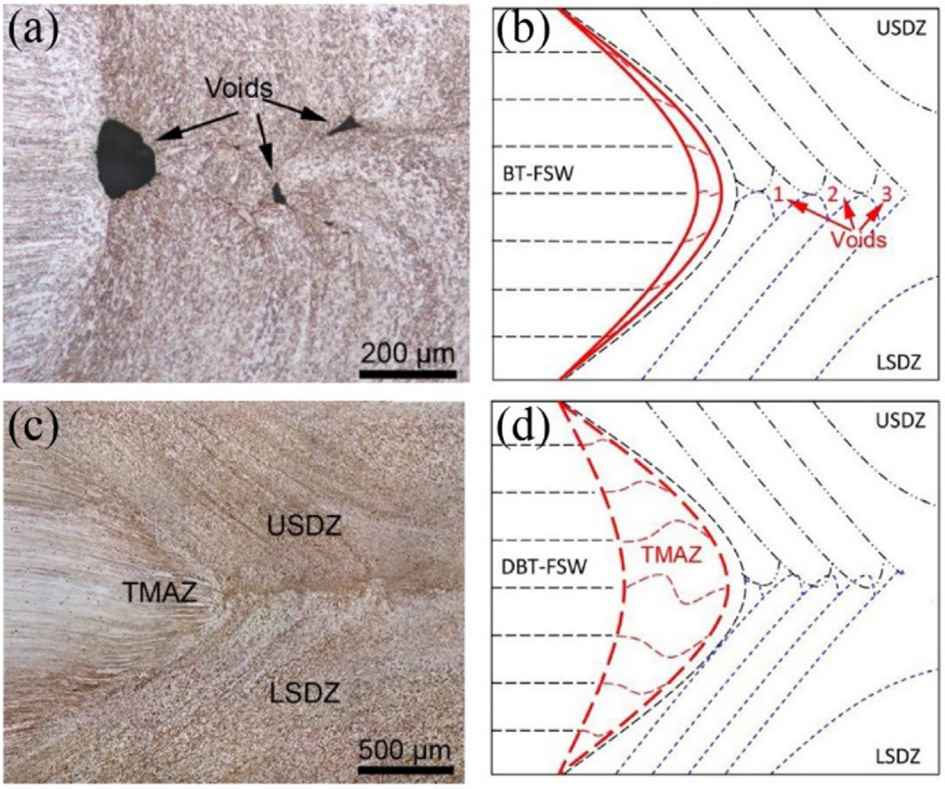


Fig. 20. Typical microstructures on the AS and illustrations for material flow: (a, b) BT-FSW and (c, d) DBT-FSW [94].

Table 3
Mechanical properties of BT-FSW and FSW joints of various materials.

Material	Thickness (mm)	Tensile strength (MPa)			Elongation (%)			Ref.
		BM	FSW	BT-FSW	BM	FSW	BT-FSW	
6061-T6	4	284		196	14		11.1	[79]
2195	8	577*	427	468	6.4*		12	[101]
2198-T851	3.2	474		379	12.5		7.5	[84]
6056-T78	4	322	268	257	12	2.1	1.1	[102]
2219-T87		459	321	331	13	7.8	7.1	[48]
2024-T3	4	469		375	18.7		3.58	[103]
6061-T651	8	290		243	10		9.2	[104]
6061-T4	6.35	246	189	229	10.5*			[96]
6082-T6	6	331*		232	12*			[105]
6061-T6	4	284		187	14		10.3	[83]
6082-T6	4	290		198	6		16	[53]
2A12-T6	6	460		345	12		5.1	[78]
6061-T6	5	300		224	13		8.9	[56]
AZ31B-O	2	345		231.9	18		2	[49]
AZ61	5	267		213	8.3		4.8	[81]
6061-T6	5	300		221	13		9.4	[106]
6063-T3	4	260		170	12		10.1	[97]
ABS	5	34.14		20.7	50*			[54]

Note: The numbers with "*" have been added by our research team from other literatures. Among them, 577* and 6.4* are from results of Zhang et al. [107]; 10.5* is referenced via the literature [108]; 331* and 12* are from Scialpi et al. [109]; 50* is from the literature [110].

USDZ and LSDZ (Fig. 20d). The LSDZ had a smaller λ value than that of the USDZ due to the higher rotational velocity, which indicated that the crests and troughs were staggered between the USDZ and LSDZ, consequently avoiding void defects.

3.1.5. Mechanical properties

Table 3 lists the mechanical properties of BT-FSW joints composed of 2xxx and 6xxx Al alloys, partial Mg alloys, and a few

polymers. The mechanical properties of the BT-FSW joints are related to joint softening and welding defects. According to published studies, mechanical properties of BT-FSW joints are all lower than those of conventional FSW joints due to severe joint softening induced by both of shoulders. For Al alloys and Mg alloys, the thermo-mechanical behaviours affect the microstructural evolutions, comprising dissolution, coarsening and reprecipitation of the precipitation phases as well as coarsening of the grains, which are attributed to joint softening and result in joint fracture. Li et al. [49] stated that a high welding speed was beneficial to grain refinement, which was attributed to a higher restriction on dislocation motion and localized plastic deformation due to the large numbers of grain boundaries. Yang et al. [96] stated that the slow cooling rate in the HAZ induced by the higher peak temperature during BT-FSW provided sufficient temperature and time for precipitation evolution. Hou et al. [83] reported that the dissolution and coarsen of precipitation phases in the HAZ occurred at higher rotational velocities, thereby decreasing mechanical properties. To reduce the severe joint deterioration induced by the higher welding heat input, Zhao et al. [97] proposed water cooling BT-FSW (WBT-FSW) in which water was sprayed on the surface of the workpieces. Using this approach, both the peak temperature and the high-temperature exposure time were significantly decreased. Hence, this process only induced the coarsening of the β'' precipitates but not the dissolution and transformation of the β'' precipitates. Consequently, the tensile strength of the WBT-FSW joint reached 178 MPa, which was 11.4% higher than that of the conventional BT-FSW joint. Moreover, some cooling mediums, such as CO_2 and argon gas, can be explored to improve the properties of BT-FSW joints. Post-weld heat treatment (PWHT) is another effective way to enhance mechanical properties of BT-FSW joints. Dalder et al. [98] heat treated AA2219-T62 BT-FSW joints under the naturally aged T4 condition, which increased the total elongation from 10.5% to 13% and tensile strength from 280 MPa to 305 MPa. For workpieces in the O condition, the welding joints were heat treated to the T62 condition, and ductility increased to 6.6%.

In addition to joint softening, welding defects, the sites of stress concentration, easily become the nucleus of tensile cracks, subsequently decreasing mechanical properties. The common defects in BT-FSW joints are voids, tunnels and lazy S defects, which are generally found close to the centre of the TMAZ or the joining interface. Warsinski et al. [99] verified that the concentration of oxygen along the fracture surface of lazy S was roughly twice that on the fracture surface of the NZ. There are three mechanisms for defect formation: (i) volume deficiency, (ii) inadequate material flow and mixing induced by low heat input [100], and (iii) accumulation of symmetrical material flow induced by the upper and lower shoulders in the centre of the TMAZ [94]. Hou et al. [83] and Pirizadeh et al. [54] stated that void formation due to the overflow of materials at certain high rotational velocities deteriorated the joint strength. Moreover, a high welding speed easily caused insufficient material flow, which further resulted in deficient pin-driven material flow, leading to void formation.

During universal mechanical tests, the integral mechanical properties of the joints were considered in greater detail. The characterization of the local mechanical properties is always neglected. Only Wang et al. [111] investigated the local mechanical properties of the NZ, TMAZ and HAZ via digital image correlation. They reported that the local elongation in the HAZ and TMAZ (13.1%) was higher than the global elongation in the whole joint (5.1%). Moreover, the NZ exhibited a local elongation of 13.8%, whereas the BM exhibited a local elongation of 13.5%, indicating that the BM exhibited better ductility, which was attributed to the heterogeneous deformation induced by the highly inhomogeneous microstructure in the whole joint. During conventional FSW, the tensile properties and the hardness have good correspondence. For third-generation Al-Li alloys with complex strengthening phases or Mg alloys, in which the texture is strongly dominant, the failure mechanism of the joint is not clear. Moreover, the relationships between the microstructures and mechanical properties need to be investigated systematically.

3.1.6. Prospects

Although BT-FSW has achieved many satisfactory results in laboratory or manufacturing fields, some technical problems still exist.

(1) Severe stress in the welding tool: Because the diameter of the pin is far lower than those of the shoulders, the welding pin easily fractures due to the advancing resistance and the large torque induced by the lower shoulder. The design of welding tools according to different welding requirements needs to be studied.
(2) Higher requirements of welding control: Compared to conventional FSW, BT-FSW has more complex contact conditions and a higher welding difficulty, especially for thin-walled structures or materials with low thermal conductivity.
(3) Preset hole at the beginning and ending stages during the BT-FSW process: Before or after welding, the preset holes need to be

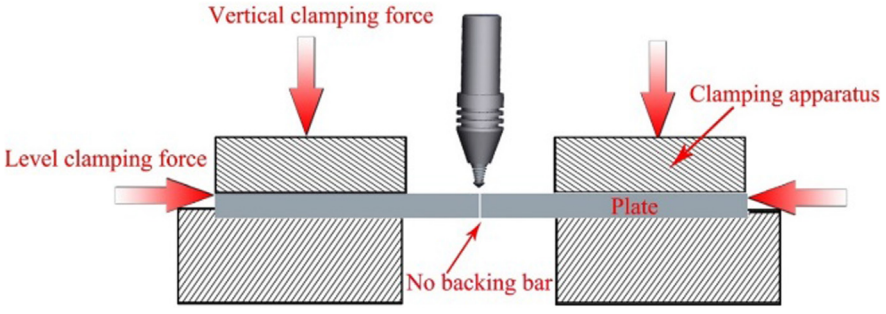


Fig. 21. Schematic of $SSFSW_1$ [113].

fabricated to facilitate the plunge and retraction of the BT-FSW pin. Especially for the enclosed structure, the installation and disassembly of the lower shoulder are more difficult.

(4) High welding heat input: The existence of a lower shoulder causes the total heat input of BT-FSW to be far higher than that of conventional FSW, which results in severe joint softening, thereby deteriorating mechanical properties. Moreover, aiming at thin-walled structures, the higher heat input is prone to cause serious buckling distortion, resulting in bad formation and joint integrity.

(5) Narrow welding process window: The tilt angle in the BT-FSW process is zero; hence, this process cannot provide sufficient forging force, which results in the narrow welding process window and high requirements of welding equipment fixtures.

3.2. Self-support friction stir welding

3.2.1. Principle

To overcome the disadvantages of severe joint softening and preset holes in the BT-FSW process, Huang et al. [112] proposed $SSFSW_1$ technique, which overcome the inherent issue of a single shoulder in conventional FSW. The welding tool used for $SSFSW_1$ is composed of a concave upper shoulder with a large diameter, a convex lower shoulder with a small diameter and a rotating pin. The high-quality joining of hollow or enclosed structures can be realized by adjusting the tilt angle and the asymmetric shoulders, as shown in Figs. 21 and 22. In contrast to BT-FSW, the convex lower shoulder in $SSFSW_1$ can realize the adjustment of the tilt angle, which is beneficial to broadening welding process windows. The thickness adaptation of $SSFSW_1$ is achieved without a tilt angle (Fig. 21). During $SSFSW_1$, the preset holes during the beginning and ending of BT-FSW are avoided, simplifying welding procedures. Due to the complete plunge of the rotating pin along the thickness direction, the lack of root penetration can be avoided. Additionally, aiming at special structures with a narrower welding area at the back of a workpiece, the smaller convex shoulder enables this method to be more effective than BT-FSW.

3.2.2. Design criterion of welding tools

The $SSFSW_1$ tool can realize the thickness adaptation of the workpieces due to the convex lower shoulder, as shown in Fig. 23. During $SSFSW_1$, the tilt angle can be adjusted from 1° to 4°. The distance between the concave upper shoulder and the root of the tapered pin is H, whereas h represents the distance between the root of the tapered pin and the convex lower shoulder. The angle between the centre axis and the lower shoulder is β. Moreover, α represents the tilt angle that the $SSFSW_1$ tool can be adjusted.

The thickness of the workpieces can be adjusted from d to $d + d_1$. From Fig. 24, the following equations can be drawn:

$$H = R\tan\alpha + d/\cos\alpha - r_1\tan\alpha \tag{1}$$

$$H + h = R\tan\alpha + (d + d_1)/\cos\alpha - r\tan\alpha \tag{2}$$

where R is the radius of the upper shoulder, $2r$ is the diameter of the lower shoulder and $2r_1$ is the diameter of the root tapered pin.

$$d = H\cos\alpha + (r_1 - R)\sin\alpha \tag{3}$$

$$d + d_1 = (H + h)\cos\alpha + (r - R)\sin\alpha \tag{4}$$

$$h = L\cos\beta \tag{5}$$

$$d + d_1 = (H + L\cos\beta)\cos\alpha + (r - R)\sin\alpha \tag{6}$$

When α is 0, the minimum thickness of the workpieces is $d = H$, and the maximum thickness of the workpieces is $d + d_1 = H + L\cos\beta$. The thickness of the workpieces can be changed from H to $H + L\cos\beta$, as shown in Fig. 24b–d. According to

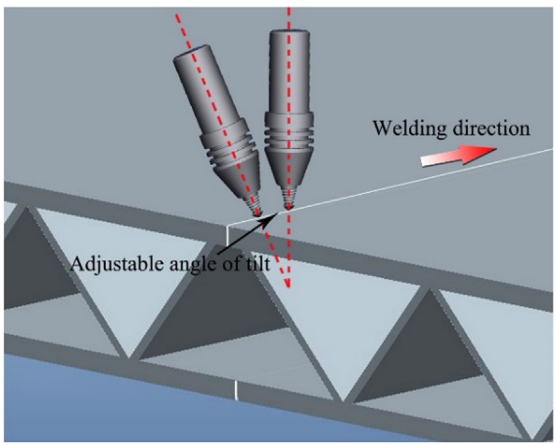


Fig. 22. Adjustable tilt angle of the $SSFSW_1$ welding tool [113].

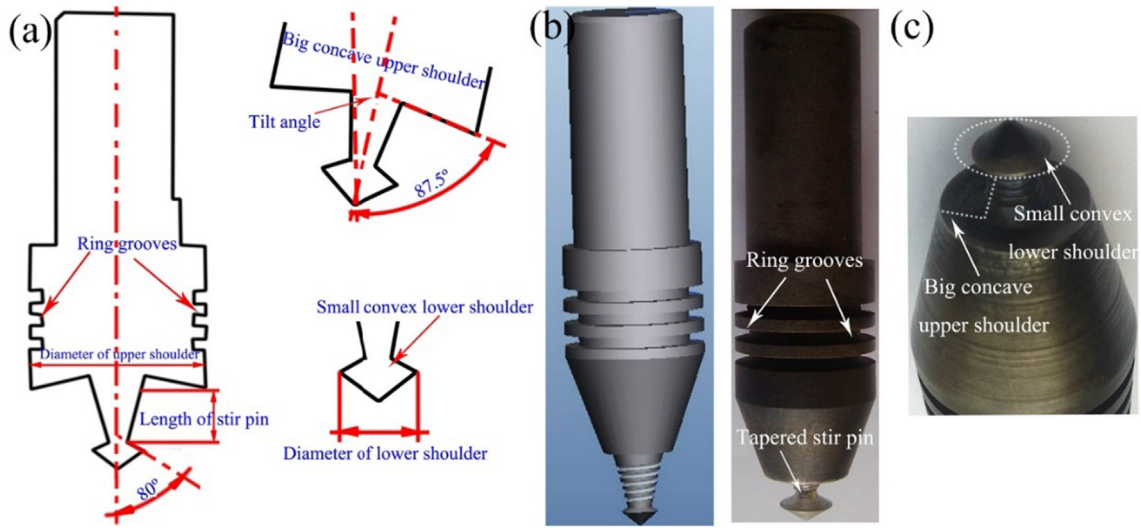


Fig. 23. Welding tools of $SSFSW_1$: (a) design view, (b) model and (c) physical picture [114,115].

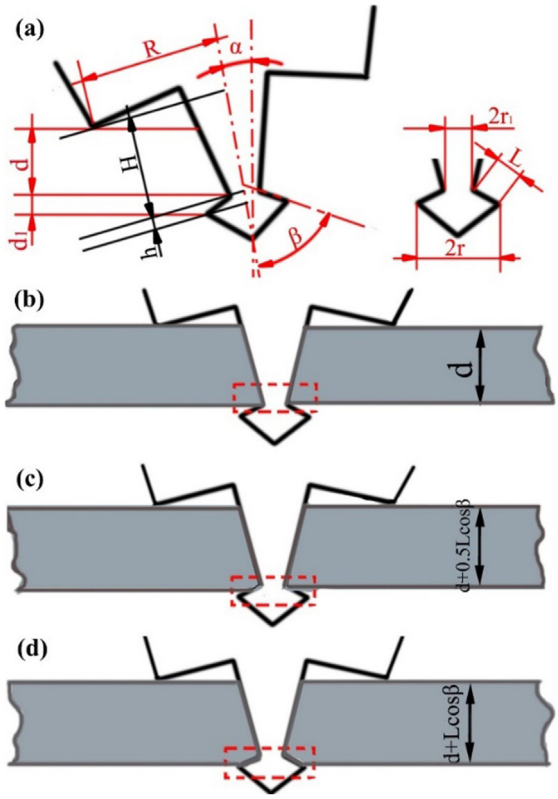


Fig. 24. Thickness adaptability of the $SSFSW_1$ tool: (a) key parameters related to the adjustability of the workpiece thickness when α is 0, (b) minimum workpiece thickness, (c) workpiece thickness changing from d to $d + 0.5L\cos\beta$ and (d) maximum workpiece thickness [112].

Eqs. (3) and (6), the variation in the tilt angle α is related to the thickness of the workpieces to which the $SSFSW_1$ tool can adapt. When other parameters are fixed, the range of thickness of the workpieces is reduced as the tilt angle α increases [112]. As shown in Fig. 25, the upper and lower surface appearances produced by $SSFSW_1$ are free-defects, which avoid the indentation induced by the shoulder plunge.

The design of the welding tool is closely correlated with the thermal and mechanical properties [116]. The mechanical properties of the welded workpieces, such as yield strength, ductility and hardness, significantly influence plastic deformation and heat

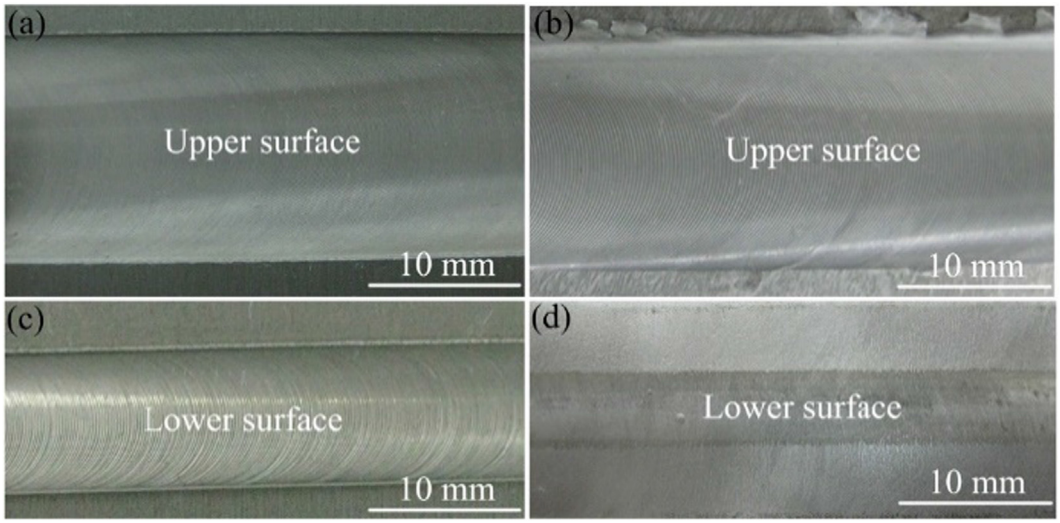


Fig. 25. Surface appearances of the typical $SSFSW_1$ and conventional FSW joints: (a) upper and (c) lower surfaces of a $SSFSW_1$ joint; (b) upper and (d) lower surfaces of a conventional FSW joint.

generation. The thermal properties, such as thermal conductivity and specific heat, affect the heat transfer in the welding workpieces. Focusing on different materials, rational selections of the materials and topologies of the welding tools are essential. In published studies, 6xxx Al alloys with low yield strength and good flowability, such as 6061-T6 and 6005-T6 Al alloys, have been successfully joined via the $SSFSW_1$ tool containing a threaded pin and a lower shoulder with a small diameter. Compared with 6xxx Al alloys, 2xxx and 7xxx Al alloys have higher yield strength, lower ductility and worse flowability. A $SSFSW_1$ welding tool with good ductility and improved material flow effect is urgent.

Fig. 26 shows the design of the $SSFSW_1$ tools, which are all made of H13 steel due to the better balance between strength and ductility at high temperature; note that W6 steel was not used due to the high loss in ductility. The circular pin and the three-facet pin do not easily fracture, whereas they have difficulties in producing sufficient material flow and deteriorate joint formation. The threaded pin can realize the material flow along the thickness direction, obtaining good joint integrity. For threaded pins with three facets, the material flow can be promoted, and the fracture risk of the welding tool is reduced during conventional FSW [117,118]. The partial stress concentrations and reduction of load bearing easily improve the fracture risk during $SSFSW_1$ of 7xxx Al alloys due to the high torque. In addition to the rotating pin, which can improve the material flow, the diameter of the lower shoulder is another important parameter that provides sufficient forging force and frictional heat, thereby reducing the welding torque and avoiding pin fracture risks. For 3-mm-thick 2xxx or 7xxx Al alloy sheets, the diameter of the rotating shoulder should be twice as high as the thickness of the workpieces to be welded.

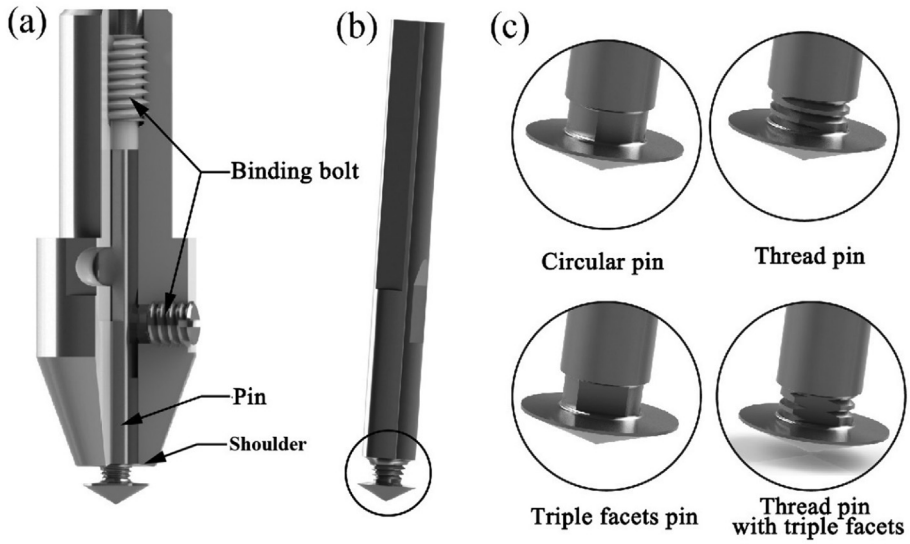


Fig. 26. Schematics of (a) detachable welding tool, (b) macroscopic rotating pin and (c) different rotating pin morphologies.

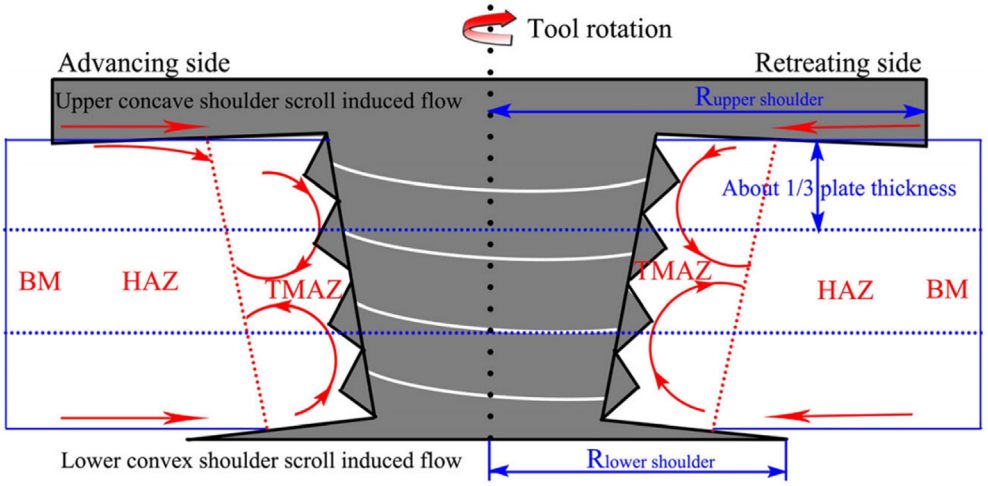


Fig. 27. Material plastic flow model during the $SSFSW_1$ process [119].

3.2.3. Formation mechanism

During the $SSFSW_1$ process, the material flow in the TMAZ is demonstrated schematically in Fig. 27. When the $SSFSW_1$ pin is plunged into the welding workpieces, a cavity remains besides the rotating pin, and the shape of the cavity is determined by the profile of the rotating pin. The volume of the plasticized materials below the upper shoulder and upon the lower shoulder depends on the rotational velocity, welding speed and tilt angle. When the $SSFSW_1$ tool goes forward, the materials in the RS are dragged by the shoulder over the weld to the AS and flow into the pin-affected zone. The materials in the pin-affected zone flow in layers around the pin in depth, and the layers are stacked on the welding line. Once the restriction of material flow from the leading edge to the trailing edge increases, flashes should occur on the RS. This results in insufficient material filling in the AS, leading to the formation of tunnel or pore defects. The upward pressure, which prevents the collapse of the NZ, depends on the diameter of the lower shoulder and the heat input. When the diameter of the lower shoulder is small, the upward pressure is not sufficient to prevent the collapse of the NZ, and the defect or converged point shifts downward.

3.2.4. Microstructural characteristics

The macrostructure of a typical $SSFSW_1$ joint is shown in Fig. 28, which presents an hourglass shape, and the LSAZ is narrower than that in BT-FSW. Similarly, the cross-sections are identified as HAZ, TMAZ, upper nugget zone (UNZ) and lower nugget zone (LNZ). The mechanical properties of Al-Mg-Si alloys are strongly dependent on the metastable precursors of the equilibrium β (Mg_2Si) phase. The precipitation behaviour of Al-Mg-Si alloys is generally reported to be supersaturated solid solution (SSS) → cluster → Guinier-Preston (GP) zones → β'' → β' → β [120,121]. The dissolution of the precipitates is observed in the TMAZ. The homogenously distributed precipitates are generally smaller in the NZ, and there are far fewer large precipitates in the NZ than in the BM. A considerable number of precipitates are randomly distributed in the UNZ. Dong et al. [122] found that the materials in the NZ experienced the highest peak temperature and the precipitates β'' dissolved into the α-Al matrix during FSW of AA6005A-T6. Moreover, coarsening of second-phase particles and dissolution of the rod-shaped precipitates and needle-shaped precipitates are also observed in the HAZ. This easily results in severe joint softening in the HAZ.

PWHT is performed to change the microstructural morphologies and improve the mechanical properties. The nanoparticles become increasingly denser. The particles include the precipitates along grain boundaries, which are broken by the rotating pin. The

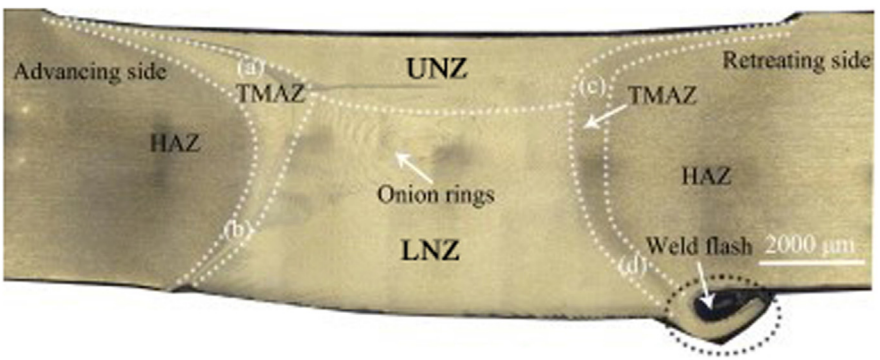


Fig. 28. Macrostructure of a $SSFSW_1$ joint of 5-mm-thick 6082-T6 Al alloys [115].

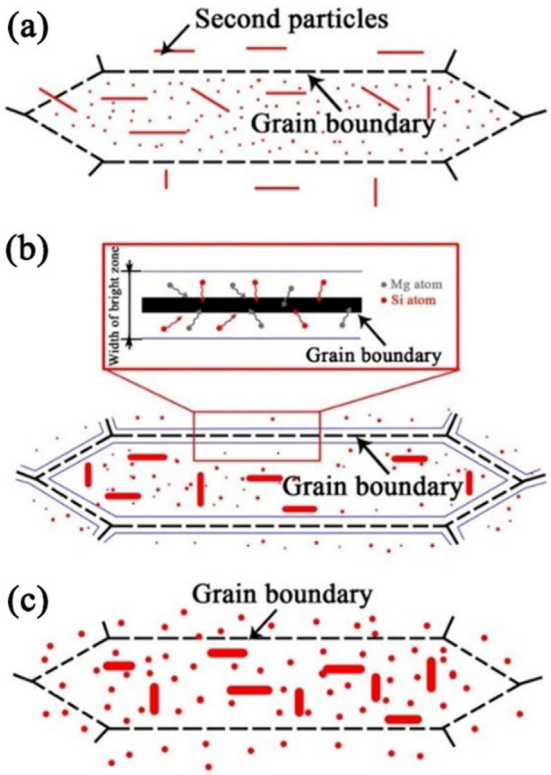


Fig. 29. Schematic maps of microstructural evolution with PWHT: (a) BM, (b) precipitate-free zone and the precipitates and (c) coarsening of precipitates [123].

heat input coarsens the small metastable precipitates. The maximum temperature of 723 K cannot induce the dissolution of the stable Mg_2Si phase particles but benefits atomic diffusion. The diffusive flows of Mg and Si atoms from nanoprecipitates and the α-Al matrix strongly contribute to the growth of the grain boundaries (Fig. 29). As a result, the concentrations of Mg and Si at the interfaces of grain boundaries and matrix decrease [123]. With the increase in holding temperature, the microhardness increases and tends to uniform due to the complete solution of the overaged strengthening particles and new precipitation of fine needle-shaped precipitates.

3.2.5. Mechanical properties

The microstructural evolution of the $SSFSW_1$ joint markedly affects the mechanical properties associated with joint softening, which is dominated by the welding parameters, such as rotational velocity, welding speed and shoulder diameter. The microhardness distribution in the cross-section presents a "W" shape, in which the lowest microhardness value is located at the interface between the TMAZ and HAZ due to severe joint softening induced by the coarsening and dissolution of the precipitates. With the increase in welding speed, the softening degree is reduced because of the short exposure time at high temperature. Table 4 lists the tensile properties of $SSFSW_1$ joints. For 5-mm-thick 6082-T6 Al alloy sheets, the maximum tensile strength with a corresponding joint efficiency of 69% was achieved at a welding speed of 200 mm/min, a rotational velocity of 800 rpm, a tilt angle of 4° and a plunge depth of 0.1 mm [114]. Moreover, the tensile fracture all located at the AS rather than at the RS due to the more severe joint softening in the AS induced by the high welding peak temperature. By increasing the lower shoulder diameter to a certain extent, the overflow of the plasticized materials is reduced, contributing to an increase of mechanical properties. Only the influences of welding speed and shoulder diameter are investigated in a narrow process range. The other welding parameters, including rotational velocity, tilt angle and plunge depth, still need to be studied to enable high-speed FSW with high quality to satisfy the requirements in the

Table 4
Tensile properties for SSFSW joints of different Al alloys.

Material	Thickness (mm)	Tensile strength (MPa)		Elongation (%)		Ref.
		BM	$SSFSW_1$	BM	$SSFSW_1$	
6005A-T6	5	270	190	16.5	6.9	[112]
6082-T6	5	320	220	14	12.8	[114]

manufacturing fields.

3.2.6. Prospects

The formation characteristics, material flow processes and mechanical properties of $SSFSW_1$ joints of 6xxx Al alloys have been extensively reported by our research group. However, 2xxx and 7xxx high-strength Al alloys have not been joined via $SSFSW_1$. Potential topics include but are not limited to the following:

(1) Design criterion of the welding tool: Tool materials and design of the tool shape are the key factors influencing the service life of the welding tool and joint quality. For 2xxx and 7xxx high-strength Al alloys, high-quality welding tools with high strength, good ductility and special tool shape need to be designed to guarantee the service life of the welding tool and the joint integrity.
(2) Static and fatigue performances: The tensile performance has been extensively studied, whereas the other static performances, such as shear tests, impact tests and corrosion tests, need to be further investigated to evaluate the overall static performances. Fatigue performance, which affects the service life of the structural parts, is immature and should be emphasized to ensure stability.
(3) Non-weld-thinning $SSFSW_1$: During $SSFSW_1$, due to the plunge of the rotating shoulder and the small lower shoulder, weld thinning easily appears in the joint, which decreases joint strength. Hence, adjusting the structures of the welding tools and workpieces is extremely necessary.
(4) Commercial applications of $SSFSW_1$: With further research efforts and thorough understanding of the FSW process, an increasing number of applications have been realized for conventional FSW in the fabrication of Al alloys with high quality in aerospace and transportation fields. Although many challenges and difficulties still exist, $SSFSW_1$ provides very attractive possibilities for commercial success in some special parts, such as hollow and enclosed structures.

3.3. Penetrating friction stir welding

To improve surface finishing and eliminate the kissing bond in the root of the weld, Liu et al. [124] proposed penetrating friction stir welding (PFSW), which used stationary-shoulder support and a tilting pin. This method can guarantee a sufficient forging force, which improved joint formation and mechanical properties by increasing the back supported force.

3.3.1. Principle

Fig. 30 shows a schematic of the PFSW process, which consists of a slide, a pedestal, a stationary shoulder and a mounting platform including two separate segments. The slide realizes relative motion between the welding workpieces and the stationary shoulder. The plasticized materials under the rotating shoulder are supported by the stationary shoulder. To guarantee the complete penetration of the rotating pin, a blind hole is made in the centre of the stationary shoulder. The two separate parts of the mounting platform are placed beside the slide with the purpose of fixing the sheets. Before the PFSW process, the slide and the mounting platform need to be fastened to the workbench. The relative positions of these components are shown in Fig. 30a. The tilt angle of the rotating tool is kept constant, as illustrated in Fig. 30b. Under a pseudo-steady state, the cross-sectional view of softened materials surrounding the rotating pin tool is depicted in Fig. 30c [124].

3.3.2. Joint formation

Fig. 31 depicts the upper and lower surface appearances of a typical PFSW joint, in which no grooves or other visible defects are observed. The upper surface of the PFSW joint is similar to that in conventional FSW, and the width is equal to the diameter of the rotating shoulder. The lower surface presents good surface finishing due to the relative motion between the welding workpieces and

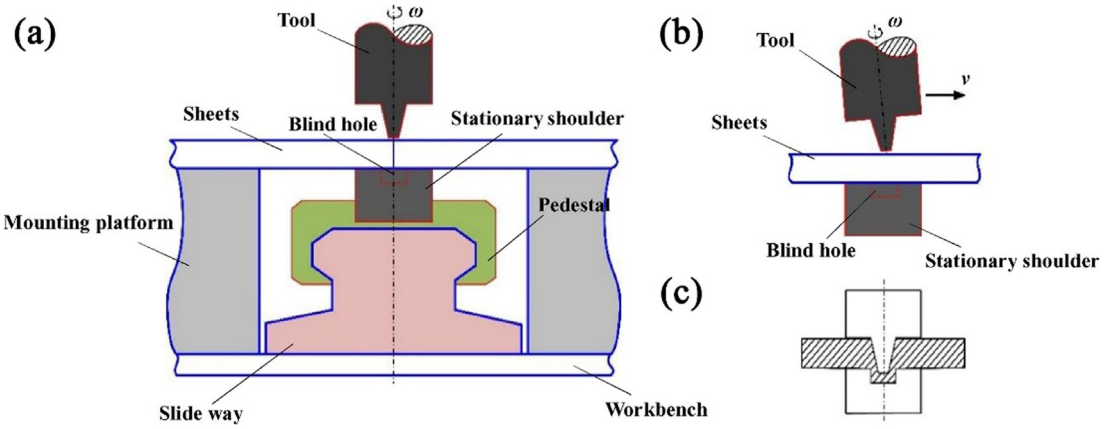


Fig. 30. Schematics of the PFSW process: (a) equipment and relative positions, (b) lateral view parallel to the welding direction and (c) local cross-sectional view [124].

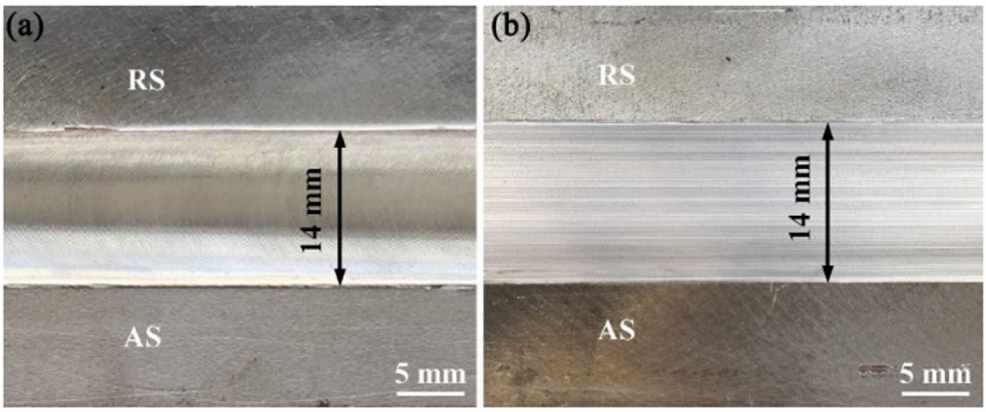


Fig. 31. Surface appearances of a typical PFSW joint: (a) upper and (b) lower surfaces [124].

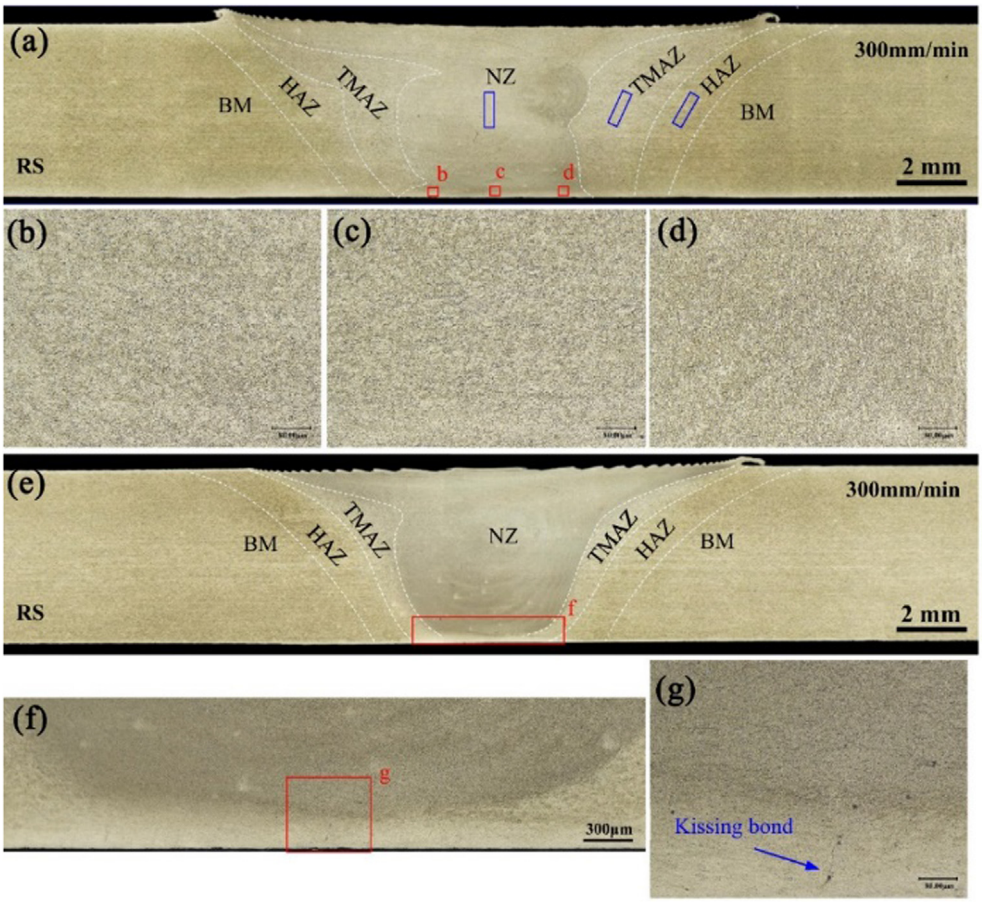


Fig. 32. Microstructures of 2219-T6 Al alloys in (a–d) a PFSW joint and (e–g) a conventional FSW joint [125].

the stationary shoulder, which indicates that the plasticized materials in the NZ are successfully supported by the stationary shoulder.

The macrostructure in the cross-section of the PFSW joint differs from that in conventional FSW joint, presenting an hourglass shape that is obviously asymmetric along the thickness direction, as shown in Fig. 32. The upper and lower materials in the NZ are subjected to different deformation and heat exposure during the PFSW process, resulting in the formation of the asymmetric hourglass shape. Furthermore, the NZ is divided into the SAZ, PAZ and stationary shoulder affected zone (SSAZ). The SSAZ is a typical feature of a PFSW joint. Moreover, no kissing bond defect is detected in the root, which indicates that the continuous oxide film in a conventional FSW joint can be successfully destroyed when the welding workpieces are completely penetrated by the rotating pin during the PFSW process.

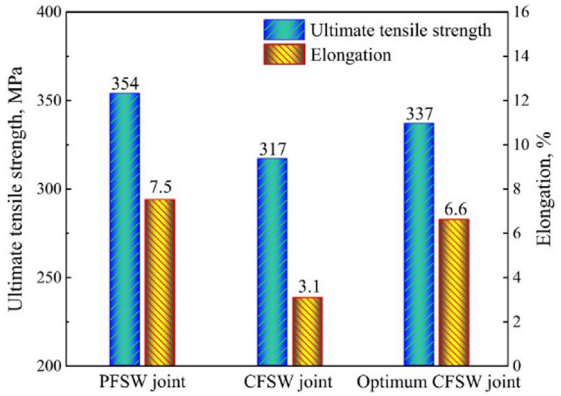


Fig. 33. Comparison of mechanical properties between PFSW and conventional FSW joints of 5-mm-thick 2219-T6 Al alloy plates [125].

3.3.3. Mechanical properties

Fig. 33 illustrates the mechanical properties of the PFSW joints. The tensile strength and elongation of the PFSW joint reached 354 MPa and 7.5%, respectively, which were approximately 79.2% and 58.6% of those in the BM (447 MPa and 12.8%) [125]. By comparison, the tensile strength and elongation of the conventional FSW joint at the same welding speed of 300 mm/min were 317 MPa and 3.1%, respectively, which were lower than those of the PFSW joint. It is concluded that the PFSW effectively realizes back support from the stationary shoulder and then eliminates the kissing bond, improving mechanical properties.

3.3.4. Prospects

PFSW has been used to successfully join 2219-T6 Al alloys, wherein back support was realized and a sound joint with a smooth surface was obtained. This method can reduce the softening degree and eliminate weld thinning of the joint, thereby improving mechanical properties. PFSW has the potential to join fuel tanks in rockets. The structural complexity of the welding tool restricts its broader adoption, including applications in hollow or enclosed structures with narrow spaces.

4. Non-weld-thinning friction stir welding

Regardless of conventional FSW [65] or its derived welding technologies [126,127], weld thinning always forms at the joints and easily results in the strength loss. This is because that a rotating shoulder plunges into the welding workpieces to a certain thickness ($\geq$0.05 mm, which is determined by the thickness of the workpieces) to produce intense frictional heat and result in the overflow of the plasticized materials. The plunge of the rotating shoulder cannot be neglected, and weld thinning cannot be avoided, as shown in Fig. 34. With wide applications of conventional FSW in manufacturing fields, such as aerospace, railway and automobile industries, the negative problems caused by weld thinning have been progressively visualized [128]. First, the formation of weld thinning always produces flash defects and deteriorates the surface finishing and integrity. Second, weld thinning is prone to decrease the area of effective load bearing [129]. Kumar et al. [130] stated that when the plunge of the rotating shoulder increased to a certain extent, weld thinning markedly increased, which easily caused joint fracture in the weak region of the weld, drastically deteriorating the mechanical properties. Third, the acute edge induced by weld thinning usually forms between the BM and the NZ. Although mechanical properties of the joint with weld thinning can satisfy the service requirements, the acute edge still becomes a potential safety hazard during service. Under the action of load, the crack source is prone to form at the acute edge, which further reduces the anti-fatigue properties and service life [131,132]. Especially in some fields that need a long service period, the acute edge of the

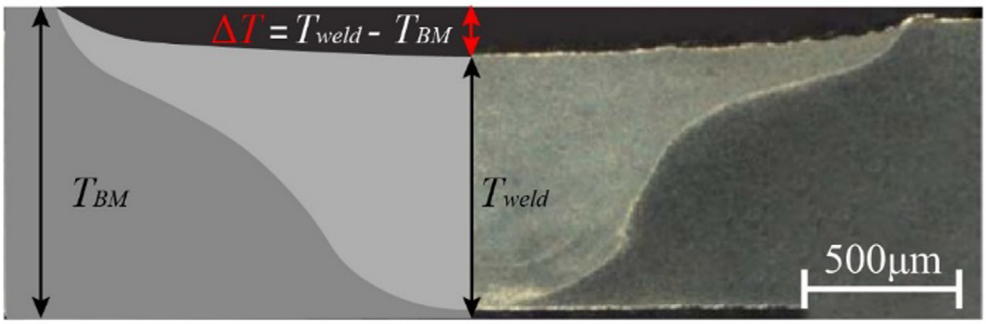


Fig. 34. Weld thinning of a typical FSW joint (the value of weld thinning (ΔT) is defined by the difference between the weld thickness (T_{weld}) and the BM thickness (T_{BM})).

workpieces must be avoided. Even if the acute edge can be burnished and transformed into a smooth transition, the potential safety hazard cannot be eliminated completely. Last, accurate welding and conformal welding concepts are widely mentioned and focused, which mean strict requirements for the appearance dimension of the structural parts without weld thinning. Hence, weld thinning is a substantial obstacle to achieving high-quality FSW joints.

Especially in military manufacturing fields, mechanical properties of the joints are not the sole criterion to evaluate the FSW joint quality. With the increasing requirements of joint quality, the FSW joint not only needs excellent mechanical properties but also requires superior surface integrity and outstanding service reliability. How to reduce or eliminate weld thinning and then achieve high-quality FSW joints is a key to expand FSW technological applications. To reduce or eliminate the weld thinning of the FSW joint and improve joint quality, researchers have performed extensive investigations from the viewpoints of the design in both of welding tool and workpiece structures as well as the assisted processes. The used welding technologies to reduce or eliminate weld thinning mainly consist of three categories. The first technology category seeks to prevent the overflow of plasticized materials, which comprises stationary shoulder FSW ($SSFSW_2$) or non-rotating shoulder assisted FSW (NRSA-FSW). The second technology category seeks to avoid the loss of plasticized materials, which is characterized by MPD-FSW or zero-plunge-depth FSW. The last technology category seeks to increase the additional materials to compensate for the loss of plasticized materials under the premise of adequate frictional heat and material flow, which comprises additive FSW (surface compensation FSW, T-plate assisted FSW and *in-situ* additive FSW) and reductive FSW.

4.1. Stationary shoulder friction stir welding

According to the previously presented information, weld thinning is attributed to the plunge of the rotating shoulder that provides a sufficient forging force on the materials of the NZ. The frictional heat generated by the rotating shoulder always results in weld overheating, which deteriorates mechanical performance. Moreover, the generated frictional heat is useless for materials with low thermal conductivity, such as Ti alloys [21,133] and polymers [134–136]. $SSFSW_2$ or NRSA-FSW, a solid-state joining technology derived from conventional FSW by TWI, has been extensively studied in the scientific community and applied in industry, which has achieved satisfactory results for butt-, lap- and T-type joints [137]. $SSFSW_2$ is deemed to be the next generation FSW technology by the European aeronautic defence and space company (EADS) [138]. Compared with conventional FSW, $SSFSW_2$ has many advantages, which are detailed hereafter:

1) A smooth joint surface is beneficial to reducing surface machining after FSW and improving fatigue properties.
2) Low heat input decreases the width of the HAZ, and the temperature distribution along the thickness direction is uniform.
3) Stationary shoulder can transform the tensile stress in conventional joints into compressive stress, reducing the residual stress and welding distortion.
4) Quasi-non-weld-thinning increases the effective area of load bearing.
5) $SSFSW_2$ has the advantage of joining materials with low thermal conductivity and welding T joints or corner joints.
6) $SSFSW_2$ can realize the filling of materials and provide a technical method for exploring additive manufacturing FSW.
7) $SSFSW_2$ reduces the torque and advancing resistance, which is helpful to the development of robotic FSW.

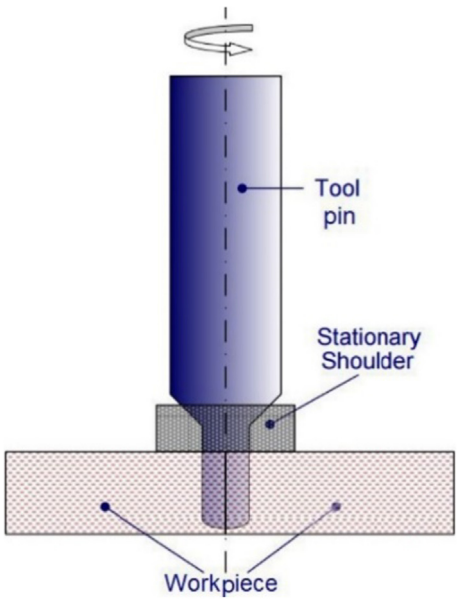


Fig. 35. Illustration of $SSFSW_2$ [137].

In this chapter, welding tools, process parameters, material compatibilities, technical development, microstructural evolution and mechanical properties of $SSFSW_2$ joints are comprehensively reviewed. Additionally, the advantages, limitations and industrial applications of $SSFSW_2$ are neutrally discussed, laying the theoretical foundation for expanding the industrial manufacturing fields of $SSFSW_2$.

4.1.1. Principle

$SSFSW_2$ is a novel solid-state welding method, whose welding tool consists of a stationary shoulder and a rotating pin, as shown in Fig. 35 [137]. During $SSFSW_2$, the rotating pin plunges into the workpieces, while the stationary shoulder tightly contacts the top surface of the workpieces without a plunge depth. The welding workpieces can be heated and stirred by the thermo-mechanical effects induced by the rotating pin alone, which is different from that of conventional FSW. Under the enclosed chamber, which is composed of the stationary shoulder, rotating pin, surrounding hard materials and backing plate, the overflow of the plasticized materials is prevented, thereby achieving a sound non-weld-thinning joint.

The heat generation mechanism during $SSFSW_2$ is very different from that during conventional FSW, which further influences joint surface integrity and microstructural characteristics. During conventional FSW, approximately 70–80% of the main heat generation is produced by the friction between the rotating shoulder and the welding workpieces, whereas 20–30% of the heat generation is from the frictional heat induced by the rotating pin and the plastic deformation heat. Due to the relatively high heat input on the surface of the workpieces, the materials are easier to be softened and plasticized, and then overflow from the weld, causing weld thinning. For $SSFSW_2$, the primary heat input is produced by the rotating pin with either no or low heat generation provided by the rotating shoulder. $SSFSW_2$ effectively reduces the softening degree of the materials on the surface of the workpieces and is beneficial to reducing or eliminating weld thinning. Moreover, for FSW of thick plates, when the heat generation and material flow induced by the rotating pin are optimized to guarantee structural integrity during conventional FSW, surface overheating forms and deteriorates the joint performance. $SSFSW_2$ can produce a uniform temperature distribution along the thickness direction and attribute to homogeneous microstructures, thereby improving mechanical properties. During conventional FSW, the translation of the rotating shoulder generally produces some flashes and regular semi-circular shoulder marks on the surface, as shown in Fig. 36a. The smoother surface results from the sliding effect of a stationary shoulder across the weld surface (Fig. 36b). The roughness in the $SSFSW_2$ joint is markedly reduced by over an order of magnitude compared with that in the conventional joint (Fig. 36c), whereas the weld thinning in the $SSFSW_2$ joint was also substantially reduced from ~1 mm to less than 0.2 mm (Fig. 36d) [139].

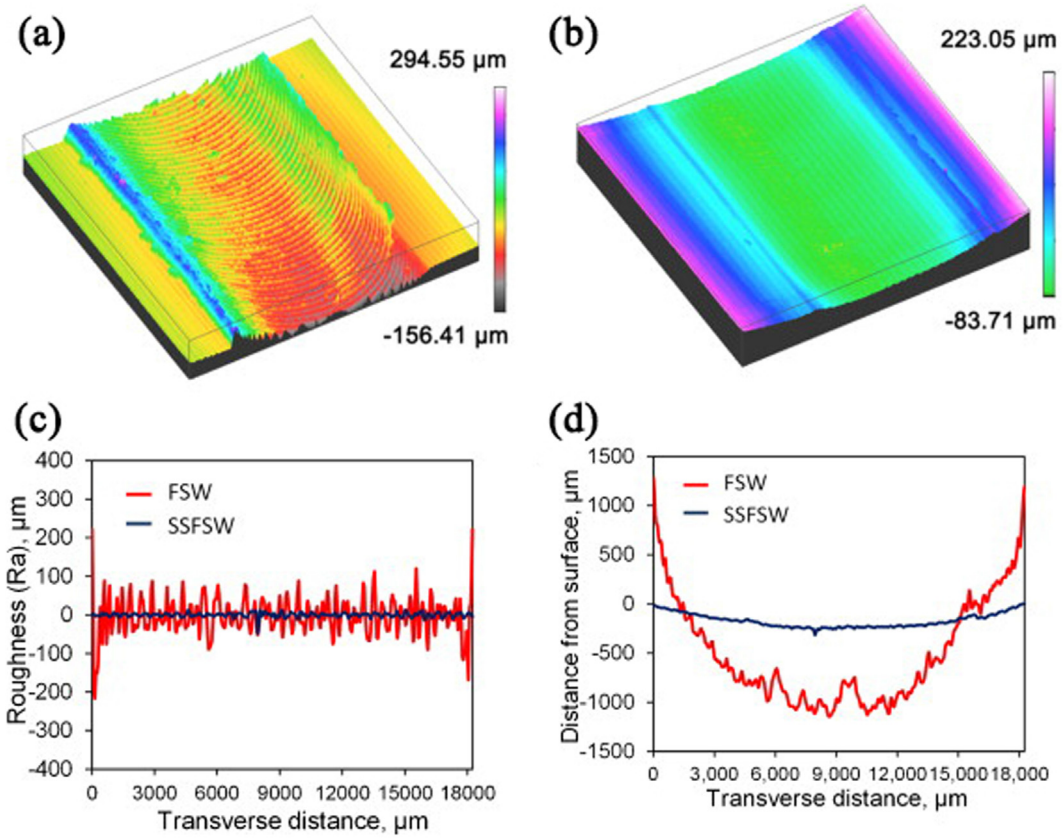


Fig. 36. Comparison of the surface quality with both processes: surface displacement maps of (a) conventional FSW and (b) $SSFSW_2$; (c) surface roughness (Ra) and (d) local displacement relative to the original sheet surface [139].

4.1.2. Welding tools

During $SSFSW_2$, the rotating pin is the key factor of frictional heat and material transfer, which is primarily responsible for achieving high-quality joints. First, the rotating pin squeezes the plasticized materials and is subjected to bending force and torque, which requires the tool materials to have high strength, stability, ductility and anti-fatigue properties at high temperature. Second, the wear resistance is another important factor to guarantee welding stability due to the severe friction between the rotating pin and the workpieces. Third, to improve the material flow around the surface of the rotating pin, the tool materials demand good machinability so that the surface morphologies of the rotating pin can be carved, such as threads and facets. Last, an important aspect is the gap between the stationary shoulder and the rotating pin. During $SSFSW_2$, the viscoplastic materials under the forging effects are easily squeezed into the gap, which result in weld thinning induced by the loss of plasticized materials or even the fracture of the rotating pin for long-term work conditions. This problem is the main difficulty facing $SSFSW_2$, which should be solved urgently in the industrial manufacturing fields.

TWI first designed an $SSFSW_2$ system for Ti alloys, as shown in Fig. 37, which mainly consisted of a stationary shoulder (10), a rotating pin (11), an inert gas protection system (13–15) and water cooling jackets (4) [140]. Water cooling jackets can protect the safety of welding equipment due to high heat generation induced by the high strength of Ti alloys, whereas inert gas protection can avoid oxides and nitrides. These tools significantly increase the complexity of the $SSFSW_2$ system. To reduce or eliminate tool wear and increase the homogeneity of microstructures, a tapered rotating pin and a stationary shoulder are made of W-Re alloys and WC materials, respectively. The gap between the stationary shoulder and the rotating pin has not been reported. Russell et al. [141] also proposed additive manufacturing of Ti parts by multiple $SSFSW_2$ processes using both 1D and 2D welding paths, as displayed in Fig. 38. Brassington et al. [142] also stated that the new development of $SSFSW_2$ tools was considered as a step change in the process evolution, in which the low heat input and smooth surface profile could have the potential to join Ti propellant tanks. EADS developed a robotic $SSFSW_2$ approach for Al alloys called Delta-N [138]. The welding system was significantly simplified without the gas protection or cooling device used for Al alloy butt joints, which only contained a stationary shoulder and a rotating tool, as shown in Fig. 39. The robotic $SSFSW_2$ approach successfully manufactured a 3D space structure.

Liu et al. [6] and Ji et al. [144] used $SSFSW_2$ to join AA2219-T8 and AA6005A-T6, respectively, wherein the rotating tools consisted of a small rotating shoulder and a rotating pin, as shown in Fig. 40. Here, the stationary shoulder only assisted the surface formation of joints. Due to the small rotating shoulder, this method can only be used for butt or lap welds, and it is difficult to join corner or complex structural parts.

The heat generation during FSW depends on the strength and hardness of the workpieces. The higher the strength and hardness, the higher the heat generation, the better the material flow. Due to the higher strength and hardness of metals, such as Ti alloys and Al alloys, relatively higher heat generation can be produced. Thermoplastic polymers or polymer matrix composites have relatively low strength and hardness, making it difficult to generate sufficient frictional heat and material flow. Moreover, the fluidity of the thermoplastic polymer is good, which easily overflows from the NZ, causing groove defects or weld thinning [146]. A modified $SSFSW_2$ called stationary shoe FSW is proposed, whose stationary tool is rectangular rather than circular to guarantee joint integrity, as shown in Fig. 41. A closed-loop thermo-controller was responsible for supplying additional heating to the workpieces and slowing the cooling rates of the materials, which has realized the high-quality joining of polymers, such as polypropylene (PP) [147], acrylonitrile butadiene styrene (ABS) [110] and high-density polyethylene (HDPE) [135].

In addition to butt joints, $SSFSW_2$ also has the feasibility and potential to fabricate T or corner joints [149–152], which avoids the

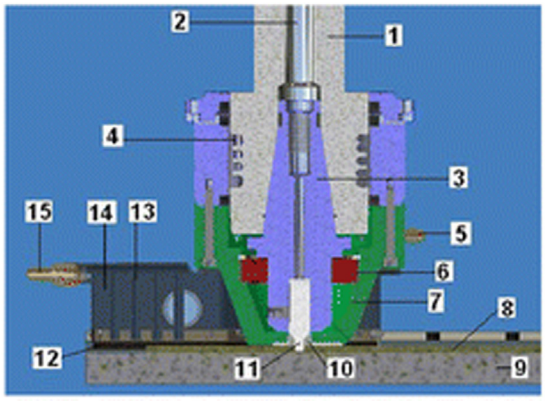


Fig. 37. A cross-sectional view of the $SSFSW_2$ assembly [143].

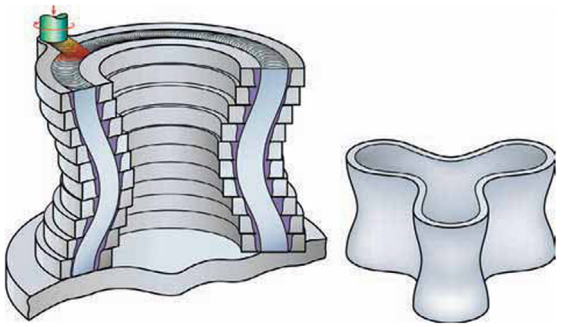


Fig. 38. Additive manufacturing by $SSFSW_2$ [141].

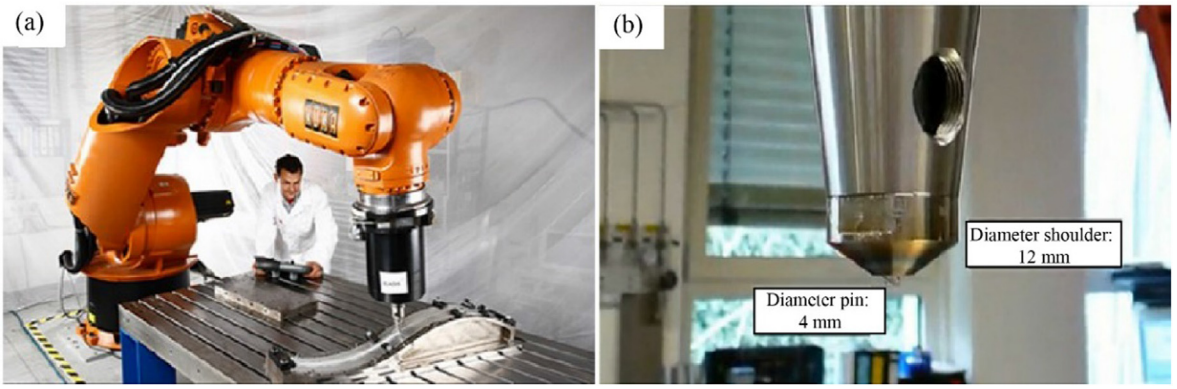


Fig. 39. Robotic $SSFSW_2$ by EADS: (a) welding equipment and (b) stationary shoulder [138].

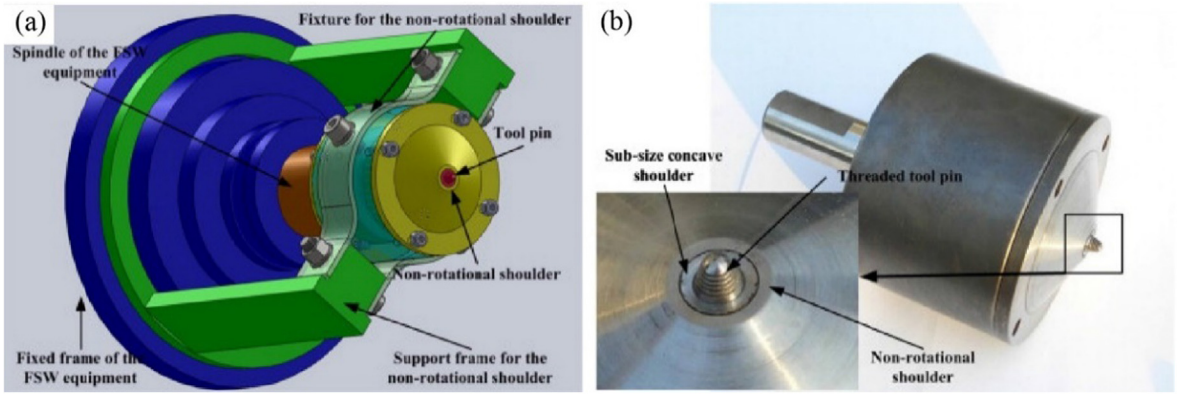


Fig. 40. Design of the $SSFSW_2$ tool: (a) model and (b) photograph [145].

problems of severe weld thinning and lap defects, such as cold lap or kissing bond defects during conventional FSW of lap structures in T joints [153–155]. Schematic diagrams of the $SSFSW_2$ equipment for the T joints are shown in Figs. 42 and 43, containing non-additive and additive processes. The stationary shoulder is machined into a corner structure similar to the angle of the corner joints, which can ensure the plasticized materials in the enclosed chamber and then avoid the overflow of materials. The weld thinning in the skin and the lap defects between the skin and stringer are completely eliminated, overcoming the limitations of conventional FSW in the T-type or corner joints. Moreover, the filling materials can be added into the transition between the skin and the stringer, which is called additive $SSFSW_2$; this approach reduces the stress concentrations at the corner and then effectively improves the static and fatigue properties. Both additive and non-additive $SSFSW_2$ joints exhibit satisfactory joint coefficients.

4.1.3. Material compatibilities

Table 5 highlights the recent progress of $SSFSW_2$ in chronological order with a summary of research findings, in which one can note that the publication rate in this area has steadily increased since 2004 [150]. $SSFSW_2$, which is characterized by several factors, including uniform temperature distribution, non-weld-thinning, and smooth surface, has been successfully used to join Ti alloys,

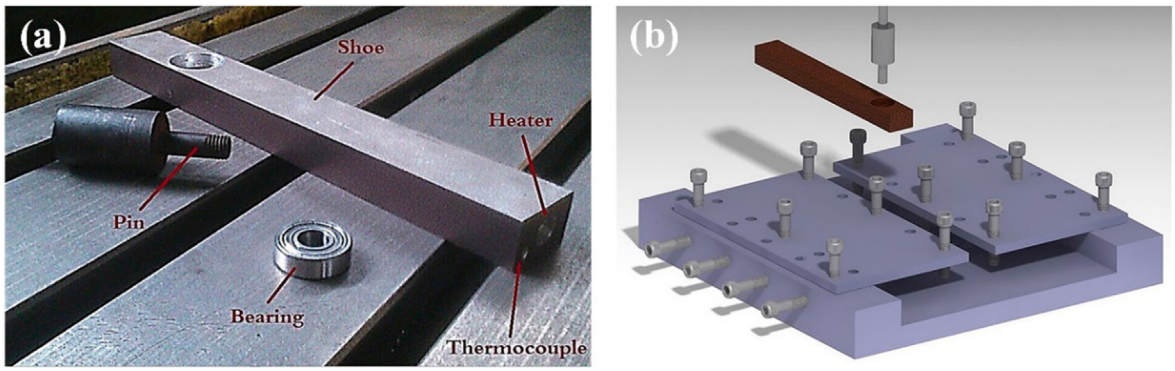


Fig. 41. Heat-assisted SSFSW$_2$: (a) stationary shoe and (b) schematic of the designed fixture for heat-assisted SSFSW$_2$ [148].

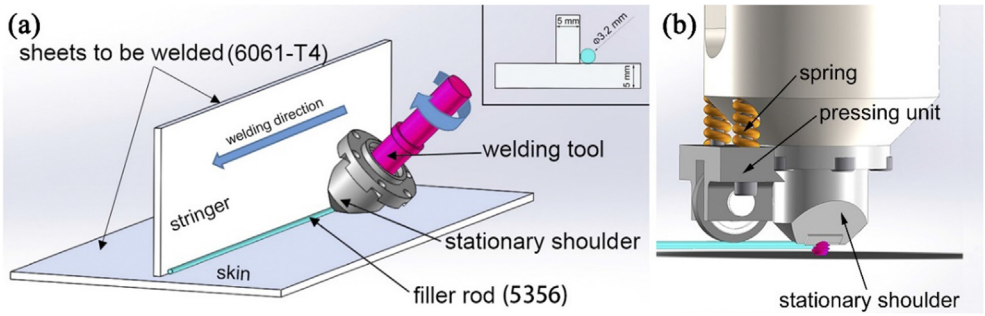


Fig. 42. Schematics: (a) welding process and (b) tool package for an additive T joint [149].

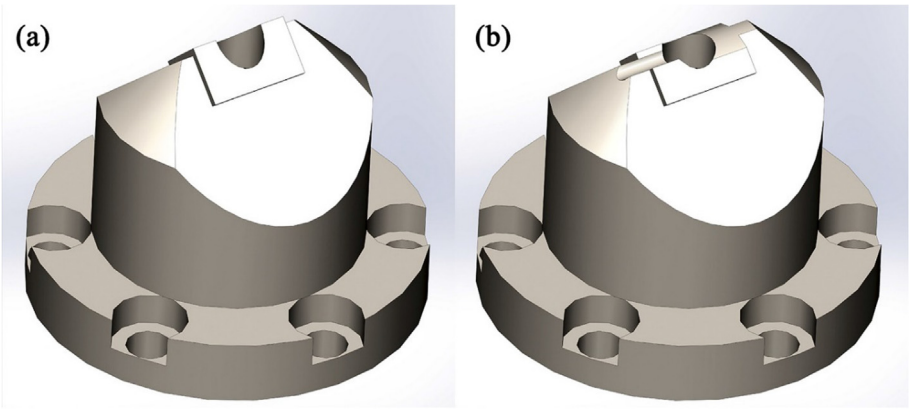


Fig. 43. Illustrations of stationary shoulders: (a) non-additive and (b) additive SSFSW$_2$ [149].

steels [151], coppers, Al alloys (especially high-strength Al alloys (2xxx [6] and 7xxx [156]) that cannot be welded by conventional fusion welding) and thermoplastic polymers [110]. Moreover, the other advantages induced by the stationary shoulder are remarkable and have also been used to join dissimilar materials in butt and lap joints, such as Al/Mg alloys [157,158] and Al/polymers [159]. Aiming at materials with low thermal conductivity, SSFSW$_2$ produces a more uniform temperature distribution along the thickness direction and is firstly developed to join Ti alloys [143]. Al alloys, including the 2xxx, 6xxx and 7xxx series, have been most commonly used and extensively studied from the viewpoints of welding parameters and design of welding tools [6,144,160]. This is hardly surprising, considering that these materials are widely used in the industrial sectors because of their excellent properties [161]. Additionally, with the increasing demands of light weight, thermoplastic polymers and polymer matrix composites, SSFSW$_2$ has also attracted extensive attention for these materials. Due to the good flowability, the weld thinning phenomenon easily appears due to the overflow of the plasticized materials during conventional FSW [146]. Moreover, the extremely low thermal conductivity of the polymer (compared with that of Al alloys) always results in a non-uniform temperature distribution and overheating of materials at the top surface of the joint. Strand [162] firstly employed stationary shoe FSW, named SSFSW$_2$, to join PP and achieved remarkable results. Subsequently, Mostafapour et al. [148] proposed a stationary shoe with a heating system to preheat the materials in front of

Table 5
$SSFSW_2$ in chronological order with focus/findings.

Authors (Ref.)	Year	Materials	Focus/findings
Russell et al. [143]	2007	Ti-6Al-4V	$SSFSW_2$ was first developed by TWI primarily to improve FSW of Ti-based alloys.
Russell et al. [141]	2008	Ti-6Al-4V	Additive manufacturing of Ti parts by $SSFSW_2$ processes performed using both 1D and 2D welding.
Ahmed et al. [171]	2011	AA6082-T6	Plastic deformation in the through thickness direction was dominated by the pin in $SSFSW_2$.
Li et al. [145]	2013	AA2219-T6	$SSFSW_2$ prevented the plasticized materials from escaping from the NZ and eliminated flash defects and weld thinning, achieving a tensile strength of 307 MPa.
Liu et al. [6]	2013	AA2219-T6	Microstructure and weld formation were dominated by the rotating pin and small concave shoulder.
Li et al. [172]	2014	AA6061-T6	AA6061-T6 $SSFSW_2$ joint had narrower TMAZ and HAZ, the microstructures were more symmetrical and homogeneous, and the maximum tensile strength was 77.3% of that of the BM.
Ji et al. [144]	2014	AA6005-T6	The width of SAZ was small. The tensile strength and elongation of the joint reached 82% and 65% of those of the BM.
Wu et al. [139]	2015	AA7050-T7651	The cold surface temperature dramatically decreased the normal workpiece thickness and can lead to “speed cracking” similar to that found in extrusion under hotter welding conditions.
Ji et al. [163]	2016	AA6061-T6/AZ31B	Excellent material mixing happened and IMCs were reduced due to heat sink from stationary shoulder.
Sun et al. [173]	2017	AA7010-T7651	A considerably smaller thermal field was developed with $SSFSW_2$, which reduced the size of the region of inhomogeneous compression created by the local temperature rise ahead of the tool.
Sun et al. [174]	2018	AA7050	The longitudinal residual stress distributions from all three techniques showed good agreement within the uncertainty limits. A high tensile residual stress field (~170 MPa) was found in the NZ.
Barbini et al. [175]	2018	AA2024/AA7050	$SSFSW_2$ decreased both the welding area and the diffusion at the interface of the two alloys.
Meng et al. [165]	2018	AA6061-T6/AZ31B	Stationary shoulder coupled with ultrasonic improved the surface formation of Al/Mg joint and broke the IMCs into pieces, thereby increasing mechanical properties.
Regensburg et al. [176]	2018	AW1050 H14/CW024A R240	$SSFSW_2$ was applied to produce 2-mm-thick EN AW1050/CW024A lap joints with minimized intermixing at the interface, lap defects and significant IMCs.
Huang et al. [159]	2018	SCF/PEEK and AA2060-T8	Stationary shoulder enhanced the surface finishing, and the maximum tensile shear strength of 33 MPa was higher than that achieved by the-state-of-the-art technology.
Strand [162]	2004	PP	Stationary shoe FSW was first proposed to join thermoplastic PP.
Mostafapour et al. [177]	2012	HDPE	HDPE could be welded at a high shoulder temperature and rotational velocity and a low welding speed. Tool coating improved mechanical properties and surface qualities.
Kiss et al. [178]	2012	PETG	A stationary shoe without a heating system was used to join amorphous PETG, which was difficult to be welded using conventional tools. The rotating pin could break and randomly distribute spherulite.
Bagheri et al. [179]	2013	ABS	A high rotational velocity and shoe temperature and a low welding speed improved welding quality.
Rahbarpour et al. [180]	2014	Wood/plastic	FSW of wood/polymer composites by a stationary shoe with a heating system was performed to eliminate voids and poor mixing. The maximum tensile strength of the joint was 92.95% of that of the BM.
Mendes et al. [181]	2014	ABS	A high-quality joint was obtained for a tool temperature of 115 °C, an axial force greater than 1.5 kN, a rotational velocity higher than 1250 rpm and a low welding speed of 50– 100 mm/min.
Eslami et al. [136]	2015	PP/PC	One of the main challenges was to prevent material overflow inside the shoulder, which caused shoulder failure, especially in long joints. A Teflon polymeric stationary shoe was the best option.
Kiss and Czigány[182]	2015	Glass fibre-reinforced PP	$SSFSW_2$ realized the homogenization and interlocking of fibres. A screwed pin with eight teeth reduced the length of fibres, thereby decreasing mechanical properties.
Mostafapour et al. [148]	2016	Nylon 6	Nylon 6 was joined via heat-assisted $SSFSW_2$ with an external heat source. A high-quality joint with over 98% of the base strength was obtained.
Eslami et al. [183]	2018	HMHDPE	The vertical positioning of the tool was responsible for the axial force, thereby providing both the forging pressure and frictional heat.

the rotating tool, further improving the surface quality and mechanical properties of the joints. Huang et al. [159] also reported that the stationary shoulder improved the surface finishing of short carbon fibre-reinforced polyether ether ketone (SCF/PEEK)/AA2060-T8 hybrid joint and that the maximum tensile shear strength of 33 MPa was higher than that produced by the state-of-the-art techniques. Additionally, $SSFSW_2$ has been used to create high-quality dissimilar joints of Al/Mg alloys. Compared with conventional FSW, $SSFSW_2$ has a lower peak temperature and simpler material flow driven by the rotating pin, which can effectively reduce the IMCs and the cold lap defect. Ji et al. [80,163] first noted that $SSFSW_2$ could not only reduce the peak temperature and pin adhesion but also improve the joint formation and material mixing, thereby enhancing mechanical properties. They also combined $SSFSW_2$ with ultrasonication to join dissimilar Al/Mg alloys and eliminated pin adhesion, producing a maximum tensile strength of 152 MPa [158,164,165]. During friction stir lap welding (FSLW), the material flow behaviour is dominated by two modes: rotating pin affecting the hook and rotating shoulder controlling the cold lap [166,167]. The application of $SSFSW_2$ in FSLW of similar or dissimilar materials significantly reduces lap defects and improves mechanical properties [168–170].

4.1.4. Microstructural characteristics

Because the shoulder is static, the material flow and heat generation are significantly reduced, thereby decreasing the

inhomogeneity degree of microstructures in the through-thickness direction. The primary frictional heat is generated around the rotating pin, further affecting the microstructural evolution, which presents significant differences relative to conventional FSW. The NZ in the conventional FSW joint presents an irregular shape, and the TMAZ in the conventional FSW joint exhibits asymmetry. These findings are attributed to the differences in shear stress and material flow on the AS and RS [66]. The NZ in the $SSFSW_2$ joint is similar to the shape of the rotating pin because the shoulder is static, and the width of the SAZ in this joint is far lower than that in a conventional FSW joint. In fact, the microstructural evolution is closely connected with the welding thermal cycle that depends on the thermal and mechanical properties of the welding workpieces. In this chapter, three kinds of typical materials are emphasized: Ti alloys with low thermal conductivity and high strength, Al alloys with high thermal conductivity and medium strength, and thermoplastic polymers with low thermal conductivity and low strength.

4.1.4.1. Ti alloys. Ti alloys, due to their high specific strength and good corrosion resistance, have been the first choice for the next generation of jet engines in the aerospace industry. FSW of Ti alloys is the primary focus of researchers. Due to low thermal conductivity, a large temperature gradient along the thickness direction easily results in inhomogeneous microstructures or tearing defects in the NZ, reducing mechanical properties [137,184]. A back-heat-assisted FSW method was proposed to improve the uniform temperature distribution and eliminate tearing defects [133,184], which always required heating equipment. $SSFSW_2$ arises at a historic moment to improve the homogeneous distribution of microstructures and phases. Based on the characteristics of Ti alloys, the FSW joint is mainly divided into three distinct zones: NZ, TMAZ and HAZ, as shown in Fig. 44. Some researchers have stated that no TMAZ occurred in the $SSFSW_2$ joints of Ti alloys [185], whereas scholars claimed that a narrow TMAZ existed when observing an obvious microstructural evolution due to the limited plastic deformation and heat input [186,187]. The microstructural evolution in the TMAZ and HAZ is primarily affected by the microstructures of the BM. The microstructure in the NZ is a result of processing conditions, tool geometry, cooling rates and material compositions.

The microstructural evolution of Ti alloys involves transformation, nucleation, and growth of the α and β phases in the BM. Ti-6Al-4V, a kind of Ti alloy, is the most extensively studied Ti alloy due to its extensive industrial applications. Fig. 45 shows a schematic of the microstructural evolution of Ti-6Al-4V during FSW, which is divided into the welding stage and cooling stage. When the peak temperature in the NZ is above the β-transus temperature, the BM is destroyed and DRX occurs in the welding stage. Then, fine, equiaxed and transformed β phases are achieved at the end of the welding stage. In the cooling stage, the materials in both the upper and lower surfaces of the NZ suffer from fast cooling, and small grain boundary α phases are formed. At the end, smaller lamellar $\alpha + \beta$ phases within the prior β grains are obtained. Due to low thermal conductivity, the materials in the middle region of NZ undergo longer high-temperature exposure times. The slower cooling process is attributed to the larger lamellar $\alpha + \beta$ phases within the prior β grains in the end. In the HAZ, the temperature is below the β-transus temperature. However, the heat cycle still causes grain coarsening, leading to an $\alpha \rightarrow \beta$ transus. In the cooling stage, $\beta \rightarrow \alpha + \beta$ occurs; hence, bimodal microstructures, which is characterized by primary coarser α grains and lamellar $\alpha + \beta$ phases within prior β grains, can be observed. In the welding stage, after being broken by the rotating tool, a higher temperature but below the β-transus can be obtained at the NZ top. Hence, some $\alpha \rightarrow \beta$ occurs. Upon cooling, $\beta \rightarrow$ lamellar $\alpha + \beta$ occurs; hence, small lamellar structures can be obtained. In the middle and bottom regions of NZ, the temperatures are far below the β-transus temperature. The stirring action plays a more important role, and only fine and equiaxed grains can be observed. Reducing the temperature gradient can be beneficial to achieving uniformly distributed microstructures by $SSFSW_2$.

4.1.4.2. Al alloys. Al alloys are classified into precipitation-strengthened alloys and solid-solution-strengthened alloys. Precipitation-strengthened Al alloys, such as 2xxx, 6xxx and 7xxx Al alloys, are the most investigated materials by $SSFSW_2$ due to their increasing demands and extensive applications in railway and aerospace fields [188]. It is known that the peak temperature during FSW can approach ~0.8 T_m or even 0.95 T_m, which is higher than the solution temperature of many precipitation-strengthened Al alloys [189]. The welding heat cycle and mechanical stirring influence the evolution of the grain size, dislocations and especially precipitates, which further influence the subsequent mechanical properties. The thermo-mechanical behaviours simultaneously affect the joint formation. As shown in Fig. 46, the SAZ is significantly reduced or even eliminated due to the stationary shoulder, and the widths of the TMAZ and HAZ are decreased due to the reduced heat input on the top surface of the joint compared with that in the conventional FSW joint. For the sound $SSFSW_2$ joint of the precipitation-strengthened Al alloys, the fracture location of the joints easily occurs at



Fig. 44. Macrostructure of a Ti-6Al-4V $SSFSW_2$ joint [137].

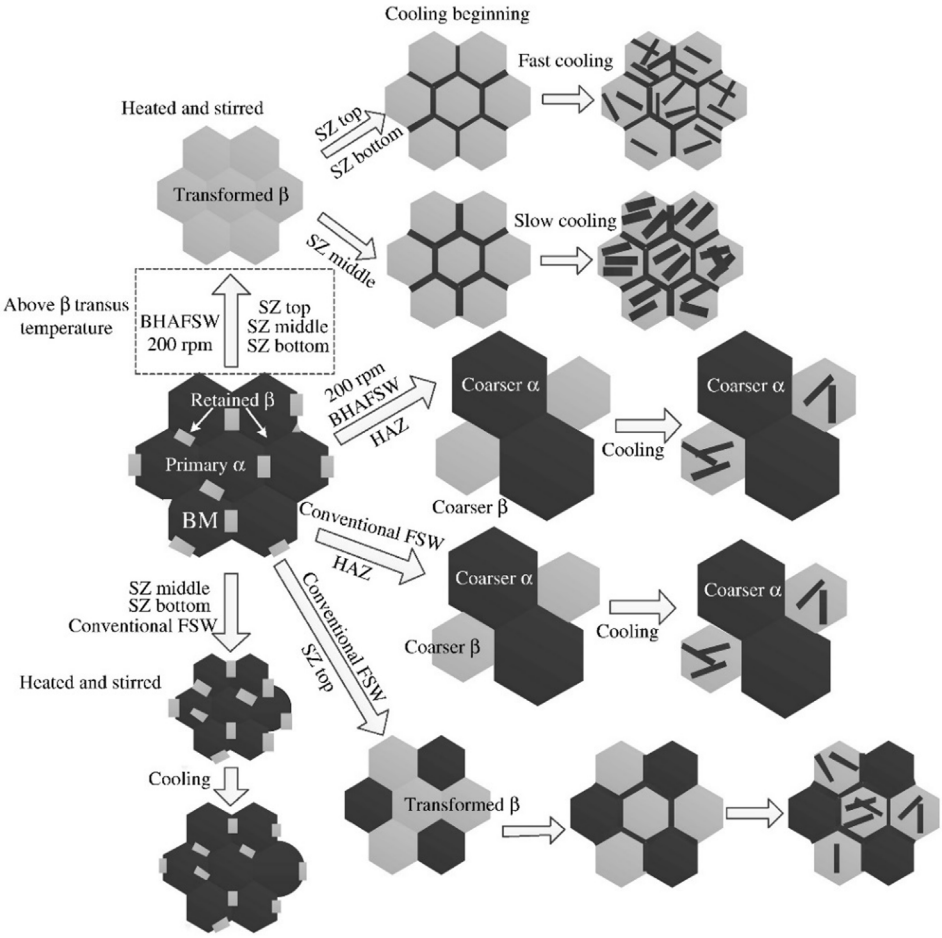


Fig. 45. Diagrammatic sketch of microstructural evolution during FSW of Ti-6Al-4V alloys [133].

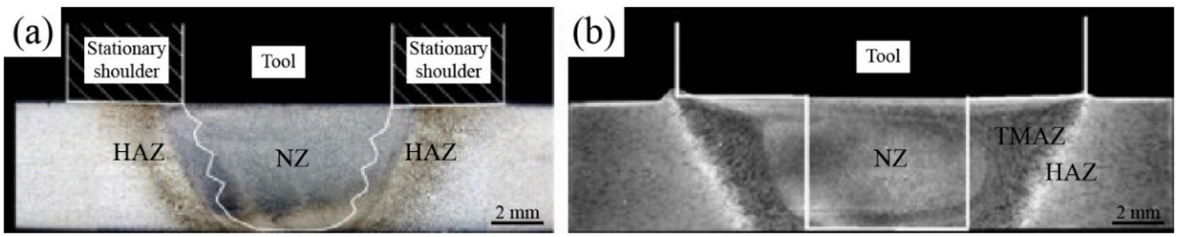


Fig. 46. Macrostructures: (a) $SSFSW_2$ and (b) conventional FSW joints [172].

the HAZ with the severest softening degree. Therefore, the microstructural evolution in the HAZ directly determines the global mechanical properties of the $SSFSW_2$ joints.

For the typical age-hardened 2xxx Al-Cu-(Mg) Al alloys, the evolution sequence of precipitates is as follows: SSS → GP(I) → GP (II) → metastable phase θ'' → metastable phase θ' → stable phase θ (Al_2Cu). In 6xxx Al-Mg-Si Al alloys, Mg and Si are the major alloying elements, contributing to precipitation strengthening. The precipitation sequence is as follows: SSS → clusters → initial β'' → (pre-β''/needle-shaped β'' precipitate) → (rod-shaped precipitates β'/lath-shaped β' precipitates/U1, U2) → (β-Mg_2Si/Si). In the 7xxx Al-Zn-Mg-(Cu) Al alloys, the precipitation sequence is as follows: SSS → metastable phase η'→ stable phase η [190–192]. The BM consists of a large number of uniformly distributed fine precipitates (approximately 5 nm in size) and some larger dispersoids. Li et al. [156] reported that the distribution and quantity of dispersoids in the HAZ are similar to those in the BM. However, the precipitates in the HAZ are larger than those in the BM. In the NZ, fine precipitates are absent, and the dispersoids are much larger than those in the BM. Liu et al. [6,125,145] examined the microstructural evolution of SSFSW of 2219-T6 Al alloys. The thermal cycle drives metastable phases (GP zones and θ'') to transform to θ' and θ phases and then inhibits the growth of recrystallized grains in the NZ. The microhardness is increased by the formation of θ' phases, but the coarsening of θ' phsases explicitly causes a reduction in the

microhardness of Al-Cu alloys. Sun et al. [193] also stated that the needle-like precipitates grew and transformed into short rod-like precipitates as a result of the welding thermal sycle in the HAZ, while the NZ was the only one that showed a large GP zone dissolution peak and a high β'' precipitation peak.

4.1.4.3. Thermoplastic polymers. Thermoplastic polymers were firstly joined via $SSFSW_2$ by Strand [162], whose cross-sectional macrostructure is shown in Fig. 47. The $SSFSW_2$ joint is separated into BM, NZ, TMAZ and bottom disturbance. Due to the extremely low thermal conductivity, no HAZ appears in the $SSFSW_2$ joints of polymers. The NZ is characterized by onion rings and a relatively narrow TMAZ. A typical defect occurs near the bottom disturbance due to insufficient stirring and low thermal conductivity and becomes the weakest region during the tensile test, which can be eliminated by double-pass FSW [194,195]. Kiss and Czigány [178] stated that stirring action of the rotating pin could break and randomly distribute spherulite. Additionally, for fibre-reinforced thermoplastic composites, the main difficulty is the lack of continuity between the fibres in the BM and NZ. Moreover, Kiss and Czigány [182] performed $SSFSW_1$ of glass fibre-reinforced composites and reported that this method could realize the homogenization and interlocking of the fibres, as indicated in Fig. 48. The fracture surface showed that fibres are extracted from the NZ, indicating interlocking with each other inside the NZ.

Gao et al. [197] performed differential scanning calorimetry (DSC) for different regions of the PE joint and analysed the crystallization behaviour induced by the uneven temperature distribution with the following formula:

$$W_c = \frac{\Delta H_m}{\Delta H_m^0} \times 100\% \tag{7}$$

where ΔH_m is the melting enthalpy of the sample and ΔH_m^0 is the melting enthalpy of perfectly crystalline PE, for which the value is 293 J/g. The crystalline contents of the BM, HAZ, TMAZ and NZ were 54.5%, 54.0%, 51.1% and 48.2%, respectively (Fig. 49). There is no obvious HAZ due to the low thermal conductivity. The crystallinity of the TMAZ and NZ was significantly reduced due to the low cooling rates.

4.1.5. Process development

During $SSFSW_2$, heat generation and material flow are mainly provided by the rotating pin, which are completely different from those in conventional FSW. The heat generation provided by the rotating pin during conventional FSW is only 20–30% of the total heat input. The optimum welding parameters during conventional FSW that can be beneficial to obtaining excellent joints may not be suitable for $SSFSW_2$ due to insufficient frictional heat and material flow resulting from the loss of frictional heat generated by the rotating shoulder. There are obvious differences in welding parameters between conventional FSW and $SSFSW_2$. Moreover, $SSFSW_2$ can also prevent the plasticized materials from overflowing from the weld at extremely high heat inputs during conventional FSW and broaden the welding parameter windows. According to the theories of heat generation during FSW [198–200], heat input is closely correlated with base properties of workpieces (yield strength, hardness, etc.), welding parameters (welding speed, rotational velocity, plunge depth, etc.) and equipment parameters (shoulder or pin diameter, pin morphology, etc.). Table 6 lists the optimum welding parameter windows for $SSFSW_2$ of different materials with different thermal and mechanical properties.

For materials (Ti, Ti alloys, etc.) with high yield strength and low thermal conductivity, the relatively low rotational velocity and welding speed are feasible. Russell et al. [143] stated that sound joints could be achieved at rotational velocities of 400–500 rpm and welding speeds of 60–80 mm/min during $SSFSW_2$ of Ti-6Al-4V alloys. Maltin et al. [151] also stated that defect-free $SSFSW_2$ joints of steels can be produced at a rotational velocity of 200 rpm and a welding speed of 120 or 140 mm/min. Aiming at Cu or Cu alloys with high thermal conductivity [202], the frictional heat quickly transfers from the weld to the surrounding materials, and then results in welding defects, which always demand high heat input (high rotational velocity or low welding speed). Wei et al. [150] stated that Cu sheets with a thickness of 0.85 mm were successfully joined using a rotational velocity of 3000 rpm, a welding speed of 300 mm/min and a Z-direction force of 6 kN, in which the specially high welding speed was used to avoid the distortion of the ultra-thin sheets. No

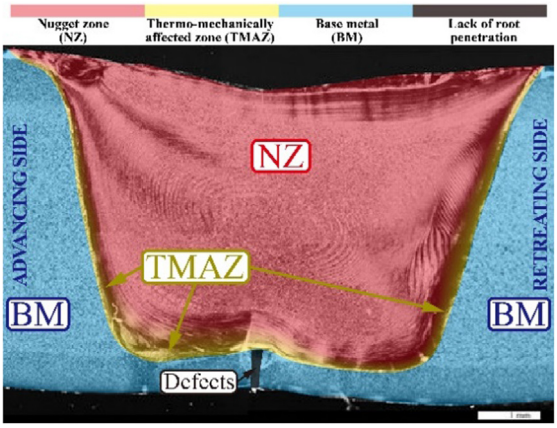


Fig. 47. Macrostructure of a typical $SSFSW_2$ joint of PP [196].

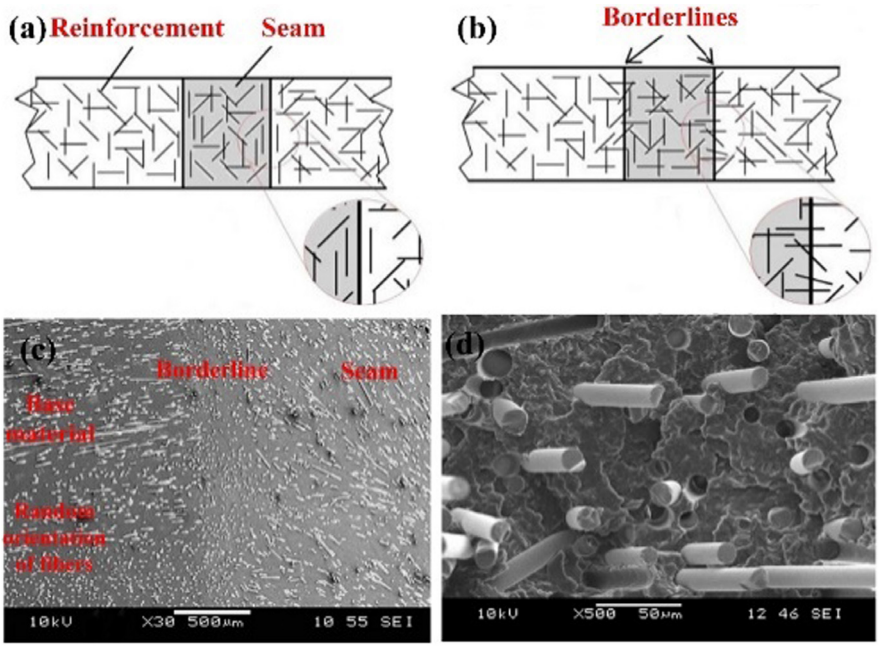


Fig. 48. Welded zone in fibre-reinforced composites with a thermoplastic matrix: (a) non-intermeshing fibres and (b) intermeshing fibres at the interface and (c) borderline between the NZ and the BM and (d) the fracture surface [182].

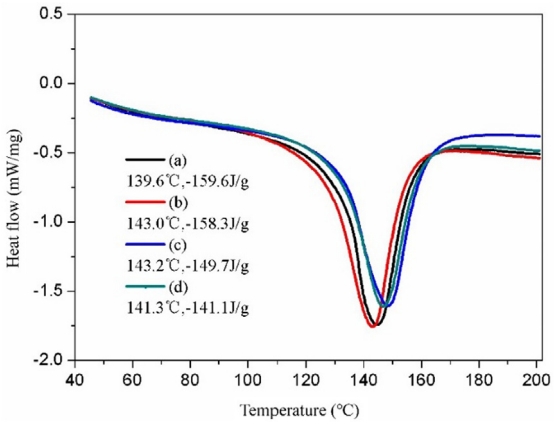


Fig. 49. DSC curves of a PE FSW joint: (a) BM, (b) HAZ, (c) TMAZ and (d) NZ [197].

Table 6
Optimum welding parameter windows for $SSFSW_2$ of different materials.

Materials	Joint type	Rotational velocity (rpm)	Welding speed (mm/min)	Preheating temperature (°C)	Ref.
Ti6Al4V	Butt	400– 500	60– 80		[143]
Steel	Butt	200	120– 140		[151]
AA2219-T6	Butt	600– 900	100		[201]
AA6005A-T6	Butt	2000	300– 600		[144]
AA6061-T6	Butt	750– 1500	100		[172]
AA7050-T7651	Butt	1500	100– 400		[139]
ABS	Butt	≥1250	≤100	115	[110]
HDPE	Butt	1400	25	100	[135]
Nylon 6	Butt	630	20	150	[148]
PP	Butt	1080	51	160	[162]
AA6061-T6/AZ31B	Butt	1000	60		[158]
SCF/PEEK/AA2060-T8	Lap	1600	30		[159]
AA6082-T6	Lap	2000	840		[150]
Pure copper	Butt	3000	300		[150]

remarkable wear was observed on the tool pin or stationary shoulder.

For Al alloys, Liu et al. [201] reported that sound joints were only obtained at a rotational velocity of 800 rpm in conventional FSW, whereas $SSFSW_2$ could produce defect-free joints in a wider range of rotational velocities of 600–900 rpm at a constant welding speed of 100 mm/min for AA2219-T6. Wu et al. [139] compared conventional FSW with $SSFSW_2$ of AA7050-T7651 based on the same size rotating pin and a welding speed of 400 mm/min. The optimum rotational velocities in conventional FSW and $SSFSW_2$ were 700 rpm and 1500 rpm, respectively. $SSFSW_2$ generated a ~30% lower heat input than conventional FSW, which achieved a narrow HAZ. Ji et al. [144] stated that a sound joint could be attained over a wide welding speed range, from 300 mm/min to 600 mm/min, based on a small rotating shoulder and a constant rotational velocity of 2000 rpm during $SSFSW_2$ of AA6005A-T6. Li et al. [172] indicated that tensile properties for $SSFSW_2$ joints of AA6061-T6 were nearly unaffected by rotational velocities of 750–1500 rpm at a constant welding speed of 100 mm/min, whereas increasing the welding speed from 100 to 300 mm/min markedly increased the tensile properties at a constant rotational velocity of 1500 rpm. The maximum joint efficiency of 77.3% (256 MPa) was achieved under welding parameters of 1500 rpm and 300 mm/min. To attain sound $SSFSW_2$ Al alloy butt joints with high strength, the rotational velocities of 500–2000 rpm and the welding speeds of 50–600 mm/min are appropriate.

For polymer materials (thermoplastic polymers or polymer matrix composites) with extremely low yield strength and thermal conductivity [203,204], it is difficult to transfer heat input to preheat the materials at the front of the rotating tool. Higher heat input (high rotational velocity and low welding speed) or a secondary heat source is required to attain sound joints. Mendes et al. [110] stated that high strength efficiency was achieved only when a high rotational velocity and a high axial force were used during $SSFSW_2$ without a heating system in 6-mm-thick ABS sheets. Rotational velocity and axial force values above a certain threshold were required to produce defect-free joints. A high-quality joint was obtained for a tool shoulder temperature of 115 °C, an axial force higher than 1.5 kN, rotational velocities greater than 1250 rpm and low traverse speed ranging between 50 and 100 mm/min [181]. Azarsa et al. [135] performed $SSFSW_2$ with HDPE and stated that a combination of high rotational velocity and low welding speed increased flexural strength by reducing the sizes of defects. The optimum welding parameters to achieve maximum flexural strength were a rotational velocity of 1400 rpm, a welding speed of 25 mm/min and a shoulder temperature of 100 °C. Aydin et al. [205] adopted backing preheating at 50 °C to join a 4-mm-thick ultrahigh molecular weight PE (UHMW-PE) sheet and then improved joint formation due to a uniform temperature gradient through the thickness direction. Vijendra et al. [206] stated that induction heating enabled materials to be plasticized in a short time and to be easily stirred. The optimum conditions for the maximum joint strength were a tool pin temperature of 45 °C, a welding speed of 50 mm/min and a rotational velocity of 2000 rpm.

Additionally, aiming at the $SSFSW_2$ of dissimilar materials, the welding parameters depend on the materials or joining types (butt or lap joints). For dissimilar materials with severe interfacial reactions, mechanical interlocking and metallurgical bonding are attributed to the joint strength. Meng and his co-workers [158,164,165] stated that a rotational velocity of 1000 rpm could be responsible for the sufficient heat input, while a low welding speed of 60 mm/min could provide much more stirring time to improve the mechanical interlocking for $SSFSW_2$ of Al and Mg alloys. A high welding speed higher than 60 mm/min easily resulted in welding defects, which can be further increased to 80 mm/min assisted by ultrasonication [207]. When using a lap configuration of polymer

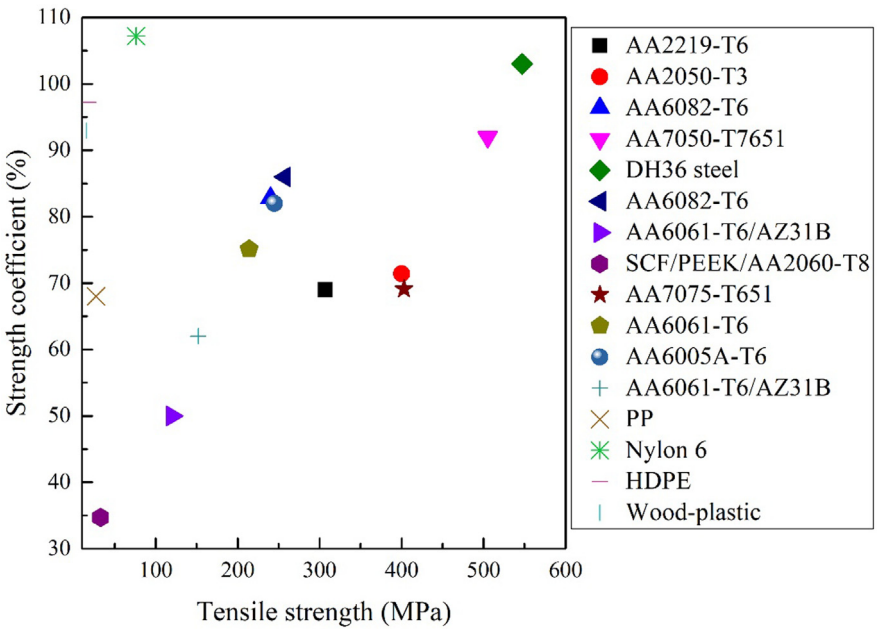


Fig. 50. Mechanical properties and strength coefficient (%) of $SSFSW_2$ in the current research and published open literature and current research. (In sequence: AA2219-T6 [201], AA2050-T3 [188], AA6082-T6 [150], AA7050-T7651 [139], DH36 steel [151], AA6082-T6 [151], AA6061-T6/AZ31B [164], SCF/PEEK/AA2060-T8 [159], AA7075-T651 [156], AA6061-T6 [213], AA6005A-T6 [144], AA6061-T6/AZ31B [158], PP [147], Nylon 6 [148], HDPE [177], Wood-plastic [180]).

at the upper and metal at the lower, the selection of welding parameters should be in accord with the joining of polymers, which needs relatively lower welding speeds lower than 50 mm/min without a secondary heating system. For lap joints of similar or dissimilar materials, the process variations are different from those of butt joints, whose rotational velocity is relatively lower [169,208] and welding speed is slightly higher due to the original interface in butt joints disappearing in the upper sheet of lap welding.

4.1.6. Mechanical properties

$SSFSW_2$ not only inherits the advantages including low peak temperature, small residual stress and distortion, simple process and non-pollution of conventional FSW, but also generates a concentrated heat input, reducing the joint softening degree and substantially improving static mechanical properties. Fig. 50 shows the mechanical properties of $SSFSW_2$ joints. Wu et al. [139] compared the mechanical properties between $SSFSW_2$ and conventional FSW of AA7050-T7651. $SSFSW_2$ provided an approximately 30% lower heat input and 20–40 MPa higher yield and tensile strength than those of conventional FSW joints, which were attributed to the compatible deformation induced by uniform thickness properties. Huang et al. [159] established a radar chart to describe the relationships between weld thinning, microstructural characteristics and mechanical properties (Fig. 51). They stated that $SSFSW_2$ could control the microstructural evolution and subsequently affect mechanical properties, which were better than those of the state-of-the-art techniques. The microstructure, surface stress state and stress concentration were investigated at the fatigue crack initiation sites. The stress concentration determines the fracture location, and the surface microstructure and surface stress state influence the fatigue properties. $SSFSW_2$ can reduce the residual stress to a certain extent since the stationary shoulder exerts residual compressive stress on the materials on the top surface, which is beneficial to improving fatigue performances. Jayaraman et al. [209] indicated that FSW increased the high-cycle fatigue endurance of Al alloys by 80% due to a deep surface layer of compressive residual stress by low plasticity burnishing. Huang et al. [210–212] proposed *in-situ* rolling FSW and fabricated ultrafine grains and a compressive residual stress layer on the surface of the joint, improving the corrosion resistance and reducing residual stress and distortion. The surface of the $SSFSW_2$ joint was characterized by ultrafine grains, which evidently enhanced the fatigue properties [149]. Li et al. [149] also stated that the stress concentration at the internal corner for additive $SSFSW_2$ joints was evidently lower than that for non-additive joints due to the additional materials filling into the corner, as shown in Fig. 52. EADS [138] also applied $SSFSW_2$ in the complex 3D structural window frame of an aircraft and stated that no failure occurred after 140,000 cycles, indicating excellent fatigue properties.

4.1.7. Prospects

$SSFSW_2$ has been used to join many kinds of materials with varied thicknesses, such as Al alloys, Ti alloys, steels and polymers. Many outstanding advantages have been applied in the manufacturing fields of aerospace and transportation, such as smooth surface, low residual stress and distortion, and high joint quality. However, some areas need to be addressed, which are detailed hereafter:

(1) Long service welding tool: During $SSFSW_2$, the plasticized materials easily overflow into the gap between the stationary shoulder and the rotating tool, which results in the overheating of the rotating pin and then acutely deteriorates the service life. A tool coating technology shall be developed to improve the heat insulation and wear resistance, increasing the service life of the rotating tool.

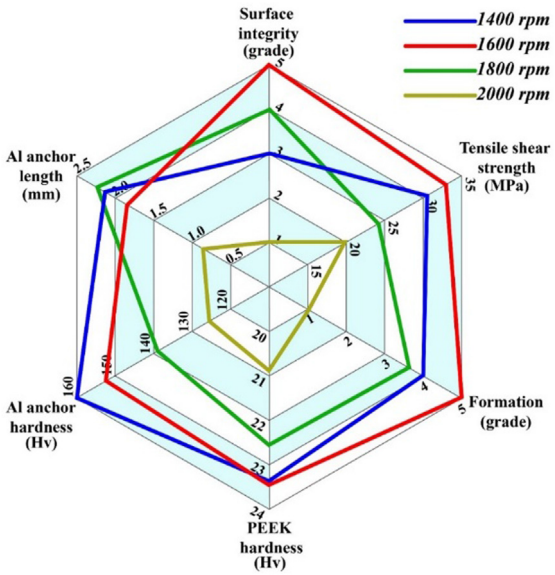


Fig. 51. Radar chart of the microstructural characteristics versus mechanical properties [159].

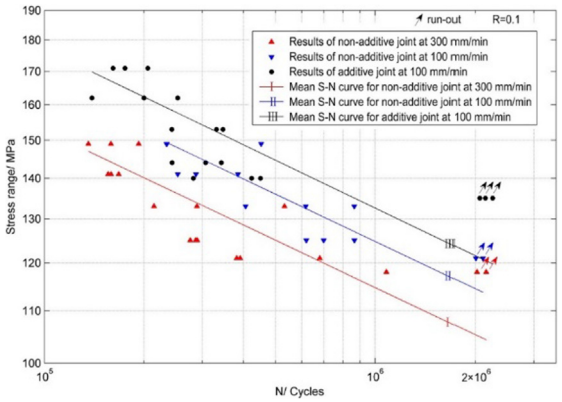


Fig. 52. S–N curves for additive and non-additive T joints produced by $SSFSW_2$ [149].

(2) $SSFSW_2$ of metal matrix composites (MMCs): Initial tool wear can also proceed without an optimized shape at high wear rates. The tool wear in FSW of MMCs is attributed to particle erosion and abrasion from the reinforcements during rotating and translational vortex flow. In addition to the excessive cost effect of tool wear, the contamination of the weld by debris from the worn tool is of considerable concern. Premature failure due to the brittleness and high tool cost is the challenge encountered with these materials.
(3) $SSFSW_2$ of polymer matrix composites and between these composites and metals: $SSFSW_2$ has the remarkable advantage and feasibility to join polymer matrix composites with low thermal conductivity and strength due to the focused heat source and assisted heating. Moreover, $SSFSW_2$ has the potential to join dissimilar or monolithic materials.
(4) High corrosion and wear resistance of $SSFSW_2$ joints: Although $SSFSW_2$ can achieve high-quality joints, the corrosion and wear resistances are reduced due to the dissolution, coarsening and reprecipitation of the strengthening phases, especially in the 2xxx and 7xxx Al alloys. In addition to depositing particles, such as pure Al, Al_2O_3, SiC_p, multi-wall carbon nanotubes or graphene hybrids with surface friction stir processing (FSP) or cold spraying, may become further hotspots to improve the wear and corrosion resistance.

4.2. Zero-plunge-depth friction stir welding

The welding tool is the foundation of FSW, playing significant roles in microstructures, defects and mechanical properties. During conventional FSW, the welding tool always contains a shoulder and a pin, which can realize high-quality welding under a tilt angle. The application of the shoulder plunge depth during FSW is the intrinsic reason for the occurrence of weld thinning. It can be inferred that weld thinning can be eliminated with a zero plunge depth, thereby avoiding the loss of plasticized materials. Based on this concept, a novel zero-plunge-depth FSW was proposed by Zhang et al. [214,215] and our workgroup [216].

4.2.1. Principle

Zhang et al. [214,215] developed the novel non-weld-thinning FSW (NWT-FSW), which could be performed at a zero shoulder plunge depth, as shown in Fig. 53. The weld thinning phenomenon is effectively eliminated without adding or removing any materials before or after welding, and without other assisted shoulder tools. A concave geometrical feature is utilized on the bottom surface of the rotating shoulder. The concavity is designed to provide a reservoir of pin sheared materials. Scrolls are among the most useful geometrical features for developing an inwardly directed traction force under the rotating shoulder during FSW. Three equally spaced scrolls are machined on the concave shoulder. During NWT-FSW, the concave shoulder only slightly contacts the workpieces and forms an enclosed chamber, which avoid plasticized materials overflowing from the weld. Welding heat input and material transfer are mainly provided by the rotating pin rather than the rotating shoulder, which ensure the sound joint without weld

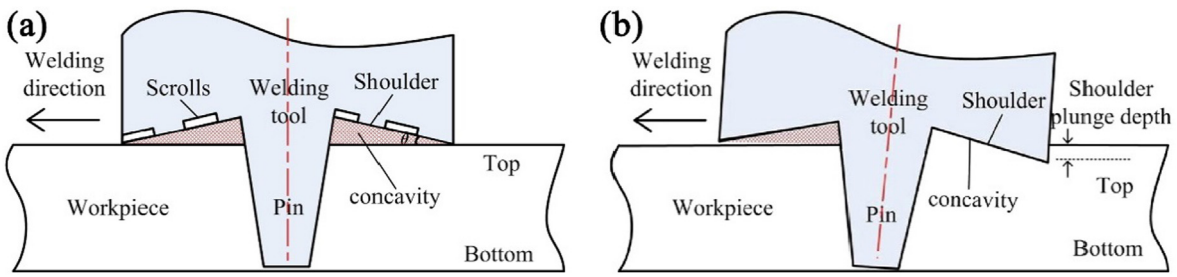


Fig. 53. Schematic views: (a) NWT-FSW and (b) conventional FSW [214,217].

thinning.

Although the NWT-FSW proposed by Zhang et al. [214] can eliminate weld thinning, the zero tilt angle narrowed the welding process window due to the small forge effects induced by the rotating shoulder. Our research group at Harbin Institute of Technology proposed a novel FSW method named “single welding and double forming” MPD-FSW, which overcome the conventional inherent issues wherein the plunge of the rotating shoulder at a tilt angle made it difficult to achieve non-weld-thinning joints [216]. This welding tool was designed to be detachable, as shown in Fig. 54, which was composed of an outer rotating shoulder, an inner rotating shoulder and a rotating pin. The plunge depths of the inner and outer rotating shoulders could be changed by controlling the relative height between the outer and inner shoulders. The concave shoulder morphology is specially designed to increase the forging and gathering effects on the plasticized materials, thereby improving the joint formation. During welding, the inner rotating shoulder and pin plunge into the workpieces to a certain depth, which are responsible for the “single welding”, and then ensure the joint inner integrity. Without the plunge depth, the outer rotating shoulder only slightly contacts with the workpieces and was attributed to “double forming”, which further rolls the plasticized materials on the surface and subsurface. The flash defects are eliminated, and weld thinning is avoided. Moreover, the rational choice of the rotating pin is essential to increase the stirring effect and heat generation due to the decrease in heat generation induced by the relatively smaller inner rotating shoulder. A tapered threaded pin with three facets was designed to improve the material flow behaviour.

4.2.2. Formation mechanism

Fig. 55 shows the surface formation of MPD-FSW joints. The surface appearance is divided into two affected zones: the outer rotating shoulder affected zone, and the inner rotating tool affected zone. The plunge depth of the inner rotating shoulder is larger than that of the outer rotating shoulder, which corresponds to the subzone.

The MPD-FSW process was mainly separated into “single welding” and “double forming”. During welding, the inner rotating shoulder and pin plunged into the workpieces and generated frictional heat and deformation heat, which further attributed to the transfer of the plasticized materials, and then a metallurgical bond was achieved. The heat generation of the “single welding” was completely from the frictional heat between the inner rotating tool and the workpieces. Furthermore, the outer concave shoulder slightly contacted the workpieces and formed an enclosed chamber, which restricted the overflow of the plasticized materials that were squeezed from the inner rotating shoulder affected zone. With the rotation and advancement of the outer rotating shoulder, the plasticized materials from the inner rotating tool affected zone were refilled into the weld thinning location induced by the plunge of the inner rotating shoulder, thereby achieving non-weld-thinning joints (Fig. 56). The outer rotating shoulder only squeezed and forged the plasticized materials, which caused the total heat generation of the MPD-FSW to be lower than that of conventional FSW. No-weld-thinning appeared in the MPD-FSW joints.

In addition to heat generation, the material flow behaviour could be separated into three types. The first type was the layer flow induced by the welding speed, in which the plasticized materials around the rotating tool flowed backward as the tool advanced. The second type was the rotation flow induced by the rotating welding tool via friction, during which the flow rate gradually decreased as distance from the centre of the welding tool increased. The last prominent type was the flow induced by the rotating pin, which made the plasticized materials near the subsurface of the pin flow downward and then upward away from the pin. In particular, the special design of the pin morphologies, such as threads and facets, can significantly improve this flow.

An illustration of the material flow behaviour induced by the novel welding tool is displayed in Fig. 57 [218]. During the MPD-FSW process, the material flow rate was divided into v_{shear} and v_{normal} due to the presence of the three facets on the rotating pin. The v_{shear} mainly provided shear force to improve material transfer, whereas the v_{normal} significantly pushed the plasticized materials and further promoted the material flow rate, as shown in Fig. 57a and b. Under the relatively lower peak temperature induced by the inner small rotating shoulder, the improved material flow rate effectively avoided the macroscopic welding defects and further enhanced the material transfer rate through the thickness direction. The plasticized materials flowed downward to the bottom near the pin surface (marked by red arrows in Fig. 57b) and then flowed upward away from the pin surface (marked by blue arrows in Fig. 57b). As shown in Fig. 57c, the partially plasticized materials easily flowed out of the NZ due to the small shoulder diameter

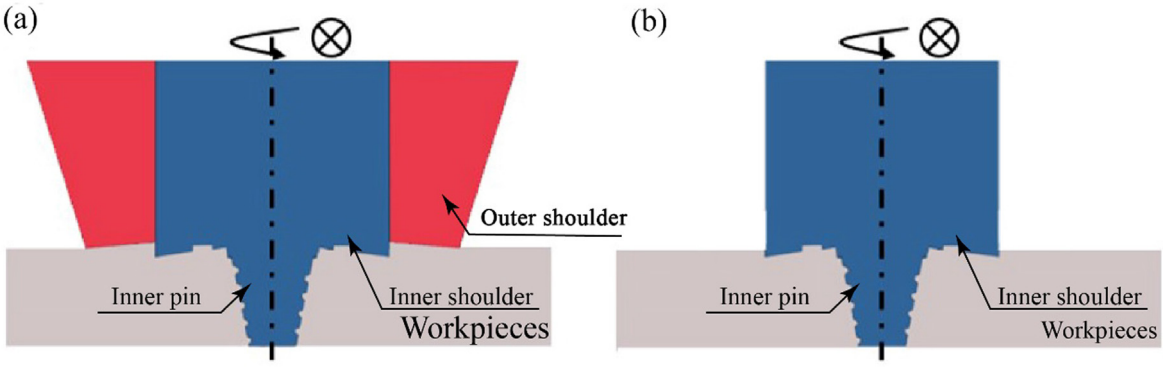


Fig. 54. Schematics of (a) MPD-FSW and (b) conventional FSW.

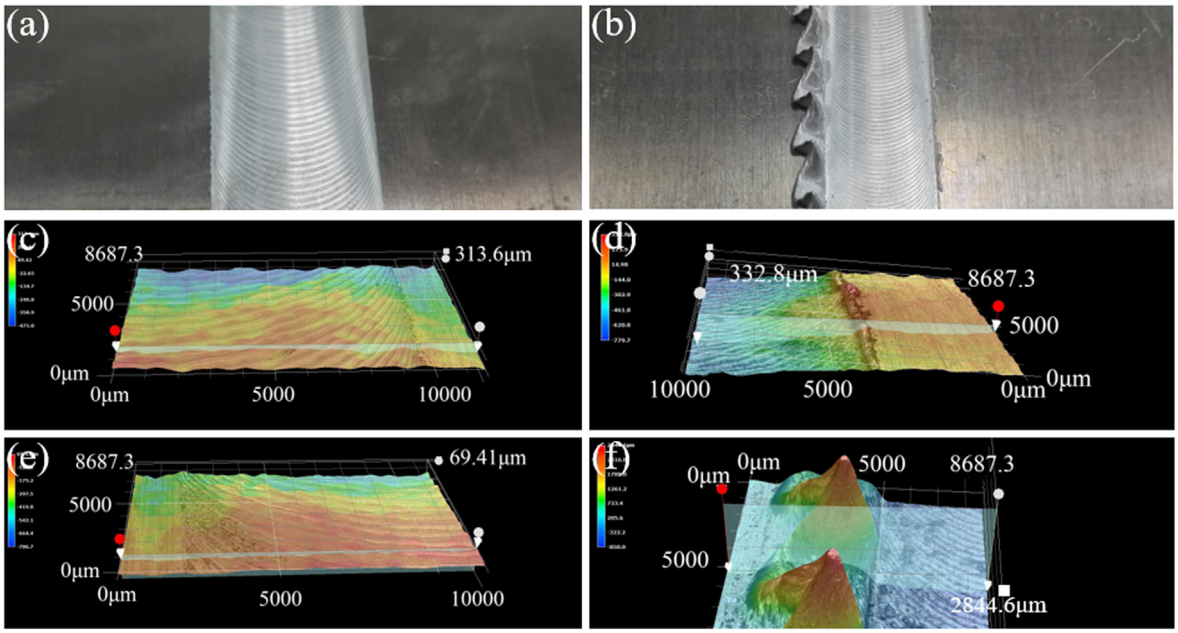


Fig. 55. Surface morphologies of MPD-FSW and conventional joints: schematics of surface appearances in (a) MPD-FSW and (b) conventional joints, 3D morphologies at the AS of (c) MPD-FSW and (d) conventional joints, and 3D morphologies at the RS of (e) MPD-FSW and (f) conventional joints.

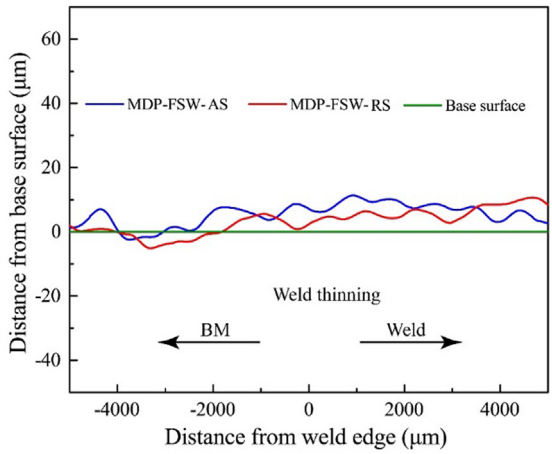


Fig. 56. Variations in the heights of the different joints.

when the outer rotating shoulder was not employed (marked by green arrows in Fig. 57c). Moreover, the outer rotating shoulder contacted the rotating tool in the clearance fit, which can preheat the overflowed materials and provide a downward pressure. This pressure can prevent the plasticized materials from overflowing from the weld and refill these materials into the NZ, as shown in Fig. 57d. Hence, favourable surface integrity without weld thinning can be achieved.

4.2.3. Microstructural characteristics

The microstructure of an MPD-FSW joint is shown in Fig. 58. The morphology is mainly divided into the outer SAZ, inner SAZ, TMAZ, HAZ and NZ. During welding, the plunge depth of the outer shoulder was only 0.05 mm and that of the inner shoulder was 0.15 mm, which caused the outer SAZ to be located only at the subsurface of the workpieces. In the top, the grains were the smallest in the whole joint, implying that this zone experienced severe plastic deformation at high strain rates. After being subjected to the rotating pin, the upper part of the weld underwent additional deformation by the rotating tool shoulder. Huang et al. [210,211] also stated that a plunge depth of 0.05 mm of rolling balls could fabricate a gradient surface layer on Al alloys, thereby improving the microhardness on the subsurface. Apparently, the grain structures for each NZ layer of the NWT-FSW joint exhibited different sizes from those of conventional FSW joints. Furthermore, the grains of both joints presented different distributed characteristics along the thickness direction, as shown in Fig. 59. First, the grain size of the NWT-FSW joint was smaller than that of the conventional FSW

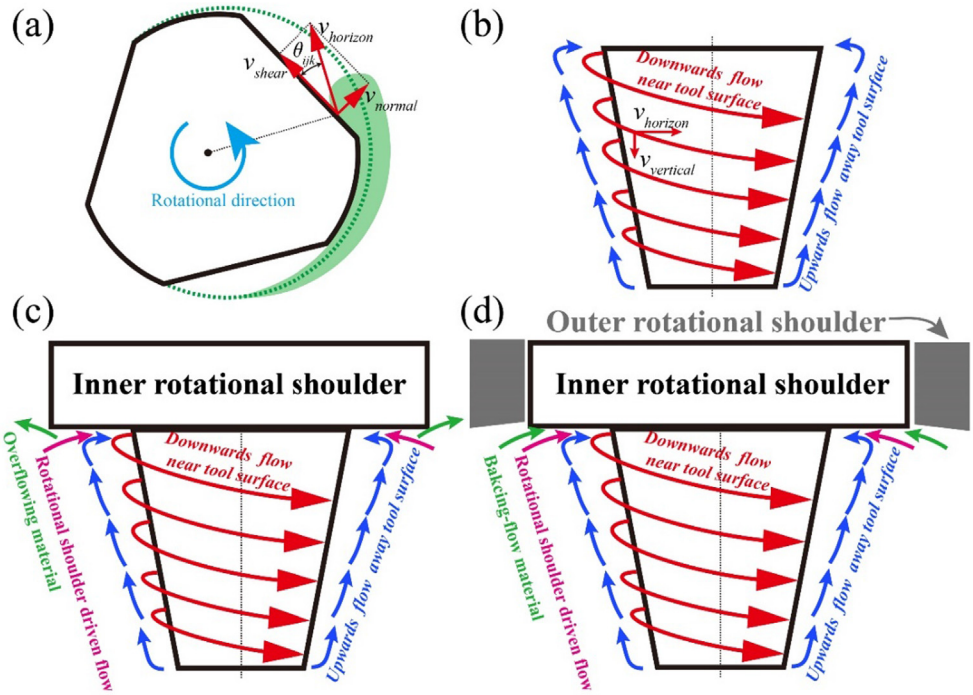


Fig. 57. Material flow and velocity distributions during FSW with controlled shape and performance: velocity distributions in the (a) horizontal section and (b) vertical section; material flow in (c) conventional FSW and (d) MPD-FSW [218].

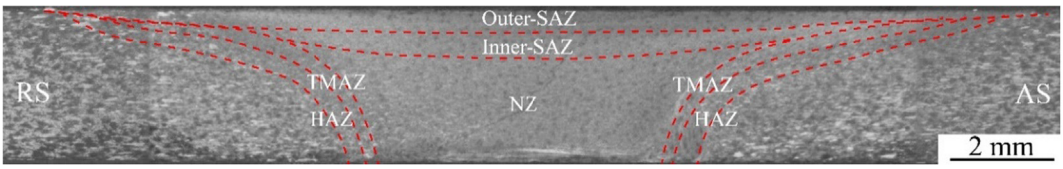


Fig. 58. Macrostructure of a typical MPD-FSW joint.

joint at each layer of the NZ. Second, the grain size of the conventional FSW joint gradually decreased from the upper to lower parts of the NZ, as commonly observed in the conventional FSW joints of other Al alloys [219,220]. For the NWT-FSW joint, the grain size was nearly uniform along the thickness direction. Compared with conventional FSW, the thermal and mechanical effects of the rotating shoulder on NWT-FSW or MPD-FSW joints were weakened and became more uniform along the thickness direction.

4.2.4. Mechanical properties

The decreased heat input during zero-plunge-depth FSW (compared with that in conventional FSW) was obtained due to the loss of frictional heat generated by the rotating shoulder, which was the intrinsic reason for grain refinement and the reduction in the SAZ. These useful microstructural evolutions further narrowed the softening regions and degree, which provided the higher mechanical properties of the NWT-FSW joint. The maximum tensile strength of the optimized joint reached 218 MPa, whereas the maximum elongation of 24.3% was comparable with that of base 5052 Al alloys [214], as shown in Fig. 60a. Additionally, the effect of the outer rotating shoulder and welding parameters on the tensile properties of the MPD-FSW is shown in Fig. 60b. The addition of the outer rotating shoulder provided significantly higher tensile strength than that provided by only the inner shoulder. Moreover, when the rotational velocity was 600 rpm, the tensile properties first increased and then decreased as the welding speed varied from 100 mm/min to 600 mm/min. The maximum tensile strength of the AA6082-T4 joint reached 231 MPa, which was equivalent to 90.8% of the BM [216].

4.2.5. Prospects

The novel design of the welding tool and process can eliminate weld thinning and obtain high-quality joints, providing technical support for the high requirements of joint integrity. The innovative welding concept is beneficial to reducing the welding temperature and refining the grain size, thereby improving the mechanical properties. Moreover, the detachable welding tool is simpler than the stationary shoulder tool system and had more potentials in the industrial manufacturing fields. Some aspects remain to be addressed, as detailed hereafter:

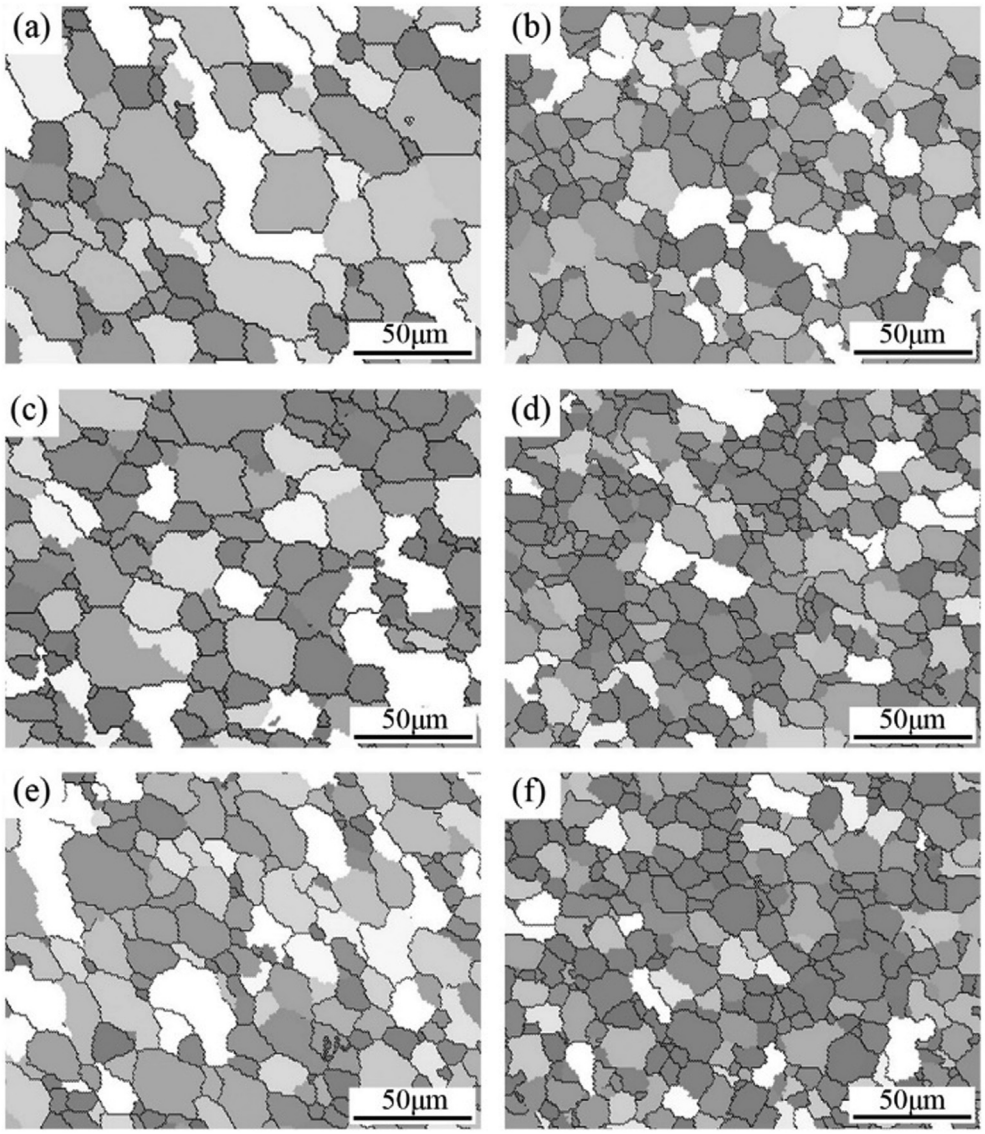


Fig. 59. Grain structures of the NZ: (a–c) upper, middle and lower parts of the conventional FSW joint and (d–f) upper, middle and lower parts of the NWT-FSW joint [219,220].

(1) For different kinds of materials with different thicknesses, the design criterion of the welding tools needs to be established from the viewpoints of joint formation, defect elimination and control of microstructures and mechanical properties.
(2) The design of the MPD-FSW tool can potentially be combined with the lower shoulder in BT-FSW or SSFSW$_2$, realizing non-weld-thinning of hollow or enclosed structures, subsequently expanding the industrial applications.
(3) Technical and fundamental issues need to be elucidated, including the design of the welding tool or structure, heat generation, material flow behaviour, microstructural evolution and mechanical properties.
(4) Hybrid joining processes, such as electricity-assisted FSW, heat-assisted FSW, ultrasonic-assisted FSW and underwater FSW, can be combined with advanced NWT-FSW to simultaneously improve the microstructure and mechanical properties by utilizing their individual advantages.

4.3. Additive friction stir welding

In addition to the methods that prevent or avoid the overflow of the plasticized materials, under the condition of a sufficient forging force, additive FSW can solve these issues through the introduction of additional materials.

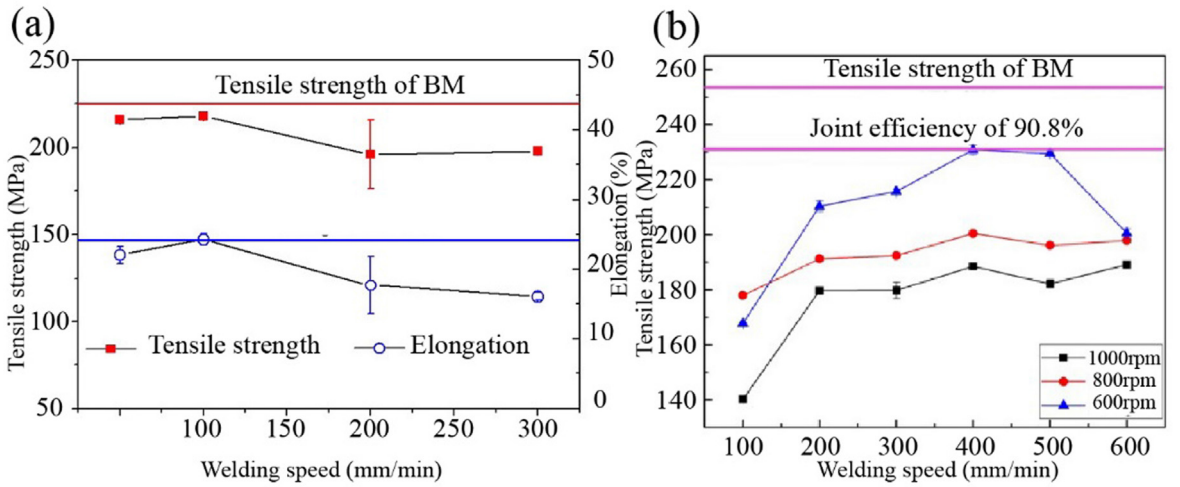


Fig. 60. Tensile properties of zero-plunge-depth FSW joints: (a) AA5052 [214] and (b) AA6082-T4.

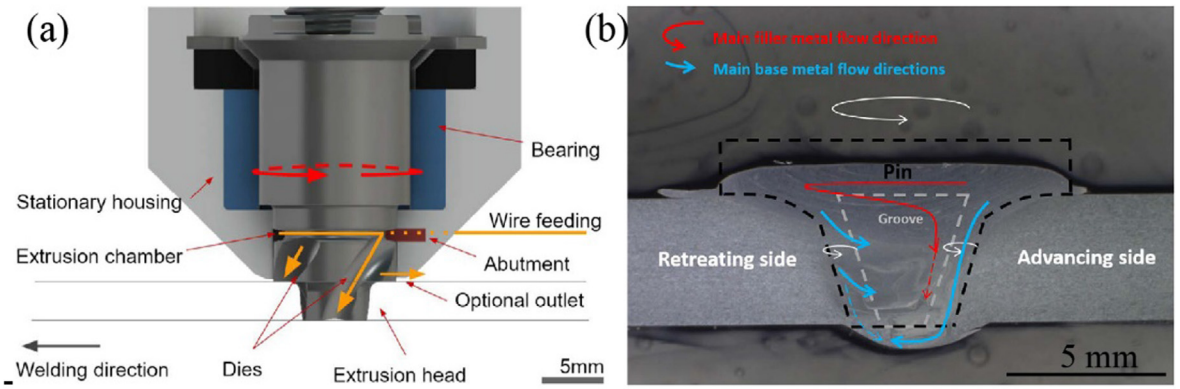


Fig. 61. Schematic and microstructure of the HYB process: (a) schematic and (b) macrostructure [221].

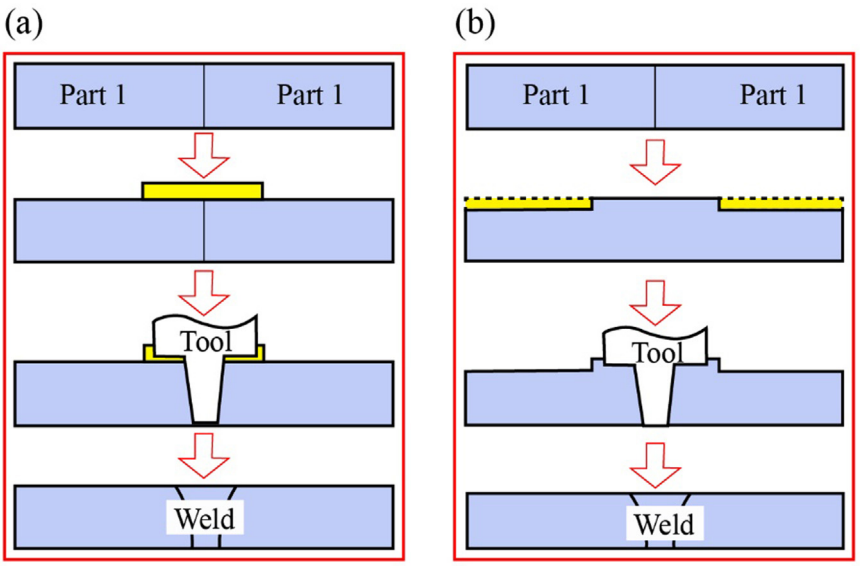


Fig. 62. Schematics of (a) additive FSW [230] and (b) reductive FSW.

4.3.1. Friction adstir welding

Sandnes et al. [221] proposed a hybrid metal extrusion and bonding (HYB) process by adding filler materials and introducing plastic deformation. During this process, an extruder head was clamped against the welding workpieces. The welding workpieces were separated from each other so that an I-groove formed between them. The diameter of the rotating pin was slightly larger than the width of the groove to ensure complete contact between the sidewalls of the groove and the pin, as indicated in Fig. 61. During the rotation and advancement of the pin, the materials along with the oxide layer on the groove sidewalls were stirred and mixed as they flowed downward into the groove and consolidated behind the pin. A sound joint with a thickness of NZ greater than the thickness of BM was obtained. Typically, the peak temperature in the groove between the welding workpieces is between 350 °C and 400 °C, which is below the peak temperature reported for FSW; this lower temperature is beneficial to reducing the joint softening and improving joint quality. Li et al. [222,223] employed cold spraying with FSW joints to improve corrosion resistance, in which weld thinning was eliminated by the addition of pure Al or Al_2O_3 particles. Partial weak bonding easily formed at the interface between the coating and the workpieces; meanwhile, cold spraying equipment is relatively expensive. Huang et al. [224] applied for a patent called *in-situ* additive FSW to solve the weld thinning problem, in which a banding wire was introduced into the surface of the welding workpieces by a wire feed system and a locating guide rail that made the banding wire tightly contact the welded workpieces. Under the thermo-mechanical effects, the banding wire and the welding workpieces could be joined, and weld thinning was avoided. Moreover, the type of banding wire could be changed according to the surface requirements, such as wear and corrosion resistances, thereby creating a stronger interface than that produced with cold spraying [225]. However, note that the joining between the banding wire and the workpieces involved a butt-lap interface, which easily led to lap welding defects, such as hook or cold lap defects [169,226].

4.3.2. Compensation friction stir welding

Mika [16], Meng et al. [227] and Wen et al. [228] introduced additional solid-state materials to the joint region along the welding line during FSW of butt workpieces, which were named surface compensation FSW (SCFSW) or level compensation FSW (LCFSW), as shown in Fig. 62a. The achieved joints had a larger cross-sectional thickness than conventional joints. After FSW, the materials in the upper surface higher than the planar surface of the base workpieces were machined, producing a non-weld-thinning joint. Although the weld thinning problem was solved, its disadvantages were also obvious. First, the addition and removal of materials before and after welding made the FSW process relatively complicate, reducing the welding efficiency. Second, many workpieces require three-dimensional contours. When FSW was utilized to join complex three-dimensional structures, it was difficult to add materials to the joint region. This method presented a relatively narrow application. Third, the upper part of the joint generally possessed more superior mechanical properties than the middle and lower parts of FSW joints, such as pure Al or 2219-O Al alloys [219,229]. Even though weld thinning could be eliminated, the mechanical properties are more prone to deterioration due to the removal of materials from the upper part of the joints. The opposite reductive FSW was also proposed, which was similar to additive FSW, wherein the thickness of the whole workpieces was higher than the thickness of the preset weld. After FSW, the materials higher than the top surface of the weld were removed, and the stress concentration caused by the weld thinning was avoided. Alternatively, before FSW, the abundant materials besides the weld were milled and formed a boss, which was further joined by FSW as in additive FSW. Although this method could eliminate weld thinning, the resource waste was very severe, and the operating procedure was more complex.

Zhao et al. [231] proposed a FSW method for eliminating weld thinning by an additional T-plate to simplify the procedures in SCFSW that required a complex extrusion process to fabricate a convex welding line. During welding, the T-plate was placed at the interface between the both workpieces, which made the surface of the weld higher than the surface of the workpieces. The lateral force ensured the T-plate was static. The frictional heat produced by the shoulder was attributed to the joining between the flange and the materials on the top surface of the welding workpieces, while the thermo-mechanical behaviours improved the welding of the web and the materials on the vertical surface of the workpieces, thereby eliminating weld thinning. Because the joining between the flange and the top surface of the welding workpieces only depended on the thermal conduction from the heat generation of the shoulder, the thickness of the flange was limited to less than 2 mm in thickness [232–234]. Moreover, the ultra-thin flange was easily deformed due to high frictional heat, resulting in poor joint integrity. Additionally, both of the joining interfaces between the flange and the web appeared at the butt joint [235,236], which always required a higher heat input to ensure good joint formation. Otherwise, the joining difficulties were greater due to the insufficient material flow induced by low heat input. Ji et al. [213] also stated that a sound joint could be achieved at a low welding speed and a high rotational velocity when an additional filler was introduced at the butt interface. The extremely high heat input was prone to severe joint softening, consequentially deteriorating the joint strength.

5. Friction stir-based remanufacturing

Metallic materials have been extensively applied in several manufacturing fields, including aerospace, railway, and shipping transportation, which have drawn increasing attention to the development of welding techniques. Conventional fusion techniques, due to coarse grains, hot cracks and pore defects, have difficulty in obtaining high-quality welding joints. FSW is a mature solid-state joining technique involving temperature, mechanics and metallurgy and their interactions. FSW has the advantages of low temperatures, high-quality joints, small residual stress and distortion, and no pollution, which can effectively avoid the problems associated with conventional fusion welding. When performed with inappropriate welding tools, process parameters or technological conditions, welding defects easily form and deteriorate the mechanical properties. Moreover, aiming at some structural parts after

long service, corrosion, wear and other severe environments are prone to causing defects, which are detrimental to the service life of the parts, as described hereafter [237]:

(1) Failure of processes or procedures during part fabrication.
(2) In-service defects were missed during fabrication or grew during operation.
(3) Degradation of parts and components through unforeseen environmental factors or extended operation, such as corrosion and wear.
(4) Damage resulting from incorrect use or external factors.

All the service lifetimes of these structural parts involve “manufacturing-servicing-scrapping” and then result in economic loss and material waste, which are detrimental to the development of the recycling economy. Introducing a repairing process into the service lifetime of the parts can enable recyclability, such as “manufacturing-servicing-scrapping-repairing”, which can significantly improve material utilization, resource conservation, energy savings and emission reduction. Green remanufacturing, with the characteristics of high efficiency, low cost and little pollution, can restore and upgrade the properties of the parts via advanced welding techniques [238–240]. It is necessary to perform green remanufacturing techniques to enhance all service lifetimes. Solid-state green remanufacturing techniques, based on friction stir-based technologies, can achieve high-quality joints due to low temperature and severe plastic deformation.

5.1. Principle and advantages

Friction stir repairing (FSR), based on the characteristics of FSW, involves temperature, mechanics, metallurgy and interactions, which has the feasibility and potential to repair the damaged structural parts. During FSR, an unconsumable or semi-consumable tool plunges into the workpieces to be repaired, and generates frictional heat and severe plastic deformation. Under the peak temperature and material flow, the defects can be repaired by filling with plasticized materials. Owing to the advantages, including low temperature, high-quality joints, and little pollution, friction stir-based remanufacturing techniques have been extensively developed and investigated, which are mainly divided into repetitive FSW and additive FSW. Fig. 63 shows the key factors affecting joint integrity and quality, which consists of equipment parameters, welding tool parameters, and material properties. The welding tool and the equipment parameters are mainly dependent on the mechanical properties of the workpieces, such as yield strength, ductility, and hardness, which play significant influences on plastic deformation [116]. High heat input is required for a high melting point or constant-pressure specific heat materials, while materials with a low melting point or constant-pressure specific heat need relatively lower heat input [241]. The thermal properties of the workpieces primarily affect the welding peak temperature and thermal transfer. For materials with high thermal conductivity that easily result in heat loss, high heat input is necessary to guarantee sufficient heat input, obtaining a sound joints [242]. In contrast, the thermal conductivity of polymers is lower than that of Al alloys, which makes it difficult to preheat the materials at the front of the rotating tool. Higher heat input is also required to attain sound joints. Reasonable selections of these parameters are the key and prerequisite to achieve excellent repaired joints.

Compared with conventional fusion repairing techniques, FSR has many advantages.

(1) Low peak temperature can reduce the degree of grain coarsening, thereby improving mechanical properties.
(2) Low heat input and severe plastic deformation can eliminate the pore and crack defects associated with fusion welding techniques.

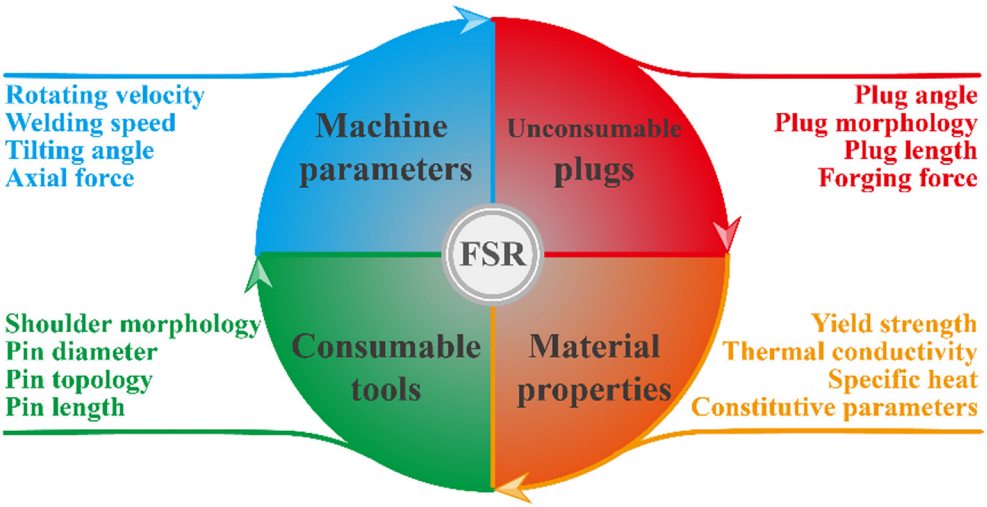


Fig. 63. Process variables of FSR [196].

(3) Low residual stress and small distortion improve the structural integrity.
(4) A smooth surface avoids subsequent surface treatment, reducing the complexity of the manufacturing processes.
(5) Strong material compatibility: FSR can also realize the repairing of high-strength Al alloys, such as 2xxx and 7xxx alloys.
(6) FSR has the potential to repair the parts of dissimilar metals according to engineering requirements.
(7) FSW equipment extensively used in the automobile and aerospace industries, which is characterized by low cost and high energy efficiency, has universal properties.

5.2. Types of FSW defects

During the FSW process, a rotating tool with a shoulder and a pin rotates and plunges into the welding workpieces, which can produce frictional heat and material flow due to the friction between the rotating tool and the welding workpieces. After completing FSW, the rotating tool retracts, and then a keyhole forms at the end of the weld, which easily deteriorates mechanical properties [243]. Moreover, other welding defects, such as cavities [244], tunnels [245], grooves [246] and kissing bonds [247], caused by improper process parameters or technological conditions are also detrimental to mechanical performance [248]. Several characteristic defects are identified as the effect of either flow or geometric. The flow-related defects occur outside the acceptable processing window with parameters that are considered either too hot or too cold [249], as shown in Fig. 64. For example, a higher welding heat input or a larger plunge depth easily forms flash defects and then results in weld thinning and stress concentration. The insufficient material flow induced by lower heat input leads to inner joint defects, such as cavities, tunnels and grooves. Khan et al. [245] stated that the kissing bond and the tunnel defects were easily influenced by the plunge depth and offset during FSW of 5083-H116 and 6063-T6 Al alloys. Tao et al. [250] indicated that the fracture behaviour of FSW joints was strongly influenced by the kissing bond featuring cracks from the lack of root penetration. Kainuma et al. [92] and Zhou et al. [93] reported that the existence of a kissing bond would seriously deteriorate the fatigue lifetimes of a joint in both low-cycle and high-cycle tests. Arici et al. [195] stated that the FSW joints of polymers could be broken by hand due to low strength resulting from kissing bond defects. Tunnelling and kissing bond defects are formed at pin offsets towards stronger materials at the AS and without offset due to insufficient mixing.

Without proper treatment or design, the flashes on the surface may cause significant problems in terms of stress concentrations, corrosion and surface finish [251]. Moreover, the kissing bond defect severely affects the mechanical properties of the welded joints compared with the tunnel defect. When the gap between the welding workpieces induced by the extrusion effect during the FSW process or accumulation of some manufacturing errors of large structures is mismatched, the kissing bond and the lack of root penetration are easily formed. Shultz et al. [252] found that increasing the gap width decreased the attainable maximum joint efficiency, while increasing the welding tilt angle was beneficial to increasing the joint efficiency to a certain degree, but the weld thinning was severe. It is difficult to obtain defect-free joints if the gap is too wide. Wanjara et al. [253] reported that when the thickness of the 6061 Al alloy was 3.18 mm, a gap greater than 0.5 mm resulted in the formation of cavity defects in FSW joints, which was determined to be the critical limit for practical application using serial industrial robots. Yang et al. [254] demonstrated that a gap between the workpieces reduced the effective area of the cross-section around the gap and led to an unsuitable welds. According to the characteristics and types of welding defects, they can be divided into global and local defects. The detailed features, definitions and causes of these defects are listed in Table 7.

Table 8 lists the recent progress for solid-state repairing of welding defects or structural inner defects. The main research objects are focused on lightweight metals, such as Al alloys and Mg alloys, among which the 2xxx, 6xxx and 7xxx series are the most common Al alloys in aerospace and railways, and AZ31 is the most typical alloy. FSR has special advantages for these lightweight metals. Moreover, the FSR of high melting point materials is rare, and few studies are associated with high melting point alloys, which are only 316L stainless steel and CuNi 70/30. This is because the wear of the FSW tool is the critical issue for harder metals with high melting temperatures [256,257] or MMCs [258,259], which is characterized by the deformation and reduction in the pin diameter and morphology. According to results of Rai et al. [143], plastic deformation, abrasion, diffusion and reaction between the environment and the tool materials were the major wear mechanisms that occurred in FSW tools. The welding tool requires higher

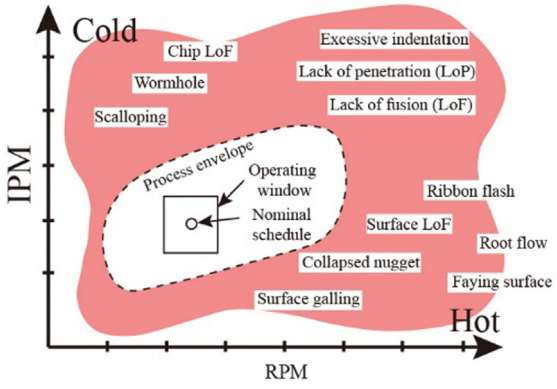
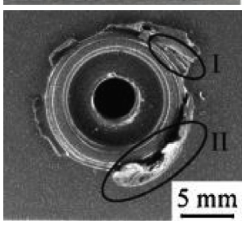
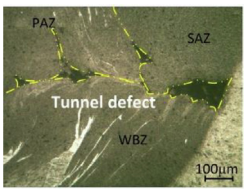
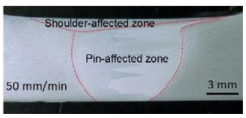
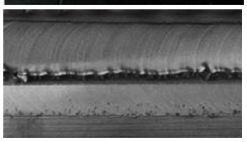
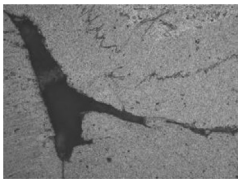
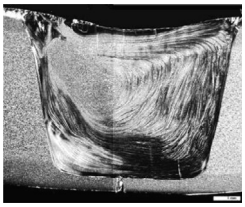


Fig. 64. Forming conditions of several defects [249].

Table 7
Typical defects appearing at the FSW joints.

Defect	Typical view	Definition	Possible causes
Keyhole [248]		A hole matching the shape of the rotating pin	A hole left by the retraction of the rotating pin
Flash [251]		Excessive overflow of materials on top surface leaving a corrugated or ribbonlike effect along the RS or AS	Excessive forge load or plunge depth; Excessively hot weld; Smaller shoulder diameter
Tunnel [255]		Internal cavity along the welding direction	Insufficient material flow; Improper welding tool; Overflow of materials;Smaller plunge depth
Weld thinning [214]		The thickness of NZ is lower than that of the BM	Larger plunge depth; Overflow of materials; Improper back support
Groove [213]		A continuous dented surface characterized by insufficient fill with plasticized materials	Insufficient material flow; Improper back support; Insufficient forge pressure; Overflow of materials
Cavity [160]		Incomplete joining induced by insufficient consolidated and forged materials at the RS	Lower heat input; Excessive travel speed; Insufficient material flow; Improper welding tool
Lack of root penetration [162]		Incomplete joining at the back area of butt plate	Shorter pin length; Smaller plunge depth;Larger fitting gap or manufacturing errors

mechanical properties at high peak temperatures, such as high compressive yield strength, good strength, dimensional stability, creep resistance and good thermal fatigue strength [22,260,261]. Moreover, these materials are usually expensive and difficult to be machined, which are detrimental to the economic benefits and repairing ability. It follows that FSR can be used for many kinds of light alloys and has strong material compatibilities for the main welding or repairing damaged defects in structural parts. From Table 8, it can be concluded that the strength coefficients of the FSR joints all reach 80% of the optimum welding joints or BM, indicating the high-quality repairing. The above-mentioned welding defects or exogenous source-induced defects are prone to causing micro cracks which propagate and severely reduce the load bearing capacity and service life. Scholars in the scientific community and industry have performed extensive investigations in this area. According to the characteristics of the defects, the repairing process is mainly composed of defect detection, location, geometrization, and repairing. In this section, highly efficient and high-quality solid-state repairing is reviewed, which provides technical support and references for the repair of metallic structural parts.

Table 8
Research progress in FSR of materials with main defects and their repairing techniques.

Materials	T (mm)	Type of defects	Repairing methods	Optimum parameters	Maximum tensile strength/ load	Ref.
Al-Cu alloy	3	Shrinkage	Repetitive FSR	w = 900 rpm; v = 150 mm/min; PD = 0.1 mm; T = 2.5°	301.6 MPa	[262]
Al-Zn-Mg alloy	6	Tunnel	Repetitive FSR	w = 800 rpm; v = 300 mm/min; F = 9 kN	207.4 MPa	[263]
304L steel	12	Cavity (gap)	FSR	w = 250 rpm; v = 100 mm/min		[264]
AA6061-T6	3.2	Flashes	Friction stir spot welding	w = 3000 rpm; v = 0.2 mm/s; DT = 0.5 s	4678 N	[251]
AA2219-T87	6	Kissing bond	Repetitive FSR	w = 600 rpm; v = 200 mm/min; PD = 0.2 mm; T = 3°	248 MPa	[265]
AA2219-T87	6	Cavity	Repetitive FSR	w = 800 rpm; v = 400 mm/min; PD = 0.3 mm; T = 3°	235 MPa	[265]
AA2219-T6	7	Groove	Offset FSR	w = 600 rpm; v = 200 mm/min; F = 4.6 kN; T = 2.5°	335 MPa	[266]
AA2219-T6	7.5	Groove	Gas tungsten arc welding (GTAW) + FSW	GTAW: I = 200 A; v = 120 mm/min FSW: w = 600 rpm; v = 200 mm/min; F = 4.6 kN; T = 2.5°	305 BM	[267]
AA6061-T6	4	Gap	Vertical compensation FSW (VCFSW)	w = 2000 rpm; v = 50 mm/min; P = 0.1 mm; T = 2.5°	214 MPa	[213]
AA7N01-T4	4	Gap	VCFSW	w = 2000 rpm; v = 50 mm/min; P = 0.1 mm; T = 2.5°	295.7	[268]
AA2024/AA7075	3.5	Gap	VCFSW	w = 2000 rpm; v = 20 mm/min; P = 0.2 mm; T = 2.5°; FD = 1.5 mm	307.2 MPa	[269]
AA2219-T6	7.8	Keyhole	Filling friction stir welding (FFSW)	FFSW: w = 800 rpm; PD = 0.1 mm; T = 2.5° FSP: w = 800 rpm; v = 200 mm/min; PD = 0.1 mm; T = 2.5°	179.6 MPa	[270]
AA2219-T87	10	Through hole	Friction plug welding (FPW)	w = 7500 rpm; AF = 50 kN; F = 60 kN; Push amount = 5 mm; FT = 5 s	329 MPa	[271]
AA2195-T8	6.35	Through hole	FPW	w = 4250 rpm; A style plug with a shank diameter of 19.1 mm	342 MPa	[272]
AA5456	7.5	Keyhole	FFSW	w = 400 rpm; v = 50 mm/min	91% of defect joint	[273]
316L steel	10	Keyhole	FFSW	FFSW: w = 1500 rpm; F = 35 kN; DT = 9 s	92% of BM	[274]
316L steel	10	Keyhole	Self-refilling FSW	SRFSW1-4: w = 1200 rpm; F = 30 kN; DT = 5 s; SRFSW5-8: w = 1500 rpm; F = 30 kN; DT = 5 s;	643 MPa	[275]
API X52 steel	16	Blind hole	Friction taper plug welding (FTPW)	w = 7500 rpm; F = 35 kN; FT = 5 s; F = 40 kN	Equal to BM	[276]
API 5L X65 steel	30	Blind hole	FTPW	w = 7000 rpm; F = 50 kN; FT = 5 s; F = 40 kN; B = 14 mm	Equal to BM	[277]
CuNi 70/30	3.13	Corrosion hole	Repetitive FSR	w = 1200 rpm; v = 12.7 mm/min; T = 3°	339.4 MPa	[278]
AZ31B	4	Keyhole	Active-passive filling friction stir repairing (A-PFFSR)	w = 1300 rpm; v = 1 mm/min; T = 2.5°; DT = 5 s	189.7 MPa	[243]
AA7N01-T4	4	Keyhole	A-PFFSR	w = 1600 rpm; v = 2 mm/min; T = 2.5°; DT = 5 s	311.1 MPa	[279]
AZ31B	1.5	Circular hole	Drilling-filling FSR (DFFSR)	w = 1600 rpm; T = 2.5°; DT = 20 s; PD = 0.4 mm	217 MPa	[280,281]
AA6061-T6	4.8	Through hole	Refill friction stir spot welding (RFSSW)	w = 2290 rpm; PS = 1.93 mm/s; F = 16 kN	213 MPa	[282]
AA2198–T851	3	Through hole	RFSSW	w = 1000 rpm; PS = 0.85 mm/s; PD = 2.9 mm	78%	[283]
AA7075-T761	6	Through hole	RFSSW	w = 1500–2100 rpm; PS = 0.7–1 mm/s; DT = 2, 4, and 6 s	425 MPa	[284]

Note: Thickness: T (mm); Rotational velocity: w (rpm); Welding speed: v (mm/min); Plunge depth: PD (mm); Forging force: F (kN); Tilt angle: T (°); Dwelling time: DT (s); Current: I (A); Filler width: FD (mm); Axial force: AF (kN); Forging time: FT (s); Plunge speed: PS (mm/s); Burn-off: B (mm).

5.3. Repetitive friction stir remanufacturing

The global defects mainly contain surface peeling, grooves, tunnels, kissing bond, lack of root penetration, surface damage and long cracks induced by the exogenous source. The above defects always appear along a certain direction, curve and depth, which are primarily repaired by repetitive friction stir remanufacturing technologies.

A concept of combining friction stir spot welding and end milling was proposed to remove flashes simultaneously. The removal process of flashes in general has little effect on the mechanical properties of friction stir spot welds, except under very low indentation rates [251]. Li et al. [263] employed repetitive FSW to reduce or eliminate the tunnel defect of Al-Zn-Mg alloy FSW joints and then avoided the stress concentrations, in which the grain size in the repaired region was reduced compared with that in the original NZ. The maximum tensile strength of the repaired joint reached 180.2% higher than that of the original joint with the tunnel defects. Zhou et al. [265] also used repetitive FSW to repair the lack of root penetration and cavity defects in AA2219-T87 FSW joints. To repair the surface groove and tunnel defects, Liu et al. [266] proposed offset FSW to eliminate groove defects in 7.5-mm-thick AA2219 FSW joints, and the offset was used so that the repairing pin was at the location of the defect rather than at the welding centreline. They stated that the offset FSR could effectively eliminate the cavity defect and an obvious aggregation of the hard-brittle phase Al_2Cu associated with the symmetrical FSR, as shown in Fig. 65. A high-quality joint repaired by offset FSR with a tensile strength of 335 MPa was achieved and fractured near the interface between the NZ and the TMAZ, presenting ductile fracture characterized by large dimples. Subsequently, Liu et al. [267] employed tungsten inert gas welding (TIG) and FSW to remove large groove defects that cannot be eliminated by repetitive FSW, in which a high tensile strength equivalent to 70% of that of the BM was achieved and the fracture feature of the repaired joint was partially plastic and partially brittle. Arici et al. [194,195] expounded that the lack of root penetration induced by the low thermal conductivity of medium-density polyethylene (MDPE) was eliminated by double-pass FSW, whereas weld thinning was increased. Saeedy et al. [285] also repaired the lack of root penetration of FSWed HDPE joints by double-pass FSW and then stated that its joint strength was twice that achieved by single-pass FSW. Cabibbo et al. [286] welded AA6082 sheets by double-pass FSW to eliminate kissing bond, in which the second pass was performed on the other side of the sheets. Compared to conventional FSW, the grains and precipitates in the TMAZ of double-pass FSW joints were coarser due to a twice overlapping heat input, thereby leading to poor tensile properties. Although double-pass FSW can solve the lack of root penetration, the surface formation is poor, and weld thinning is serious. Furthermore, the welding process still needs to be further optimized. Widener et al. [287] demonstrated that $SSFSW_2$ with a high rotational velocity can be performed in thin-gauge Al alloys with relatively low process forces, making smaller portable devices possible for repairing applications and achieving high-quality repaired joints without weld thinning.

In addition, when the welding or exogenous defects are relatively large, they easily result in the loss of extremely mass materials, such as large tunnel and groove defects and gap defects induced by either the extrusion effect during the FSW process or the accumulation of some manufacturing errors of large structures that are mismatched. Introducing additional filling materials into these locations is extremely essential. Ji et al. [213,268,288] proposed VCFSW technique to repair these defects and then selected the gap defect as the main research object, as shown in Fig. 66. Additional compensation materials were added to these defects, which were homogeneous materials similar to the workpieces to be repaired. During VCFSW, the rotating tool simultaneously rotated, stirred and mixed the welding workpieces and the compensation materials, realizing high-strength solid-state repairing of defects with large sizes for 6061-T6 and 7 N01 Al alloys, respectively. Moreover, they expounded that employing materials with low melting points and high strength easily achieved high arrangement repairing of materials with high melting points, such as the workpieces to

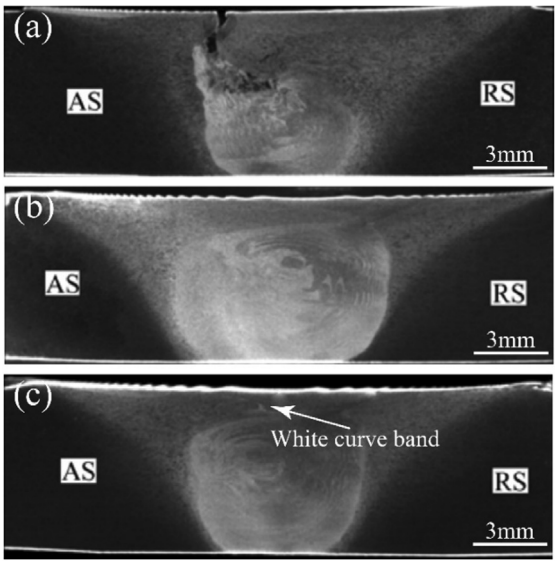


Fig. 65. Morphologies of the initial joints with groove defects and their repaired joints: (a) initial, (b) offset FSR and (c) symmetrical FSR joints [42].

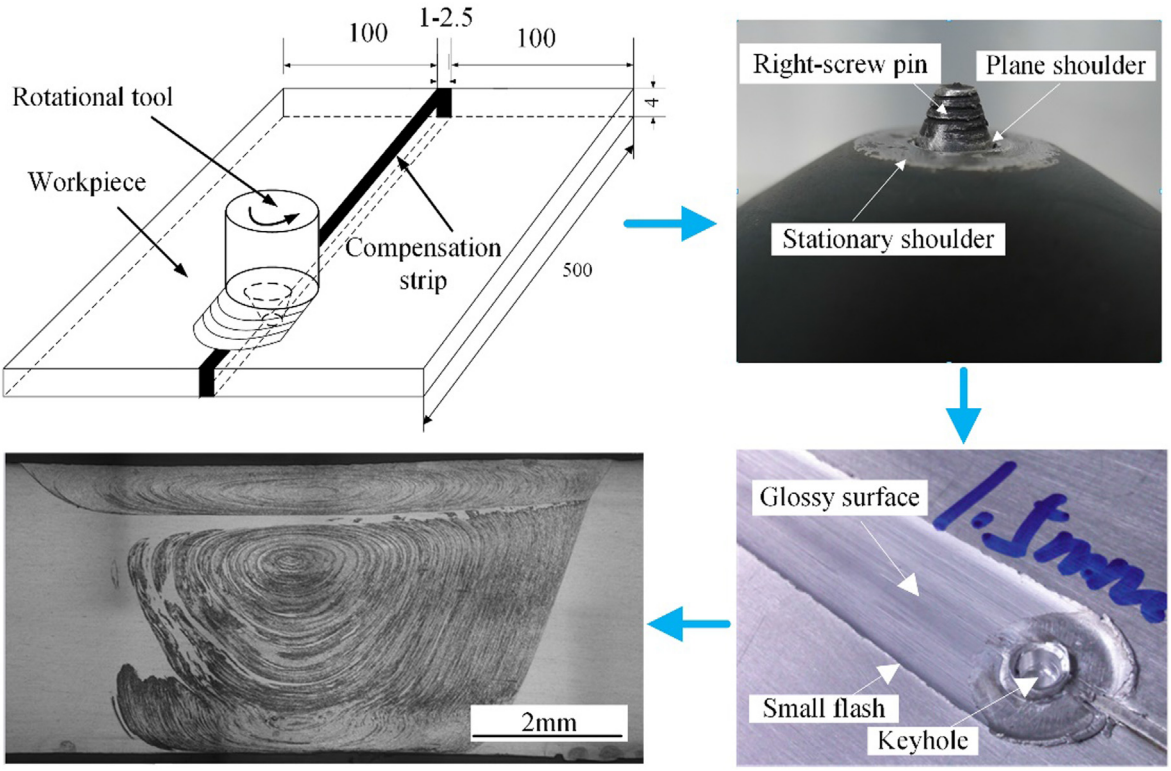


Fig. 66. Schematic of VCFSW [213].

be welded AA6061-T6 and the compensation materials AA2024-T4 [213]. Two vortex-like structures appeared in the SAZ and PAZ, which was similar to the "onion ring" pattern reported in the literature [289]. The forming mechanism of "onion ring" patterns was formed due to loads from both the external and the internal screws at each rotation [290–292]. The formation of the "onion ring" pattern markedly improved the mechanical interlocking and metallurgical bonding, enhancing the mechanical properties. Abu-Okail et al. [269] stated that the quality of the joints welded by VCFSW depended on the ability of compensation materials to fill in and mix with the BM through VCFSW. Sandnes et al. [221] used the HYB process to eliminate the insufficient material feeding induced by the lack of filler materials when strict base plate and profile tolerances were required.

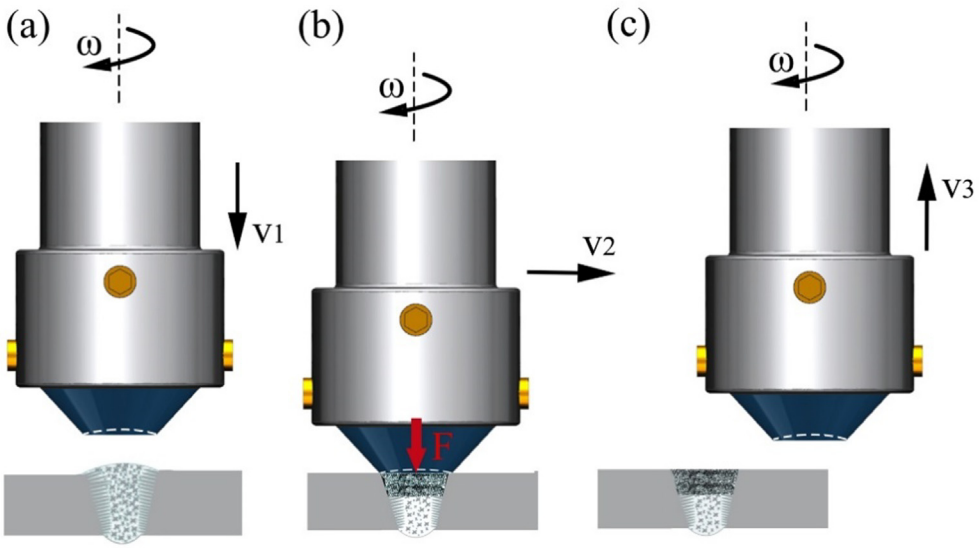


Fig. 67. Keyhole closure technique of TIG filler wire welding with subsequent FSP: (a) TIG filler wire welding, (b) FSP and (c) completion of keyhole repairing.

To eliminate the potential defects and severe joint softening induced by conventional fusion welding and the back-supported body that is needed in additive filling FSW, a hybrid between TIG welding and pinless FSP is proposed by our workgroup, as shown in Fig. 67. TIG welding is responsible for the weld reinforcement in the welding line, eliminating possible defects at the ending stage. Here, a “multi-strand welding wire” technique is used, and the shape and performance control of the filling joints can be realized by several factors, including the composition design, diameter selection, and wire assembly modes. Subsequently, a pinless tool with a special shoulder morphology and diameter is used to modify the microstructure produced by TIG welding, which transforms the coarse casting microstructures into fine and equiaxed forging microstructures, eliminating fusion defects and strengthening the repaired joints. Additionally, by regulating the shoulder topology (shoulder diameter, morphology and angle) and processing parameters (plunge depth/force, rotational velocity, processing speed and tilt angle), the microstructures and mechanical properties can be optimized, which realize the excellent repairing of volume defects.

For materials that have higher melting points than Al alloys, few studies exist due to the high cost and wear of the rotating tool. Mukherjee and Ghosh [278] combined laser-assisted direct metal deposition with FSW to repair corrosion holes in a CuNi 70/30 alloy. This additive FSW process allowed for site-specific filling and repairing of the harmful features in laser-assisted direct metal deposition microstructures, including porosity, large grain size, residual stress and solute segregation. Gunter et al. [264] employed FSW to repair crack defects in 304L stainless steel using a PCBN/W-Re tool, as shown in Fig. 68. Through this process, it was possible to heal a crack that began narrow and then progressively grew up to a width of 2 mm.

During FSW, the material intersecting the path of the pin deformed in a similar manner. As the pin approached, the materials were initially compressed, rotated around the pin, and finally deposited behind the pin at the same transverse position as its beginning (Fig. 69). The typical microstructural evolution of stainless steel during the deformation process could be presented through a microstructural analysis along the centre of the weld path. The final microstructure in the NZ was a result of DRX and some grain growth. FSW of 304L stainless steel resulted in similar levels of dislocation density, as shown in Fig. 70.

For the solid-state repairing methods, the materials around the repairing interfaces experienced severe thermo-mechanical behaviours, which further resulted in the formation of chemical and mechanical bonds at the repairing interfaces. The microstructural evolution and interfacial behaviour significantly influenced the mechanical properties. The macrostructure of the FSW welds was closely related to the workpiece materials, tool design, and offset, as well as welding variables and setup. Good metallurgical bonding may reduce the presence of defects at the repairing interface, while complex mechanical bonding promotes better stress distribution during loading and a more complex crack propagation path [294].

Investigating the interfacial microstructures and healing of the repairing interfaces can provide important references and technical support for the regulation and control of mechanical properties. Current knowledge on the interface characteristics and microstructural evolution of the repaired joint is presented in this section. During the FSR process, the materials in the repairing zone always experienced high peak temperatures and high strain rates, and then DRX occurred, which further resulted in grain refinement or phase transformation. Moreover, severe plastic deformation can improve the mechanical mixing between the filling materials and the workpieces. Ji et al. [262] stated that the casting structure in Al-Cu casting alloy was transformed into fine and equiaxed grains due to DRX, thereby improving mechanical properties.

The main aim behind solid-state repairing is to improve the mechanical properties, corrosion and wear resistance of joints. The mechanical properties mainly include microhardness, tensile strength, yield strength and elongation in addition to impact and fatigue strength. Various strengthening mechanisms contribute to the enhancement of mechanical properties. Parameter optimization and optimal welding setup are essential to produce high-quality repaired joints. Estimation of the microhardness of the repaired joints requires the consideration of contrary parameters, which further influences the tensile properties. On the one hand, severe plastic deformation refines the grain size and then increases the microhardness according to the Hall-Petch relation. On the other hand, high temperatures easily result in annealing of materials [296]. Dislocation density and residual compressive stress are decreased in the annealed materials, leading to a reduction in microhardness. The grain refinement effect dominates the annealing effect [297].



Fig. 68. FSR tool (70% PCBN/30% W-Re) [264].

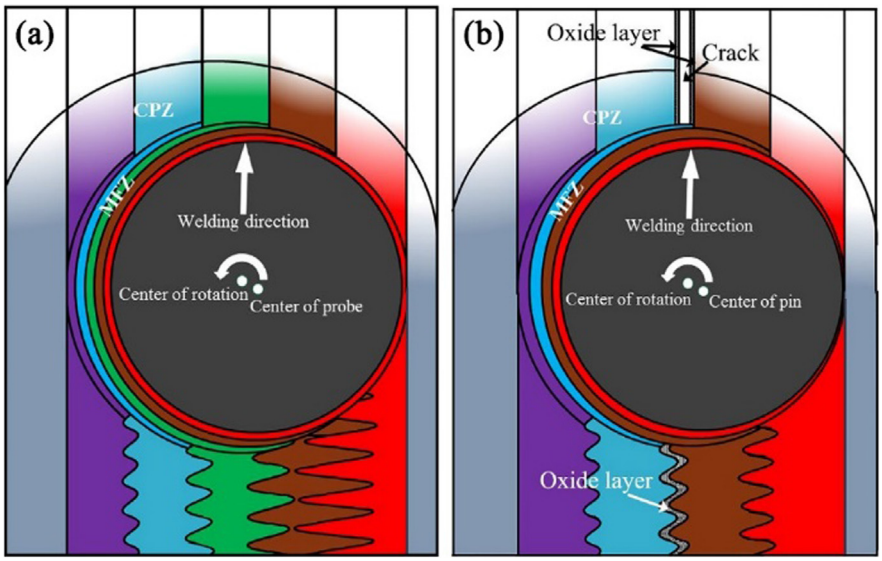


Fig. 69. Pin-driven material flow around the tool: (a) schematic of FSP performed on crack-free stainless steel and (b) schematic of FSP performed along a crack [264,293].

Consequently, the grains are refined during FSR, which increases the microhardness values. Moreover, second-phase particle strengthening is another main factor besides grain refinement contribution. It can be concluded that strengthening is a combined effect of grain refinement and strengthening phases [298]. For Al alloys and interstitial-free (IF) steel, the Hall-Petch relationship fit the data quite well. For commercially pure Ti, the relationship breaks down when the grain sizes are smaller than 6.4 μm, wherein the measured microhardness is higher than that predicted by the Hall-Petch relationship. The lack of correlation to the Hall-Petch effect for fine Ti grains was attributed to the high dislocation density within the grains.

5.4. Additive friction stir remanufacturing

For local volume defects, such as keyhole, cavity and pitting defects, digging and geometrization are the essential procedures due to the irregular distribution inside the parts, in which the loss of materials can be compensated by filling additional materials. In recent years, a series of friction stir-based closure techniques are reported that attempt to transfer the advantages of FSR to closure methods of volume defects. Additive FSR techniques mainly consist of FPW, FTPW, FFSW, and progressive FSW.

5.4.1. Friction plug welding

FPW is proposed to repair keyhole defects, which has been widely reported by relevant researchers. FPW is primarily used by TWI [299] and NASA Marshall Space Flight Center [300,301]. In this process, a taper plug is coaxially forced into a keyhole that has a similar taper. The keyhole is filled with the taper plug by the friction between the taper plug and the surface of the hole. For the FPW joints, post machining is essential to remove the redundant materials of the plug and the materials that flow out of the weld. According to the load pressure, FPW is divided into friction push plug welding and friction pull plug welding, as shown in Fig. 71 [42].

Friction push plug welding was first introduced by Lockheed Martin to repair the defects of AA2195 FSW joints in 1995, replacing manual TIG welding. Subsequently, Lockheed Martin, TWI and NASA optimized the welding parameters for a more robust process [300–302]. Friction push plug welding has become an effective repairing method in rocket tanks. During welding, excessive force on the taper plug pushes the plug into the hole, forming a compact joint. Friction push plug welding has many advantages characterized by (1) a plug unit located in front of the workpieces and withdrawing compressive stress and (2) a wide process window, high welding stability and qualified welding rate. This method is unsuitable for enclosed structures because the rigid backing plate has to withstand a great welding force. The published references have reported that a larger plug diameter in relation to the hole diameter is much more effective in repairing defects. The main process parameters affecting the friction push plug welding process and its welded joints are rotational velocity, axial force, forging force, push amount, forging time and plug morphology. A tapered plug can make the flow direction change instantly from the upper surface to the lower surface of the sheet. Metz et al. [272,303] studied the microstructures, hardness and fatigue properties of 2195-T8 FPW welds. A typical weld can be classified into six regions (Fig. 72): plug metal, plug thermo-mechanically affected zone, plug recrystallized zone (PRZ), TMAZ, HAZ and BM. The hardness variations in these zones may control the fatigue behaviour of the joints. The TMAZ that is close to the bonding interface is the weakest location of the joint due to the dissolution of precipitates and the redistribution of constituent particles. The repaired joints sustained reductions in both the tensile properties and the fatigue life when compared with the FSW joints. The reduction in fatigue life is most likely due to the complication of the weld geometry, the interacting HAZ and the strength mismatch between the BM, the FSW joint and the plug

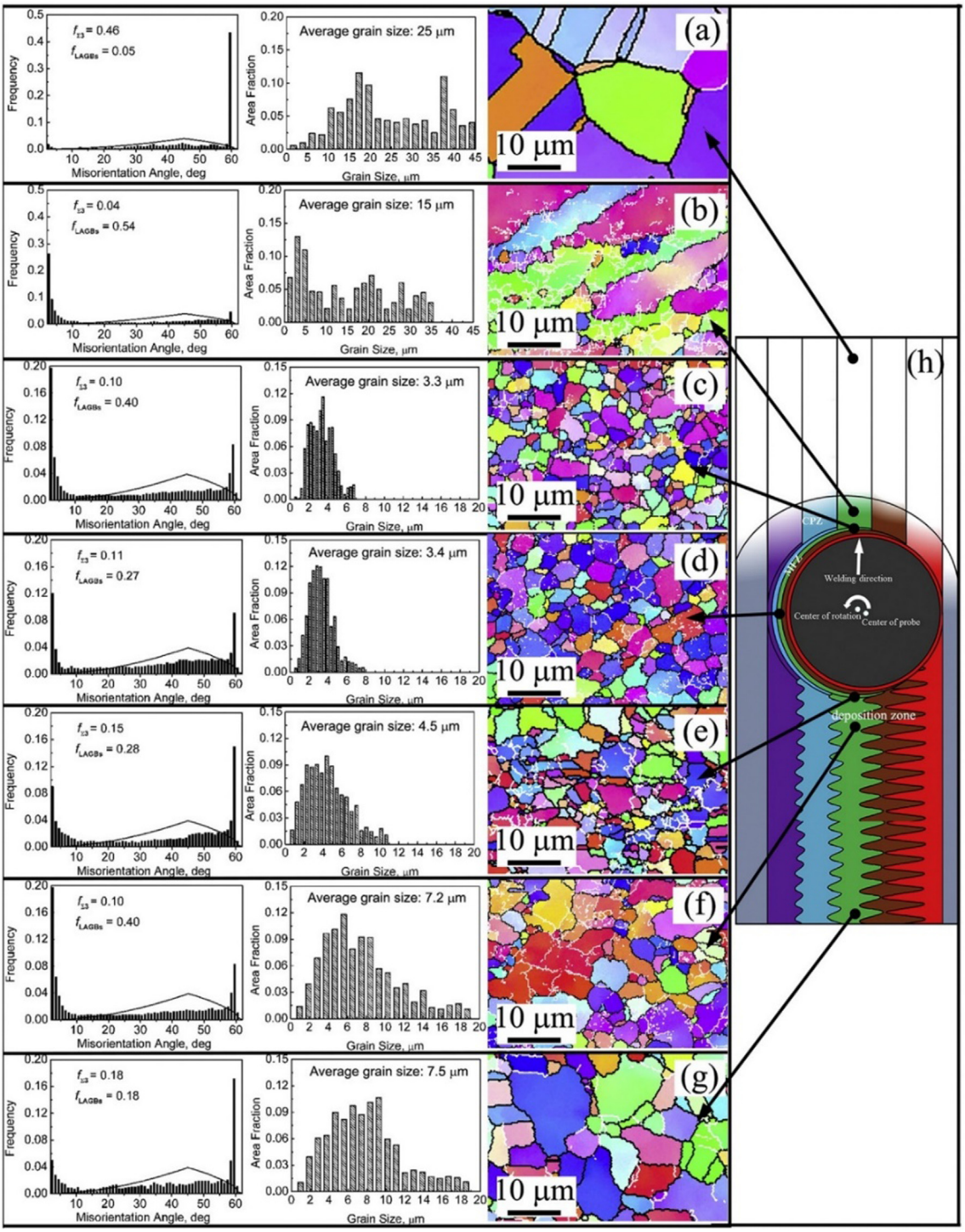


Fig. 70. Grain structure evolution in 304L stainless steel during FSW [295].

materials [272].

Michael Lange et al. [305] studied the bending, tensile and thermal characterization of AA2024-T3 plug welds. Defect-free joints were successfully achieved with optimized parameters. At the beginning of the tensile stress application ($t \leq 20$ s), the joint was under the elastic deformation stage, exhibiting uniform elastic strain across the plug joint (Fig. 73).

When the global strain reached 0.18% ($t = 35$ s), the strain concentration could be examined initially near the TMAZ. A slight plastic deformation occurred in the HAZ but was not obvious in the BM. With conducting the tensile process, the stress showed a fast

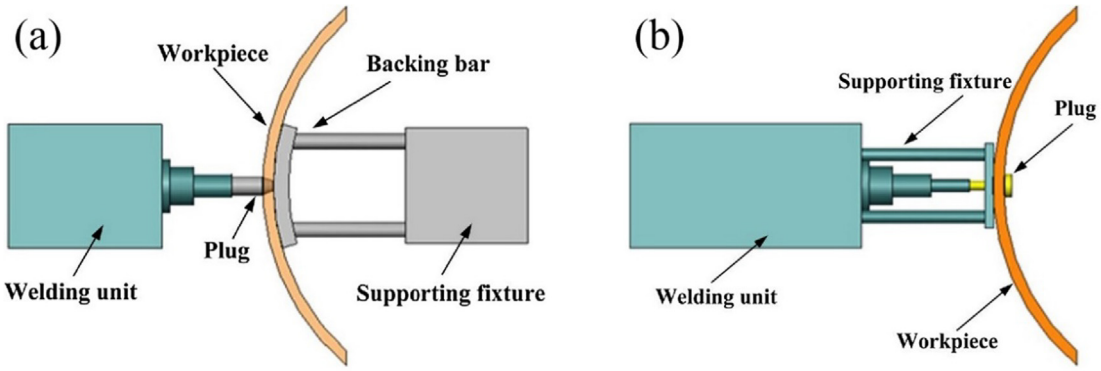


Fig. 71. Schematics of FPW: (a) friction push plug welding and (b) friction pull plug welding [42].

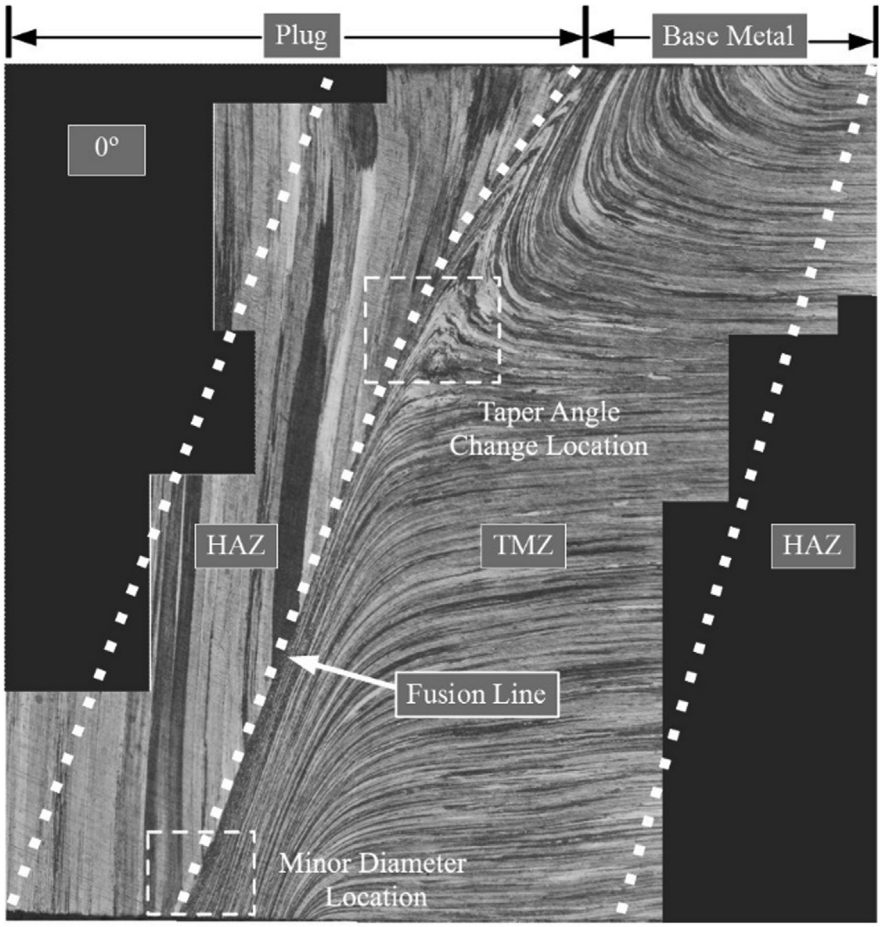


Fig. 72. A typical weld [304].

and linear increase accompanied by a slow extension of the plastic deformation zone. When the global strain reached 0.86%, yield occurred in the joint with necking. When the global strain reached 5.08%, the joint fractured with a local strain of 6.8% in the TMAZ. By optimizing the design of joint geometry, the maximum tensile strength of the repaired joint of AA2219-T87 reached 329 MPa, which is approximately 72.3% of that of the BM [271].

Friction pull plug welding was proposed and patented by Paula Hartley and Riki Takeshita from Lockheed Martin [42]. It was originally received as a key technique for the external tank of the space shuttle and the keyhole in BT-FSW [307], as indicated in Fig. 74 [308]. The welding equipment of friction pull plug welding is located on one side of the workpieces, which requires a simple fixture without rigid backing plates, indicating that friction pull plug welding is more suitable for enclosed complicated structures

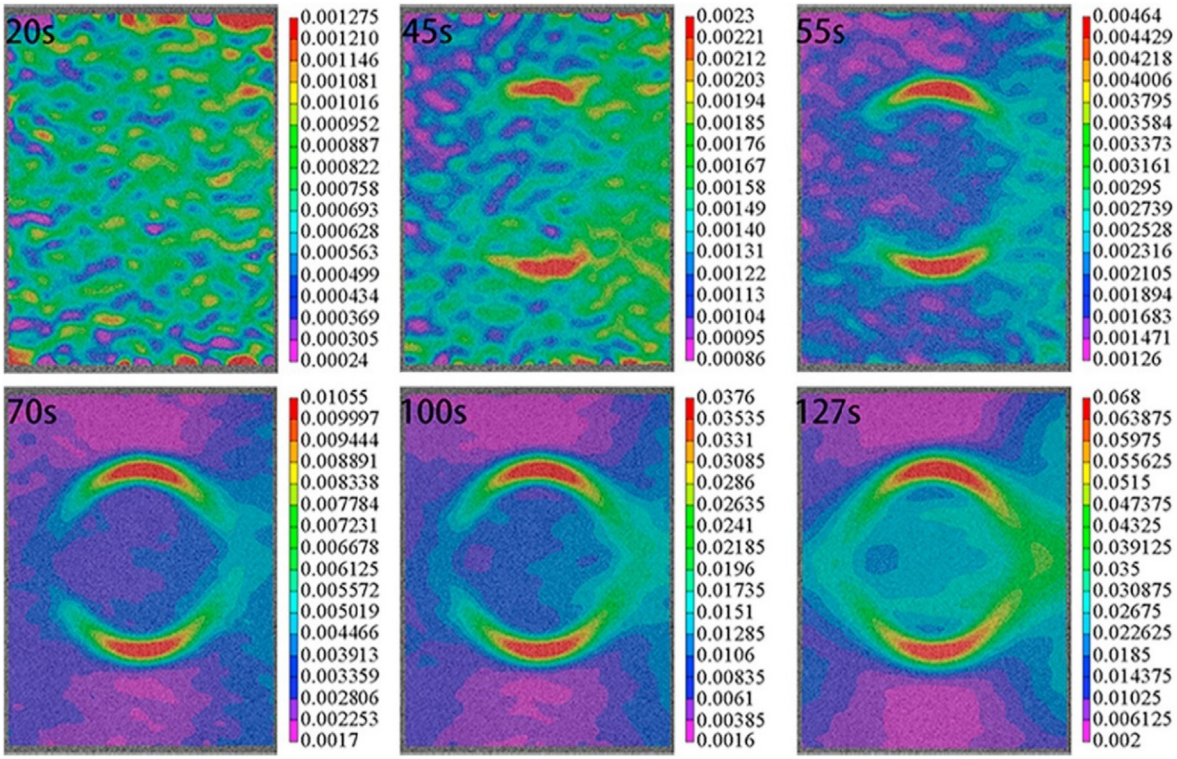


Fig. 73. Strain maps of a plug joint at different times during a tensile test [306].

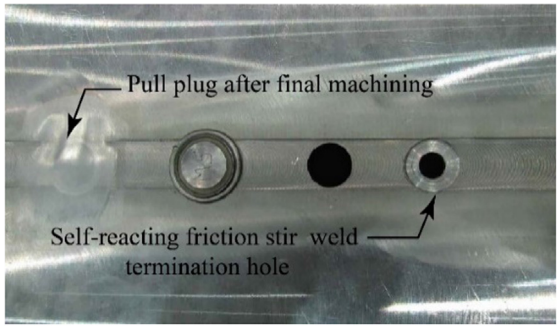


Fig. 74. Friction pull plug weld operations [308].

than friction push plug welding. The narrower process window in the friction push plug welding results in lower joint quality and less welding stability than that in the friction push plug welding. The friction pull plug welding process was applied to 4-mm-thick AA2219. By appropriate selection of the welding parameters and joint configuration, the tensile strength reached 330 MPa or above, which was equal to or even greater than that of the FSW joints.

5.4.2. Friction taper plug welding

As a new and promising solid-state repairing technique, FTPW was proposed and has been widely investigated, which has the feasibility and potential to repair underwater metal structures, pipes and thick section materials or seam thick plates or components [309,310]. Pauly and Nicholas [311,312] defined that FTPW was a hole filling process that involved drilling a blind hole and then forcing a consumable plug into the hole coaxially, similar to FPW. A schematic of the FTPW process is shown in Fig. 75. Synergistic effects between frictional heat and forging force led to the plug materials to be softened and flow continuously, and then the blind hole could be filled. After completing the plug consumption process, another axial forging force was applied immediately to forge the materials in the weld [313]. FTPW joints were mostly fabricated in underwater wet conditions, and the repairing interfaces exhibit as-forged microstructures without hydrogen-induced cold cracks [314–316]. Characteristics of the basic welding parameters have been described in previous investigations and are reviewed in Meyer and Ambroziak's works [317,318].

Thorough insight into material flow and heat generation in different welding conditions is of practical importance for the

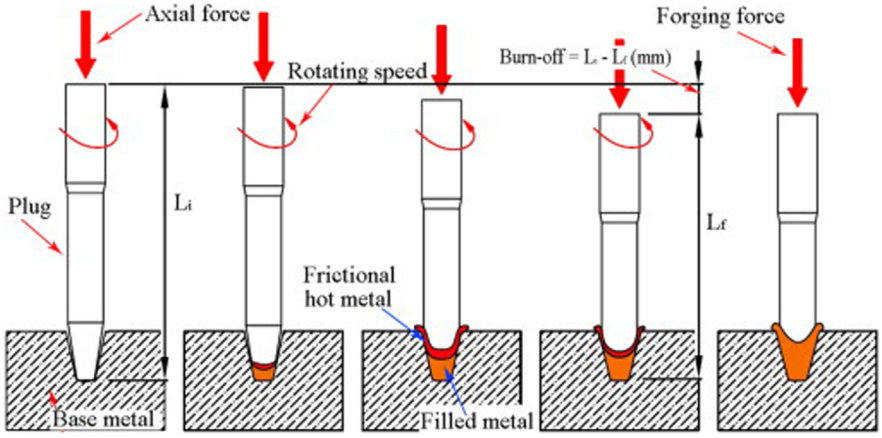


Fig. 75. Schematic of the FTPW process [319].

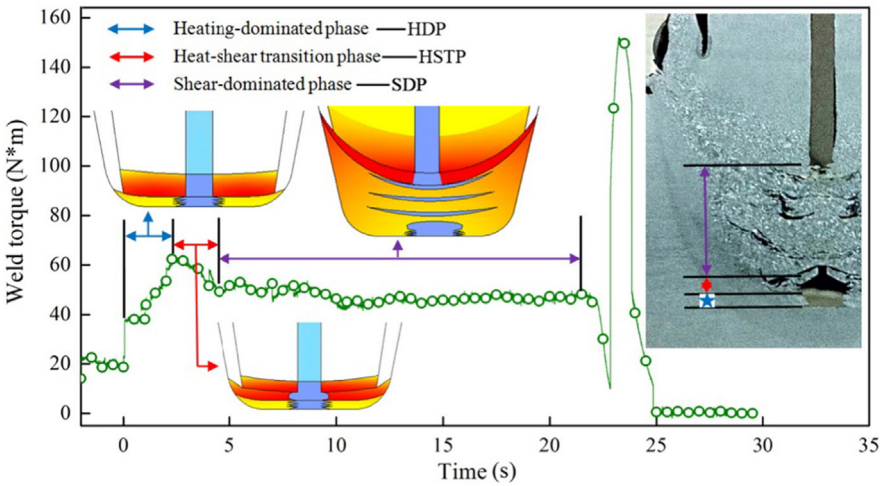


Fig. 76. Relationship between material flow behaviour and torque variation [277].

comprehension and elimination of welding defects. Yin et al. [277] showed the typical plug material flow behaviour with the variation in weld torque during the FTPW process, which contained a heat-dominated phase (HDP), heat-shear transition phase (HSTP) and shear dominated phase (SDP), as shown in Fig. 76. The HDP was defined as the time between the start of the weld and the point where substantial plastic shear occurred, which resulted in a substantial drop in peak torque. In the SDP, the torque stabilized at a considerably lower plateau level for the remainder of the weld. Under the severe heat dissipation caused by both cold workpieces and the water environment, a stable temperature field and heat input could hardly be established. The plug material flow was not sufficient to fill the hole, further forming effective bonding with the hole sidewall. Nevertheless, at the end of HDP, a certain amount of plasticized material accumulated at the plug frictional plane and pressed to the gap between the plug and BM at the start of HSTP. This “pressing behaviour” was reflected by the drop in weld torque and demonstrated by the Ni tracer since a significant amount of Ni was removed from the centre over a relatively larger area, especially under higher axial force. As the SDP began, a regular plug consumption process that was dominated by regular shear off of the plug and deposition was established. The weld torque was maintained at a quasi-stable level that was smaller than that in the other phases. Considering the severe heat dissipation and poor material flow at the HDP and HSTP, increasing material flow and the heat input during both phases was believed to be practical to eliminate root defects. Moreover, the material flow in the SDP was uniform and extensive. This should be the reason why incomplete filling defects never occur at the sidewall when the axial force is sufficient (higher than 20 kN).

The main process parameters affecting the FTPW process and its welded joints are rotational velocity, axial force, forging force, push amount, forging time, burn-off and plug morphology. Meyer and co-workers [317] found that the bonding qualities and properties of FTPW welds were significantly influenced by the weld geometry, rotational velocity, and axial force. However, the influences of the forging force and forging time were less substantial. Hattingh et al. [316] found that for AISI 4140 steel, a maximum tensile strength of 94% of that of the BM could be obtained with the following parameter combination: 6000 rpm rotational velocity, 11.7 kN axial force and 9.0 mm burn-off. The measured tensile strength and ductility were nearly equivalent to those of the BM owing to the overmatching of the welds. In Charpy impact tests, the properties would match the requirements of the standard for marine

applications [317]. Chludzinski et al. [320] found that the fracture toughness of the weld was much lower than that of the BM. The varied axial forces could rarely influence the fracture toughness. Cui et al. [321] determined that a lack of bonding and incomplete filling defects were found, which easily formed under the combination of low rotational velocity and low welding force. High-quality joints were obtained at rotational velocities up to 7000 rpm and welding forces ranging from 25 to 40 kN. It can be concluded that superior FTPW joints can be achieved by regulating and controlling the welding parameters. A high rotational velocity and a larger axial force than conventional FSW are necessary.

5.4.3. Filling friction stir welding

Huang et al. [248,270,322] proposed FFSW to repair similar keyhole volume defects, as shown in Fig. 77. The FFSW process was performed in three main steps: friction stage, stirring stage, and joining stage. First, the FFSW depends on a friction process, where a semi-consumable bit contacts the wall of the keyhole, rubs against the inner surface of the keyhole and self-cleans the bonding surfaces (removal of oxidation). Second, a stirring step, where the semi-consumable bit is plunged into the keyhole and the rotating shoulder made of steel contacts the upper surface of the workpieces, generates frictional heating at the interface between the bit and the wall of the keyhole. The materials surrounding the keyhole and the bit are plasticized and stirred, while severe plastic deformation and flow of the plasticized materials occur. The joining step follows, while the bit and the materials surrounding the keyhole are heated by frictional heat. With the combined functions of softening and torque, the joining bit is sheared and fractured at the corner of the shoulder, becoming the filler material to repair the keyhole.

Figs. 78 and 79 show detailed images of the FFSW tool and joints. The welding tool is composed of a semi-consumable bit and a steel shoulder (Fig. 78).

The keyhole defect can be successfully filled (Fig. 79). In the following FSP, a non-consumable tool consisting of a pinless shoulder provides mechanical mixing and plastic deformation. Moreover, the flash around the filled keyhole was abraded and stirred. The semi-consumable bit and materials surrounding the keyhole have been metallurgically bonded very well. A classical formation of the elliptical “onion ring” structure parallel to the interface formed in the transition between the filling zone (FZ) and the TMAZ [248]. Mechanical interlocking is also the main bonding mechanism in dissimilar FSW joints that rely on forming a complicated geometry at the bonding interface to enhance mechanical strength. During the FFSW process, as the bit keeps inserting downward into the keyhole, the bit head begins to contact the zigzag structures on the keyhole surface. Material deformation and fierce attrition occurred at the contact region. Additionally, some of the superficial bit materials were stripped off and fell down into the bottom of the keyhole, resulting from the relatively lower hardness (96 HV) and the keyhole friction. As a result of the features of the FFSW tool, the materials at the bottom of the FZ experienced relatively gentle stirring and insufficient heating, especially compared with the NZ, and defects such as cavities and flaws are easily formed at the interlayer or interface between two adjacent layers. These problems can be solved by regulating and controlling the welding parameters in the FFSW.

The main process parameters in the FFSW process are rotational velocity, plunge speed and bit conicity degree for semi-consumable bits, though other variables such as welding speed, shoulder diameter, tilt angle, deep indentation depth for the rotating shoulder, and plate conditions may also influence the repair quality. The length of the bit should be 2–5 mm higher than the depth of the keyhole, which can guarantee sufficient filling of the keyhole. The bit conicity degree is always lower than that of the keyhole defects. Behmand et al. [273] discussed that an unsuitable geometry caused incorrect contact at the pin/exit hole faying surface, while sufficient friction and stirring were not attained. A low plunge speed is beneficial to sufficient plastic deformation at the repairing interface and improves metallurgical bonding. Moreover, the harder the semi-consumable bit is, the more severe the plastic deformation in the repairing interface and the higher the joint quality. Huang et al. [322] reported that when employing an AA2219 bit to repair the keyhole defect in AA2219 FSW joints, the average ultimate tensile strength and elongation were 172 MPa and 11.22%, which corresponded to 90% and 82% of those of the base weld without defects, respectively. Huang et al. [248,270] also repaired the keyhole defect of AA2219-T6 FSW joints by choosing an AA7075-T6 bit whose hardness was higher than the workpieces to be repaired. The maximum ultimate tensile strength and elongation of the FFSW joint were 179.6 MPa and 13.7%, which corresponded to 96.6% and 99% of those of the original defect-free FSW joint, respectively [248]. Behmand et al. [273] applied FFSW to repair a 6.5-mm-deep exit hole in AA5456 FSW lap joints. The failure load on the coupons with the refilled keyhole reached 91% of

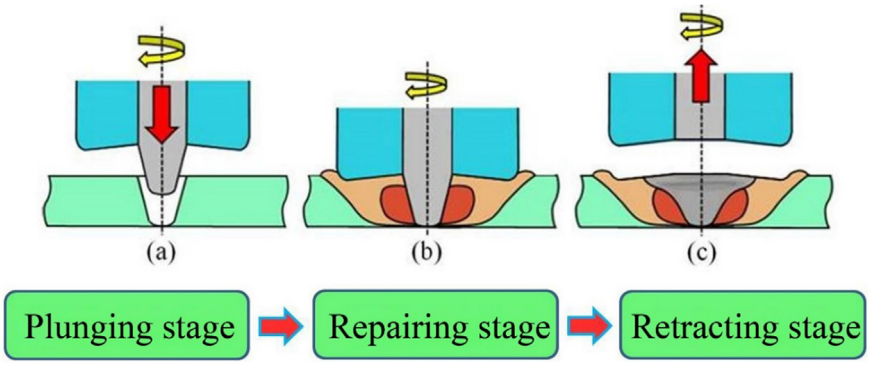


Fig. 77. Schematics of FFSW: (a) plunging stage, (b) repairing stage and (c) retreating stage.

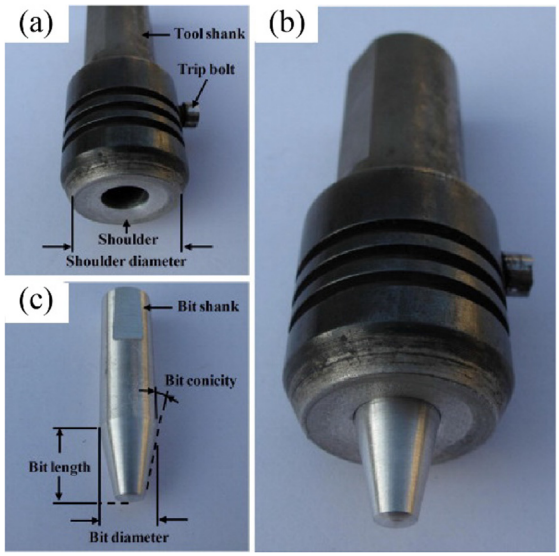


Fig. 78. Features of the FFSW tool: (a) steel shoulder, (b) AA7075 bit and (c) assembled semi-consumable FFSW tool [248].

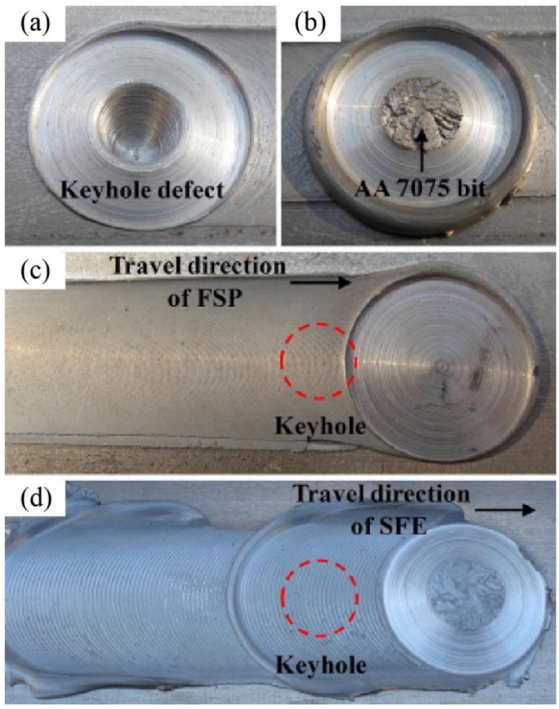


Fig. 79. Detailed images of FFSW: (a) keyhole defects, (b) repaired keyhole, (c) repaired keyhole after FSP and (d) repaired keyhole after SFE [248].

that of a corresponding defect-free FSW joint. It can be concluded that quasi-equivalent mechanical performances without weld defects have been achieved by the FFSW joints with excellent interface and mechanical properties. Based on the technical advantage of FFSW, Yan et al. [323] successfully joined ABS sheets and stated that high joint strength was achieved when using a large plug diameter, a moderate plug length and a blind hole depth. In contrast, spot welds with small plug diameters, excessive plug lengths or large blind hole depths exhibited pores and cavities in the vicinity of the joining interface.

Zhou et al. [274] reported that void defects were formed at the bottom of the refilled original conical keyholes for all the tool design and process parameters used for 316L stainless steel. A refilled joint with a defect-free interface could be obtained on the modified spherical keyhole using the corresponding filling tool under processing parameters of 35 kN, 1500 rpm and 9 s. The microstructures surrounding the interface and in the refilled zone were significantly refined for all the refilled joints. Tensile test results showed that the tensile specimen fractured at the BM. The relative tensile strength and elongation were 105% and 92% of

those of the as-received plate, respectively. Zhang et al. [324] modified the FFSW method using a pinless tool and a T-shaped filler bit to reduce the setup time for replacement of the tool between the filling and reprocessing operations. For a cylindrical bit, the failure loads were sensitive to the *in-situ* friction time. When the *in-situ* friction time exceeded 5 s, the filled samples exhibited favourable failure loads. They sealed keyholes left by FSW in 4.7-mm-thick AA1060 sheets. To eliminate voids in the lower portion of the joint, a Zn brazing foil was preset in the keyhole. The ultimate tensile strength of the keyhole closure welds reached 67.3% of the BM strength [324]. Until now, FFSW has been shown to repair keyholes left by a conical FSW tool, for which the geometry of the filler bit must be adapted and has not yet been applied to through holes. Moreover, FFSW is still in its infancy, and further investigations are necessary for its evaluation and application in manufacturing fields.

For dissimilar materials without metallurgical reactions, our research group proposed friction-based filling stacking joining (FFSJ), which is similar to the principle of FFSW, to fill the keyholes of polymer and metal FSLW joints, as shown in Fig. 80 [325]. The FFSJ was completed by filling a prefabricated hole with an additional filling stud. An excellent FFSJ joint was successfully achieved under the combined effects of frictional heat and thermo-mechanical behaviour at the interface between the filling stud and the polymer sheet. Intimate contact formed at the interface between the filling stud, the polymer and the metal, and the metal hole was completely filled with the stud. The maximum tensile shear strength of 13 MPa for the FFSJ was comparable to that produced by state-of-the-art welding. The fracture location of the FFSJ joint is located at the joining interface between the filling stud and the re-solidified polymer sheet.

5.4.4. Progressive friction stir welding

Progressive FSW is different from the other filling FSW methods employing a consumable bit, whose principle is that the materials surrounding the keyhole are used to fill the volume defects and reduce the depth of the keyhole. To improve the filling of the volume defect completely, an additional filling piece is necessary.

Pinless FSW is a solid-state joining technique based on the material transfer induced by severe plastic deformation that can realize the high-quality joining of thin sheets lower than 2 mm [326–328]. Based on the concept of friction-induced plastic flow, the keyhole of FSW joints in thin-walled sheets could be repaired. The main factors affecting the joint strength are shoulder morphology,

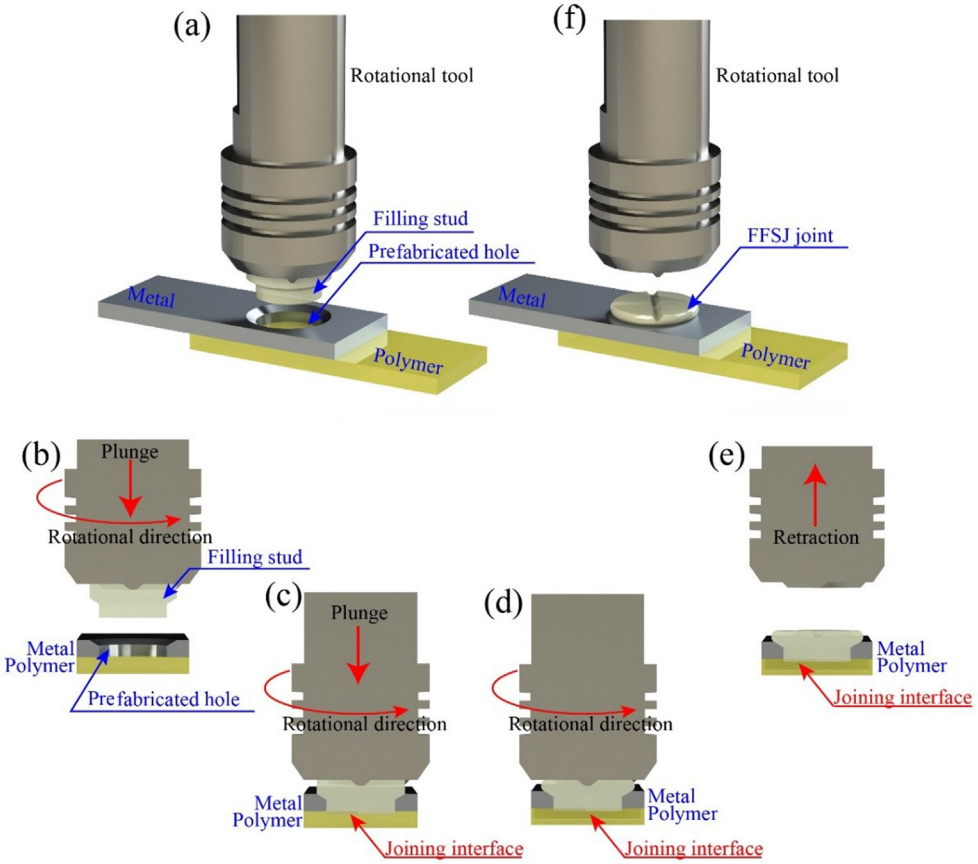


Fig. 80. Schematic of the FFSJ process: (a) positioning of the filling stud in the prefabricated hole; (b) rotation and plunge of the rotating tool and the filling stud; (c) the filling stud approaches the polymer sheet while the filling stud and polymer sheet are melted near the joining interface; (d) the rotating tool stops plunging and continues rotating for 1 s, then the tool stops rotating and the molten polymer begins to solidify; (e) the rotating tool retracts and the molten polymer continues to solidify; and (f) the hybrid FFSJ joint is achieved [325].

rotational velocity, plunge depth and dwelling time. Venukumar et al. [329] reported that a convex shoulder tool was better than a concave shoulder tool due to the complete elimination of insufficient refilling. Sajet et al. [330] reported that rotational velocity has the strongest effect on welding strength. Dwelling time has a minimum effect on the strength and maximum displacement of conventional joints and nearly no effect on refilled joints. The order of importance for parameters that affect conventional joints is rotational velocity > tool plunge depth > dwelling time. Huang et al. [280] proposed a DFFSR technique to repair the volume defects in lightweight AZ31B Mg alloy with an additional filling plug and a pinless tool. An optimized joint with a maximum tensile strength of 217 MPa was produced, which fractured at the TMAZ rather than at the interface between the filler and the BM. Niu et al. [281] employed a non-rotating shoulder to assist the PFFSR and then obtained a uniform microhardness distribution along the whole repaired region. However, the effective depth of the pinless FSW is limited to 2 mm or even smaller.

Self-refilling friction stir welding (SRFSW) was proposed by Zhou et al. [275] to seal the keyhole left by FSW in stainless steel, as shown in Fig. 81. This multistage process used a series of non-consumable tools with gradual changes in pin geometry and size. Similar to the results of Ji et al. [243], based on the constancy of the material volume, a narrow and deep keyhole was filled and changed to a wide and shallow exit hole remaining at the surface due to the lack of filler materials. SRFSW is not applicable to through holes and has not been verified to work in Al alloys. This approach can also avoid preparing a specific tapered through hole in a plate, such as that required in the FPW/FTPW processes, thereby providing better adaptability for the actual working conditions.

Based on the advantages of SRFSW [275] and pinless FSW [280], Ji et al. [243,279] proposed the A-PFFSR method to fill keyhole-based volume defects based on a series of non-consumable pinless tools and additional filler materials. A schematic diagram of the A-PFFSR process is shown in Fig. 82. The A-PFFSR process was divided into two parts: active filling (AF) and passive filling (PF). The keyhole could be repaired in several steps using different pinless rotating tools with different diameters. The keyhole in the AF process was filled with the materials surrounding the keyhole. The additional filler materials used in the PF process were the same as those used in the BM process. The diameter of the additional filler materials was the same as that of the rotating tool used in the last step, and the height was higher than the depth of the unfilled keyhole. During the AF and PF processes, the filler materials were heated and plasticized by frictional heat generated by the pinless tool. Under the stirring effect of the rotating tool, sufficient material flow behaviour can be produced, which can effectively fill the keyhole. In addition, the forging force provided by the rotating tool was beneficial to solid-state bonding between both filling layers. Significantly, to repair keyholes successfully and obtain high-quality joints, the optimum selections of the welding parameters (rotational velocity, plunge depth, tilt angle, plunge depth) and other variables (shoulder diameter and morphology and the filling piece size) were very important. Ji and his co-workers [233] stated that a six-spiral-flute shoulder was designed to improve the material flow and eliminate the interfacial defects, in which six-spiral flutes were distributed across a greater proportion of the shoulder. During the PF process, to obtain surface formation and reduce or even eliminate the possibility of kissing bonds, the pinless rotating tool moved forward along the welding direction after dwelling for 5 s. They reported that the tensile strength and elongation of the repaired joint reached 189.7 MPa and 7.6% at a constant rotational velocity of 1300 rpm and a plunge speed of 1 mm/min, which correspond to 96.3% and 98% of those of the defect-free FSW joint, respectively. The diminished plastic deformability after repairing the FSW keyhole in the 4-mm-thick AZ31B Mg alloy sheet occurred due to the limitation of the number of slip systems of the hexagonal close packed crystal lattice. The mechanical properties of the A-PFFSR joints increased as the rotational velocity increased from 1000 rpm to 1600 rpm. When the rotational velocity was 1600 rpm and the constant plunge speed was 2 mm/min, the tensile strength and elongation of the repaired joint reached maximum values of 311.1 MPa and 7.6%, which correspond to 82.1% and 95.8% of those of the defect-free FSW joint, respectively. It can be concluded that the solid-state repairing techniques, the severe plastic deformation and low peak temperature occur in the repairing interface, which can improve the interfacial bonding, and then achieve the repaired joints with quasi-equivalent strengths.

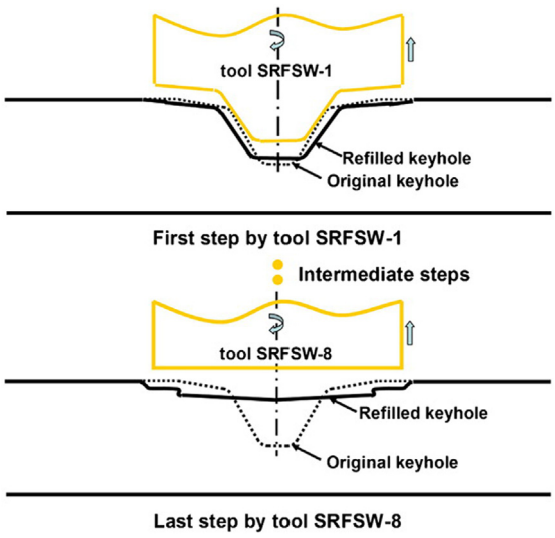


Fig. 81. New technique of SRFSW [275].

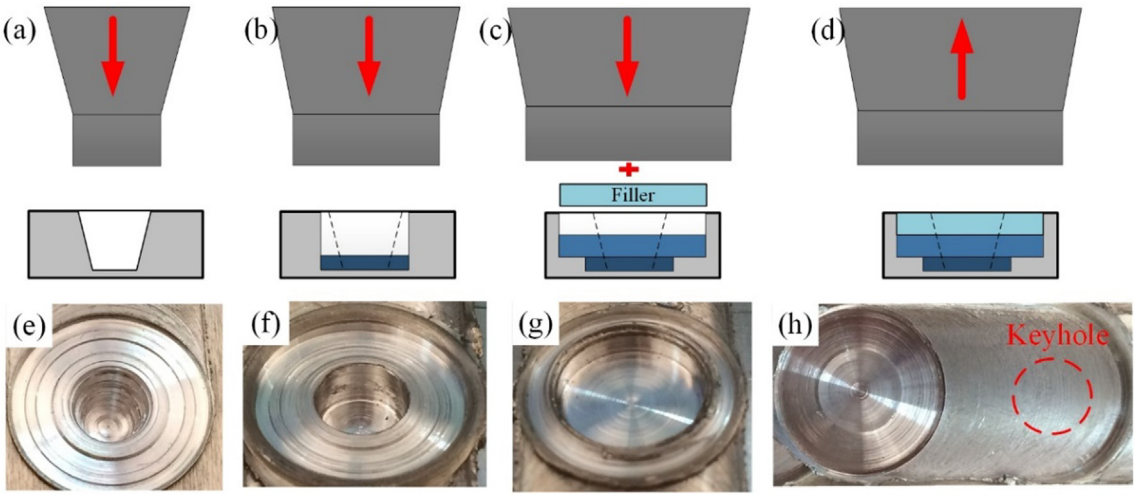


Fig. 82. Schematics and joint formations of the A-PFFSR process: schematics of the (a) first AF, (b) second AF, (c) PF and (d) completion of A-PFFSR; joint formations of the (e) keyhole, (f) after first AF, (g) after second AF and (h) after PF [243].

5.4.5. Refill friction stir spot welding

RFSSW, a solid-state spot welding process invented and patented by Helmholtz-Zentrum Geesthacht [331], was developed as an alternative to riveting or conventional fusion welding techniques to fabricate similar or dissimilar material joints, such as Al/Al alloys [332–335], Mg/Mg alloys [336], Al/Mg alloys [337], polymers/polymers [134,338,339] and polymers/metals [340–342]. The RFSSW tool consists of a clamping ring, a sleeve, and a pin, as shown in Fig. 83 [33]. The clamping ring does not rotate during welding. The main function of the clamping ring is to keep the sheets tightly joined and prevent the plasticized materials from escaping. The clamping ring always has a large diameter. The main components stirring the materials are the pin and the sleeve. Hence, both the pin and the sleeve have threads on their outer surfaces (Fig. 83). A clearance fit is used when assembling the three components to avoid their direct connections. The RFSSW process is mainly divided into four steps. In the initial step, the front surface of the rotating tool parts initially contacts the surface of the plate, generating frictional heat. In the second step, the sleeve plunges downward, displacing the materials that flow into the cavity underneath the retracting pin. In the third step, the pin moves downward and the sleeve retracts, pushing the softened materials back into the weld. In the final step, the tool retracts from the workpieces, leaving the plug and surrounding workpieces joined.

The main parameters controlling microstructures and subsequent mechanical properties are the pin morphology, rotational velocity, plunge speed and heat treatment for precipitation-hardened Al alloys. Defect-free joints were fabricated using a modified tool with three grooves or notches in the tool sleeve, which improved metallurgical bonding, material intermixing and mechanical interlocking at the interface compared with the standard sleeve with a flat surface, as shown in Fig. 84 [332]. With increasing tool wear, more materials are pressed into the gaps between the tool parts. This leads to larger required torques and forces and higher temperatures [343]. Based on numerical simulations, Ji et al. [344] studied the effects of welding tool morphology on heat generation and material flow, as shown in Fig. 85. They found that a large sleeve diameter increased the heat input and joining area, while an extremely high heat input was detrimental to the joint quality. The groove on the sleeve improved the material flow behaviour. The threaded groove on the sleeve walls or the unclosed groove on the sleeve bottom is more suitable for increasing the flow velocity along the vertical direction.

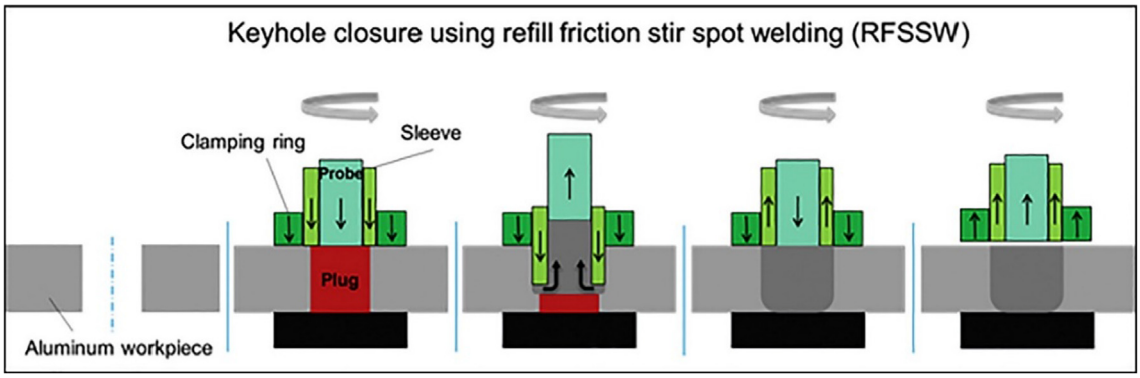


Fig. 83. RFSSW keyhole closure process [282].

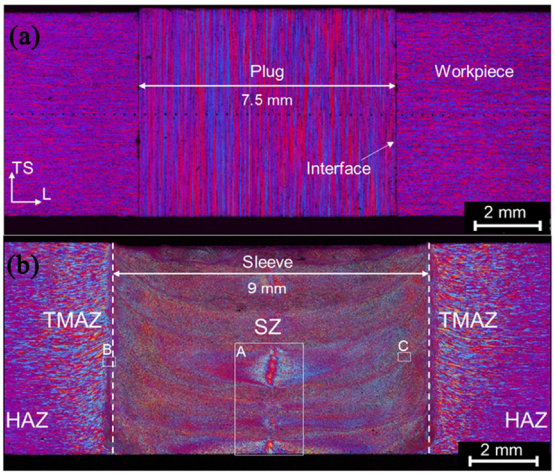


Fig. 84. Low-magnification overviews of unwelded and welded samples: (a) unwelded cross-section with extruded plug and surrounding workpieces and (b) typical appearance of the welded sample [284].

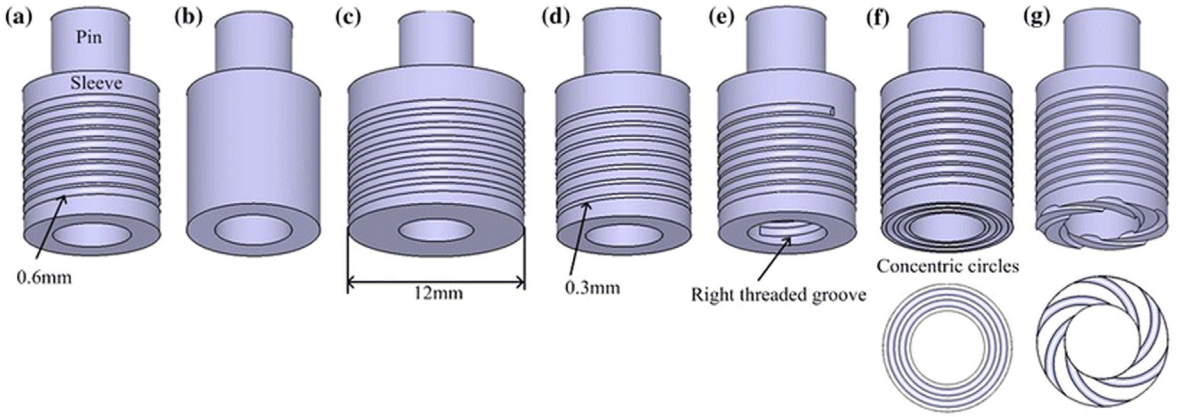


Fig. 85. Tool models in the simulation process: (a) regular tool, (b) tool with a smooth surface, (c) tool with a large-diameter sleeve, (d) tool with a smaller groove width, (e) tool with a groove on the inner sleeve surface, (f) tool with concentric circles on the sleeve bottom and (g) tool with a scrolled groove on the sleeve bottom [344].

Reimann et al. [282] employed RFSSW and a plug as filler materials to seal through holes in 6-mm-thick AA6061-T6 workpieces. The RFSSW joints reached 68% and 55% of the ultimate tensile strength and yield strength of the BM, respectively. Later, Reimann et al. [283] applied RFSSW for termination hole closure in BT-FSW joints in 3-mm-thick AA2198-T8 workpieces. The mechanical performance of the closed hole is similar to that of the RFSSW keyhole closure welds in the base metal. Coefficient of 67% for hardness, 57% for yield strength and 78% for ultimate tensile strength were achieved. They also filled the through hole of an AA7075-T761 workpiece by RFSSW [284]. Reimann and co-workers [282–284] stated that post-weld natural ageing was shown to be highly significant for the mechanical properties. During ageing, the strength increased from 58% to 70% of the BM hardness in the area of lowest hardness in the HAZ and from 46% to 55% of the yield strength of the BM. The post-weld natural ageing stabilized after 4 weeks [284]. Keyhole closure using RFSSW was demonstrated as a universal through-hole closure method that offers advantages such as defect-free welds and superior surface appearance on both sides of the weld. Fox et al. [345] developed a pre-cracking procedure to provide simulated fatigue cracks on which repairing could be performed by depositing AA2024 powders using cold spraying to fill the pre-cracks. Good repairing was also characterized and showed the improvement in fatigue life over cracks by $SSFSW_2$.

Additionally, this method does not require any surface preparation before or after the welding process and seals the keyhole in a single-step process. This method is not suitable for closed structures due to the need to install a rigid backing bar that has to withstand a large welding force. Some cross-sections of the RFSSW joints show cracks in the lower parts of the NZ, which initiated from the oxide remnants of the interface between the plug and surrounding workpieces. Moreover, the common defects are lack of mixing, incomplete refilling [346], voids [347] and tearing [348] at the TMAZ/NZ interface. Liu et al. [349] introduced ultrasonic oscillation into the RFSSW process to join AA5A06 and stated that lateral ultrasonic oscillation was more effective in improving the tensile strength of the joint.

5.4.6. Prospects

Friction stir-based remanufacturing, a high-efficiency and green joining technique based on low frictional heat and severe plastic deformation, has great potential for high-quality repairing of metallic material. However, some issues need to be addressed.

(1) Aiming at the typical defect repairing of the outer environment or complex structural parts, the portable and multiple-degree-of-freedom FSW robot combined with FSR will certainly be a research hotspot. Recently, robotic FSW systems have been utilized in various industrial applications.
(2) Although FSR has the outstanding advantages to repair light materials of Al alloys and Mg alloys, it should be developed into the production of high melting materials, such as steels, Ti or Ti-based alloys and MMCs.
(3) FSR integrates advanced manufacturing processes such as additive manufacturing to obtain variants such as friction stir additive manufacturing and additive friction stir, resulting in landmark accomplishments towards the goal of innovative and modern prototyping/tooling/manufacturing engineering applications. It is challenging to extend its applications to include tubes, in particular small-diameter tubes, and other complex geometries.

6. Conclusions and outlooks

In this review, the latest progress and rapidly growing knowledge involving the inherent issues and their control strategies for conventional FSW, with particular emphases on the technical development of self-supported FSW, non-weld-thinning FSW and frictional stir-based remanufacturing, were reviewed and summarized.

The back support problem during conventional FSW has been successfully solved by BT-FSW and $SSFSW_1$. By optimizing the welding tools and process parameters in BT-FSW, acceptable results were obtained in the joining of 2xxx and 6xxx Al alloys and partial Mg alloys. Moreover, the adjustable-gap or adaptive-gap BT-FSW, counterrotating shoulder and stationary shoulder BT-FSW were developed to enhance joint integrity and quality. Aiming at the narrow space and the preset holes in BT-FSW joints, $SSFSW_1$ with a convex lower shoulder was invented, which could directly plunge into the welding workpieces without preset holes, and successfully join 6xxx Al alloys. The design criterion of the welding tool and formation mechanism were established and expounded to improve structural integrity. Additionally, the lower surface finishing was further improved by PFSW. Some issues in the self-supported FSW were the voids and JLRs, which may be addressed by the tool design with improved material flow and process parameters.

The solution methods of weld-thinning were mainly divided into three categories. The first method aimed to prevent the overflow of the plasticized materials in the weld: $SSFSW_2$. The second method aimed to avoid the overflow of the plasticized materials: zero-plunge-depth FSW, NWT-FSW and MPD-FSW. The last method aimed to add materials into the weld by assisted devices (hybrid metal extrusion and bonding, cold spraying and *in-situ* additive FSW) or processes (SCFSW and T-plate assisted FSW). Extensive research has focused on $SSFSW_2$, which has achieved good joint integrity without weld thinning and with excellent mechanical properties for Ti alloys, Al alloys and thermoplastic polymers. $SSFSW_2$ has also been applied to the aerospace and railway manufacturing fields. One of the key issues in $SSFSW_2$ is tool wear or fracture induced by the overflowing materials between the stationary shoulder and the rotating tool, which can be addressed via tool coating or rational structural design. Zero-plunge-depth FSW was invented to avoid tool fracture, reduce the softening degree and improve the mechanical properties. The narrow parameter window restricted its further application, which may be handled by the tool design. Moreover, the solid-state joining mechanism should be further revealed and provide technical support for microstructural adjustment and property improvement.

The typical defects and causes in FSW joints or other damaged structural parts in complex and harsh environments during engineering applications were concluded. Recent progress in solid-state remanufacturing techniques based on FSW was reviewed, which provided significant reference values for improving the properties, high-quality repairing and practical engineering applications. Friction stir-based remanufacturing techniques were divided into repetitive (conventional FSW and pinless FSW) and additive (FPW, FTPW, FFSW and so on) remanufacturing. Repetitive friction stir remanufacturing, characterized by unconsumable welding tools, was suitable to repair defects with a certain length and thickness, such as surface peeling, grooves, and cracks in low melting point materials. This technique could also repair high melting point materials; however, this approach is expensive and requires special welding tools to avoid tool wear. Additive friction stir remanufacturing, featuring consumable or semi-consumable welding tools, is applicable to local volume defects with the loss of materials, such as keyholes, cavities and pitting defects. The consumable tool has the potential to repair the materials with high melting point or low melting point, as the tool directly acted as the filling materials for repairing defects, thereby avoiding tool wear.

To date, inherent issues have been solved by advanced manufacturing technologies. It should be emphasized that there are still several challenges to be approached before industry can proceed with these new strategies.

(1) Solid-state joining mechanism and numerical simulation of the whole process of FSW

FSW is a highly intricate process comprising several nonlinear physical phenomena. These phenomena include severe plastic deformation, heat generation, turbulent flow, mechanical shearing, DRX, and interfacial interaction. Multiple parameters greatly change the results of the joints. It is nearly impossible to analyse the isolated influences through experiments only. FSW is an interesting subject, for which numerical simulations and experiments are integral. The key issue is to apply the numerical method to guide the design of the experiments and achieve process-structure-microstructure-property relationships. Nonetheless, there are still several challenges that must be overcome:

1) Systematic integration of the process-structure-microstructure-property relationships.
2) Tool design based on reliability evaluation and failure analysis.
3) Multiscale numerical study from atoms to joints.
4) Multiphase flow behaviour and interfacial rapid diffusion of dissimilar joints.
5) Modelling of dynamic recovery and DRX considering severe plastic deformation.
6) Boundary flow mechanism driven by frictional shearing based on molecular dynamics.
7) Dislocation multiplication and annihilation behaviours induced by severe plastic deformation.

(2) High reliability and anti-fatigue joining

In published articles, satisfactory mechanical properties of advancing FSW joints have been achieved. To push FSW from the laboratory into industry, the improvement of wear and corrosion resistance must be thoroughly considered in the future to satisfy the application requirements in aerospace and automobile. Functional gradient coatings (composites and nano-grains) have the notable advantage in wear and corrosion resistance, which can satisfy the requirements of highly reliable and anti-fatigue joining. The current challenges in fabricating functionally gradient coatings are microstructural adjustments with assisted equipment and related process parameters. There are still some key issues to be solved, which are detailed hereafter:

1) Develop portable assisted equipment with the advantages of low cost, simple operation and high efficiency to extend industrial applications.
2) Select reasonable coating materials according to the requirements of wear or corrosion resistance.
3) Optimize the process parameters and material types to achieve reliable bonding between the coating and the substrate and satisfactory properties of the coatings.
4) Understand the bonding mechanism between the coating and the substrates, such as metallurgical bonding, mechanical interlocking and adhesion.

(3) Quasi-equal strength remanufacturing

Friction stir-based remanufacturing is a solid-state and effective technique to repair structural defects that provides better mechanical properties than other fusion repairing methods. A necessary geometrizatiio process for different types of defects in the laboratory increases the complexity of remanufacturing and restricts the repairing quality and industrial applications. Direct solid-state additive repairing based on powders with strengthening effects has the potential to further expand friction stir-based remanufacturing. Additive friction stir deposition is a fast, scalable and solid-state process characterized by refined microstructures and flexible options for feed materials. The direct deposition method has the advantages of nanostructured grains in powder metallurgy and fast diffusion induced by severe plastic deformation, significantly improving mechanical performances. Moreover, some strengthening phases, such as ceramic particles or whiskers, carbon nanotubes, and graphene nanoplatelets, can be deposited to improve mechanical, thermal or electronic properties. Some key problems remain to be solved.

1) Seek economical high-strength powders and strengthening phases as additive materials and fabrication methods for composite powders.
2) Optimize the process parameters, including the morphology and size of high-strength powders and strengthening phases, the equipment parameters to control microstructural evolution and the subsequent mechanical properties.
3) Understand the deposition growth, interfacial bonding and strengthening mechanisms; establish a relationship between the process-microstructure-joint performance (mechanical, corrosion, thermal and electronic).
4) Combining assisted processes (arc, laser or ultrasonic) with solid-state additive repairing, where thermal energy benefits the softening of high-strength materials or low thermal conductivity materials, such as Ti alloys, high-entropy alloys and polymers, and vibration energy improves atom diffusion at the repair interface.

(4) Detection, standardization and expanding applications

FSW has been widely used in industrial manufacturing fields, where welding defects inevitably appear in the weld and subsequently affect the service life. Although many methods have been developed to solve this problem, quantitative evaluations of defect types and corresponding repairing techniques are lacking. It is of vital importance to establish standards for detecting and repairing of welding defects to realize point-to-point repairing. Many non-destructive tests have been developed to characterize different volume welding defects, such as an eddy current inspection, ultrasonic non-destructive testing and evaluation techniques, acoustic emission, X-ray, magnetic methods, and ultrasound-excited infrared thermography. Some important issues remain to be addressed.

1) Detect and characterize the kissing bond defects or unsatisfactory microstructures quantitatively.
2) Reveal the effects of process parameters and external environmental conditions on defect formation, microstructures and mechanical properties.
3) Establish a database containing the defect types (shape and size) in many kinds of materials with varied thickness and the corresponding repairing techniques based on the experiments and numerical simulations.

(5) Robotic and intelligent FSW

The inherent issues of conventional FSW have been addressed by a series of innovative control strategies in linear or two-

dimensional structures by gantry FSW equipment, which has difficulties in satisfying the requirements for three-dimensional structural parts. Recently, robotic FSW equipment and techniques have become candidates to replace conventional FSW due to the relatively high flexibility and complex motion track, which can realize the welding of complex structural parts. Robotic FSW, which can operate in a large welding space and offer multi-mode control, can significantly improve production efficiency and quality; hence, this technique has been used to create door structures in the Mazda RX8 and hatches in helicopters. Some important key issues need to be addressed.

1) Develop overloading industrial robotic FSW equipment with high rigidity to improve weldable thickness and ensure the consistency between the actual and simulated welding tracks.
2) Integrate the controlling modes of robotic FSW to regulate several factors, including pressure, temperature, weld tracking, and laser positioning.
3) Study the effect of welding parameters (pressure, temperature, weld tracking, and laser positioning) on the welding track and pose through interdependent feedback to realize the accuracy control of the welding track.
4) Combine new FSW technologies (self-supported FSW, NWT-FSW and friction stir-based remanufacturing) with robotic FSW to realize flexible manufacturing of structures.
5) Introduce an assisted heating source to decrease the material stress for the accuracy control of the welding track.

Successfully addressing these important inherent issues will have large impact on FSW/P science and technology for a wide range of technological applications.

Declaration of Competing Interest

The authors declare that they have no known competing financial interests or personal relationships that could have appeared to influence the work reported in this paper.

Acknowledgements

The work was jointly supported by the National Natural Science Foundation of China (No. 51575132).

References

[1] Magalhães VM, Leitão C, Rodrigues DM. Friction stir welding industrialisation and research status. Sci Technol Weld Join 2018;23:400–9. https://doi.org/10.1080/13621718.2017.1403110.
[2] Thomas WM, Nicholas ED, Needham JC, Murch MG, Temple-Smith P, Dawes CJ. Friction stir butt welding; 1991. https://doi.org/10.1007/978-3-642-54607-5.
[3] Ma ZY. Friction stir processing technology: a review. Metall Mater Trans A 2008;39:642–58. https://doi.org/10.1007/s11661-007-9459-0.
[4] Mishra RS, Ma ZY. Friction stir welding and processing. Mater Sci Eng R Reports 2005;50:1–78. https://doi.org/10.1016/j.mser.2005.07.001.
[5] Chen Y, Liu H, Feng J. Friction stir welding characteristics of different heat-treated-state 2219 aluminum alloy plates. Mater Sci Eng A 2006;420:21–5. https://doi.org/10.1016/j.msea.2006.01.029.
[6] Liu HJ, Li JQ, Duan WJ. Friction stir welding characteristics of 2219–T6 aluminum alloy assisted by external non-rotational shoulder. Int J Adv Manuf Technol 2013;64:1685–94. https://doi.org/10.1007/s00170-012-4132-1.
[7] Zhang ZH, Li WY, Feng Y, Li JL, Chao YJ. Global anisotropic response of friction stir welded 2024 aluminum sheets. Acta Mater 2015;92:117–25. https://doi.org/10.1016/j.actamat.2015.03.054.
[8] Zhou C, Yang X, Luan G. Fatigue properties of friction stir welds in Al 5083 alloy. Scr Mater 2005;53:1187–91. https://doi.org/10.1016/j.scriptamat.2005.07.016.
[9] Lombard H, Hattingh DG, Steuwer A, James MN. Optimising FSW process parameters to minimise defects and maximise fatigue life in 5083–H321 aluminium alloy. Eng Fract Mech 2008;75:341–54. https://doi.org/10.1016/j.engfracmech.2007.01.026.
[10] Hirata T, Oguri T, Hagino H, Tanaka T, Chung SW, Takigawa Y, et al. Influence of friction stir welding parameters on grain size and formability in 5083 aluminum alloy. Mater Sci Eng A 2007;456:344–9. https://doi.org/10.1016/j.msea.2006.12.079.
[11] Shi L, Wu CS, Gao S, Padhy GK. Modified constitutive equation for use in modeling the ultrasonic vibration enhanced friction stir welding process. Scr Mater 2016;119:21–6. https://doi.org/10.1016/j.scriptamat.2016.03.023.
[12] Maggiolini E, Tovo R, Susmel L, James MN, Hattingh DG. Crack path and fracture analysis in FSW of small diameter 6082–T6 aluminium tubes under tension–torsion loading. Int J Fatigue 2016;92:478–87. https://doi.org/10.1016/j.ijfatigue.2016.02.043.
[13] Ma ZY, Mishra RS, Mahoney MW. Superplastic deformation behaviour of friction stir processed 7075Al alloy. Acta Mater 2002;50:4419–30. https://doi.org/10.1016/S1359-6454(02)00278-1.
[14] Kawashima T, Sano T, Hirose A, Tsutsumi S, Masaki K, Arakawa K, et al. Femtosecond laser peening of friction stir welded 7075–T73 aluminum alloys. J Mater Process Technol 2018;262:111–22. https://doi.org/10.1016/j.jmatprotec.2018.06.022.
[15] Bayazid SM, Farhangi H, Asgharzadeh H, Radan L, Ghahramani A, Mirhaji A. Effect of cyclic solution treatment on microstructure and mechanical properties of friction stir welded 7075 Al alloy. Mater Sci Eng A 2016;649:293–300. https://doi.org/10.1016/j.msea.2015.10.010.
[16] Ji SD, Jin YY, Yue YM, Gao SS, Huang YX, Wang L. Effect of temperature on material transfer behavior at different stages of friction stir welded 7075–T6 aluminum alloy. J Mater Sci Technol 2013;29:955–60. https://doi.org/10.1016/j.jmst.2013.05.018.
[17] Wang K, Shen Y, Yang X, Wang X, Xu K. Evaluation of microstructure and mechanical property of FSW welded MB3 magnesium alloy. J Iron Steel Res Int 2006;13:75–8. https://doi.org/10.1016/S1006-706X(06)60082-4.
[18] Singh K, Singh G, Singh H. Review on friction stir welding of magnesium alloys. J Magnes Alloy 2018;6:399–416. https://doi.org/10.1016/j.jma.2018.06.001.
[19] Pan F, Xu A, Deng D, Ye J, Jiang X, Tang A, et al. Effects of friction stir welding on microstructure and mechanical properties of magnesium alloy Mg-5Al-3Sn. Mater Des 2016;110:266–74. https://doi.org/10.1016/j.matdes.2016.07.146.
[20] Oliveira JP, Miranda RM, Braz Fernandes FM. Welding and joining of NiTi shape memory alloys: a review. Prog Mater Sci 2017;88:412–66. https://doi.org/10.1016/j.pmatsci.2017.04.008.
[21] Gangwar K, Ramulu M. Friction stir welding of titanium alloys: a review. Mater Des 2018;141:230–55. https://doi.org/10.1016/j.matdes.2017.12.033.
[22] Mironov S, Sato YS, Kokawa H. Friction-stir welding and processing of Ti-6Al-4V titanium alloy: a review. J Mater Sci Technol 2017;34:58–72. https://doi.org/

10.1016/j.jmst.2017.10.018.
[23] Shinde G, Gajghate S, Dabeer PS, Seemikeri CY. Low cost friction stir welding: a review. Mater Today Proc 2017;4:8901–10. https://doi.org/10.1016/j.matpr.2017.07.241.
[24] Guan W, Shen Y, Yan Y, Guo R, Zhang W. Fabrication of ultra-thin copper foil pressure welding using FSW equipment. J Mater Process Technol 2018;251:343–9. https://doi.org/10.1016/j.jmatprotec.2017.08.022.
[25] Heidarzadeh A, Laleh HM, Gerami H, Hosseinpour P, Shabestari MJ, Bahari R. The origin of different microstructural and strengthening mechanisms of copper and brass in their dissimilar friction stir welded joint. Mater Sci Eng A 2018;735:336–42. https://doi.org/10.1016/J.MSEA.2018.08.068.
[26] Liu FC, Hovanski Y, Miles MP, Sorensen CD, Nelson TW. A review of friction stir welding of steels: Tool, material flow, microstructure, and properties. J Mater Sci Technol 2017;34:39–57. https://doi.org/10.1016/j.jmst.2017.10.024.
[27] El-Batahgy AM, Miura T, Ueji R, Fujii H. Investigation into feasibility of FSW process for welding 1600MPa quenched and tempered steel. Mater Sci Eng A 2016;651:904–13. https://doi.org/10.1016/j.msea.2015.11.054.
[28] Zhang H, Wang D, Xue P, Wu LH, Ni DR, Xiao BL, et al. Achieving ultra-high strength friction stir welded joints of high nitrogen stainless steel by forced water cooling. J Mater Sci Technol 2018;34:2183–8. https://doi.org/10.1016/j.jmst.2018.03.014.
[29] Lee SJ, Sun Y, Fujii H. Stacking-fault energy, mechanical twinning and strain hardening of Fe-18Mn-0.6C-(0, 1.5)Al twinning-induced plasticity steels during friction stir welding. Acta Mater 2018;148:235–48. https://doi.org/10.1016/j.actamat.2018.02.004.
[30] Banjare PN, Sahlot P, Arora A. An assisted heating tool design for FSW of thermoplastics. J Mater Process Technol 2017;239:83–91. https://doi.org/10.1016/j.jmatprotec.2016.07.035.
[31] Ratanathavorn W. Hybrid joining of aluminum to thermoplastics with friction stir welding engineering. KTH-Royal Institute of Technology; 2012.
[32] Pramanik A, Basak AK, Dong Y, Sarker PK, Uddin MS, Littlefair G, et al. Joining of carbon fibre reinforced polymer (CFRP) composites and aluminium alloys – a review. Compos Part A Appl Sci Manuf 2017;101:1–29. https://doi.org/10.1016/j.compositesa.2017.06.007.
[33] Shi H, Chen K, Liang Z, Dong F, Yu T, Dong X, et al. Intermetallic compounds in the banded structure and their effect on mechanical properties of Al/Mg dissimilar friction stir welding joints. J Mater Sci Technol 2017;33:359–66. https://doi.org/10.1016/j.jmst.2016.05.006.
[34] Liu L, Ren D, Liu F. A review of dissimilar welding techniques for magnesium alloys to aluminum alloys. Materials (Basel) 2014;7:3735–57. https://doi.org/10.3390/ma7053735.
[35] Kasai H, Morisada Y, Fujii H. Dissimilar FSW of immiscible materials: steel/magnesium. Mater Sci Eng A 2015;624:250–5. https://doi.org/10.1016/j.msea.2014.11.060.
[36] Zheng Q, Feng X, Shen Y, Huang G, Zhao P. Dissimilar friction stir welding of 6061 Al to 316 stainless steel using Zn as a filler metal. J Alloys Compd 2016;686:693–701. https://doi.org/10.1016/j.jallcom.2016.06.092.
[37] Thomä M, Wagner G, Straß B, Wolter B, Benfer S, Fürbeth W. Ultrasound enhanced friction stir welding of aluminum and steel: Process and properties of EN AW 6061/DC04-Joints. J Mater Sci Technol 2017;34:163–72. https://doi.org/10.1016/j.jmst.2017.10.022.
[38] Huang Y, Lv Z, Wan L, Shen J, dos Santos JF. A new method of hybrid friction stir welding assisted by friction surfacing for joining dissimilar Ti/Al alloy. Mater Lett 2017;207:172–5. https://doi.org/10.1016/j.matlet.2017.07.081.
[39] Choi JW, Liu H, Fujii H. Dissimilar friction stir welding of pure Ti and pure Al. Mater Sci Eng A 2018;730:168–76. https://doi.org/10.1016/j.msea.2018.05.117.
[40] Eslami S, Tavares PJ, Moreira PMGP. Friction stir welding tooling for polymers: review and prospects. Int J Adv Manuf Technol 2017;89:1677–90. https://doi.org/10.1007/s00170-016-9205-0.
[41] Wu LH, Nagatsuka K, Nakata K. Achieving superior mechanical properties in friction lap joints of copper to carbon-fiber-reinforced plastic by tool offsetting. J Mater Sci Technol 2018;34:1628–37. https://doi.org/10.1016/j.jmst.2018.04.015.
[42] Wang G, Zhao Y, Hao Y. Friction stir welding of high-strength aerospace aluminum alloy and application in rocket tank manufacturing. J Mater Sci Technol 2017;34:73–91. https://doi.org/10.1016/j.jmst.2017.11.041.
[43] Space launch system: Tooling up to build the world's largest rocket; 2013. https://www.nasa.gov/centers/marshall/news/news/releases/2013/13-080.html.
[44] Schorr AA, Creech SD, Ogles M, David H. Space launch system spacecraft and payload elements: making progress toward first launch. AIAA Sp; 2016:1–14. https://doi.org/10.2514/6.2016-5418.
[45] Burkey Martin. A (much) closer look at how we build SLS. Rocket NASA's Sp Launch Syst; 2016. https://blogs.nasa.gov/Rocketology/2016/06/02/a-much-closer-look-at-how-we-build-sls/.
[46] Large-Scale Manufacturing: Advancing State-of-the-art. Mater Manuf; 2014. https://www.nasa.gov/sites/default/files/files/LargeScaleMfg.pdf.
[47] Trueba L, Torres MA, Johannes LB, Rybicki D. Process optimization in the self-reacting friction stir welding of aluminum 6061–T6. Int J Mater Form 2017:559–70. https://doi.org/10.1007/s12289-017-1365-4.
[48] Marie F, Alléhaux D, Esmiller B. Development of the bobbin tool technique on various aluminum alloys. In: 5th Int. Symp. Frict. stir Weld., Metz, France; 2004. p. 39–52.
[49] Li WY, Fu T, Hütsch L, Hilgert J, Wang FF, dos Santos JF, et al. Effects of tool rotational and welding speed on microstructure and mechanical properties of bobbin-tool friction-stir welded Mg AZ31. Mater Des 2014;64:714–20. https://doi.org/10.1016/j.matdes.2014.07.023.
[50] Thomas WM, Wiesner CS, Marks DJ, Staines DG. Conventional and bobbin friction stir welding of 12% chromium alloy steel using composite refractory tool materials. Sci Technol Weld Join 2009;14:247–53. https://doi.org/10.1179/136217109X415893.
[51] Hilgert J, Santos JF, Huber N, Hilgert J, Santos JF, Huber N. Shear layer modelling for bobbin tool friction stir welding. Sci Technol Weld Join 2012;17:454–9. https://doi.org/10.1179/1362171812Y.0000000034.
[52] Chen S, Li H, Lu S, Ni R, Dong J. Temperature measurement and control of bobbin tool friction stir welding. Int J Adv Manuf Technol 2016;86:337–46. https://doi.org/10.1007/s00170-015-8116-9.
[53] Sued MK, Pons D, Lavroff J, Wong EH. Design features for bobbin friction stir welding tools: Development of a conceptual model linking the underlying physics to the production process. Mater Des 2014;54:632–43. https://doi.org/10.1016/j.matdes.2013.08.057.
[54] Pirizadeh M, Azdast T, Rash Ahmadi S, Mamaghani Shishavan S, Bagheri A. Friction stir welding of thermoplastics using a newly designed tool. Mater Des 2014;54:342–7. https://doi.org/10.1016/j.matdes.2013.08.053.
[55] Wahid MA, Khan ZA, Siddiquee AN. Review on underwater friction stir welding: a variant of friction stir welding with great potential of improving joint properties. Trans Nonferrous Met Soc China 2018;28:193–219. https://doi.org/10.1016/S1003-6326(18)64653-9.
[56] Zhou L, Li GH, Liu CL, Wang J, Huang YX, Feng JC, et al. Effect of rotation speed on microstructure and mechanical properties of self-reacting friction stir welded Al-Mg-Si alloy. Int J Adv Manuf Technol 2017;89:3509–16. https://doi.org/10.1007/s00170-016-9318-5.
[57] A Group Sponsored Project. Assessment of bobbin friction stir welding for joining aluminium alloys. TWI; 2009:6. https://www.twi-global.com/news-events/connect/2009/march-april-2009/assessment-of-bobbin-friction-stir-welding-for-joining-aluminium-alloys/.
[58] Carter R, Kirby Lawless. Gimballed shoulders for friction stir welding. NASA Tech Briefs; 2008:27–8.
[59] Nunes AC. Counterrotating-shoulder mechanism for friction stir welding. Manuf Prototyp 2007:21–2https://ntrs.nasa.gov/archive/nasa/casi.ntrs.nasa.gov/20090041262.pdf.
[60] dos Santos JF, Hilgert J. Apparatus for sriction stir welding. US20120248174A1; 2012.
[61] Scupin P. Semi-stationary shoulder bobbin tool (S3BT): A new approach in high speed friction stir welding. Technischen Universität Hamburg; 2015.
[62] Goebel J, Martin R, Norman A, Jorge. F.dos Santos. Semi-stationary shoulder bobbin tool friction stir welding of AA2198-T851. J Mater Process Technol 2017;245:37–45.
[63] Hilgert J. Knowledge based process development of bobbin tool friction stir welding. Helmholtz-Zentrum Geesthacht; 2012.
[64] Tongne A, Desrayaud C, Jahazi M, Feulvarch E. On material flow in friction stir welded Al alloys. J Mater Process Technol 2017;239:284–96. https://doi.org/10.1016/j.jmatprotec.2016.08.030.
[65] Nandan R, DebRoy T, Bhadeshia HKDH. Recent advances in friction-stir welding - process, weldment structure and properties. Prog Mater Sci 2008;53:980–1023. https://doi.org/10.1016/j.pmatsci.2008.05.001.

[66] Huang Y, Wang Y, Wan L, Liu H, Shen J, dos Santos JF, et al. Material-flow behavior during friction-stir welding of 6082–T6 aluminum alloy. Int J Adv Manuf Technol 2016;87:1115–23. https://doi.org/10.1007/s00170-016-8603-7.
[67] Colligan K. Material flow behavior during friction welding of aluminum. Weld J 1999;75:229–37.
[68] Guerra M, Schmidt C, McClure JC, Murr LE, Nunes AC. Flow patterns during friction stir welding. Mater Charact 2002;49:95–101.
[69] Schmidt HNB, Dickerson TL, Hattel JH. Material flow in butt friction stir welds in AA2024-T3. Acta Mater 2006;54:1199–209. https://doi.org/10.1016/j.actamat.2005.10.052.
[70] Tamadon A, Pons D, Sued K, Clucas D. Formation mechanisms for entry and exit defects in bobbin friction stir welding. Metals (Basel) 2018;8:33. https://doi.org/10.3390/met8010033.
[71] Schmidt HB, Hattel JH. Thermal modelling of friction stir welding. Scr Mater 2008;58:332–7. https://doi.org/10.1016/j.scriptamat.2007.10.008.
[72] Hilgert J, Schmidt HNB, Dos Santos JF, Huber N. Thermal models for bobbin tool friction stir welding. J Mater Process Technol 2011;211:197–204. https://doi.org/10.1016/j.jmatprotec.2010.09.006.
[73] Liu XM, Yao JS, Cai Y, Meng H, Da Zou Z. Simulation on the temperature field of bobbin tool friction stir welding of AA 2014 aluminium alloy. Appl Mech Mater 2013;433–435:2091–5. https://doi.org/10.4028/www.scientific.net/AMM.433-435.2091.
[74] Hilgert J, dos Santos JF, Huber N. Investigation of the material shear layer in bobbin tool friction stir welding. Frict. Stir Weld. Process. IV; 2011. p. 187–93.
[75] Chen S, Lu A, Yang D, Lu S, Dong J, Dong C. Analysis on flow pattern of bobbin tool friction stir welding for 6082 aluminum. In: Proc. 1st Int. Jt. Symp. Join. Weld.; 2013. p. 353–8. https://doi.org/10.1533/9781782421641.353.
[76] Fraser KA, St-Georges L, Kiss LI. Numerical simulation of bobbin tool friction stir welding. In: 10th Frict. Stir Weld. Symp., Beijing, China; 2014. p. 1–15.
[77] Wen Q, Li WY, Gao YJ, Yang J, Wang FF. Numerical simulation and experimental investigation of band patterns in bobbin tool friction stir welding of aluminum alloy. Int J Adv Manuf Technol 2018. https://doi.org/10.1007/s00170-018-2750-y.
[78] Zhang H, Wang M, Zhang X, Yang G. Microstructural characteristics and mechanical properties of bobbin tool friction stir welded 2A14-T6 aluminum alloy. Mater Des 2015;65:559–66. https://doi.org/10.1016/j.matdes.2014.09.068.
[79] Liu HJ, Hou JC, Guo H. Effect of welding speed on microstructure and mechanical properties of self-reacting friction stir welded 6061–T6 aluminum alloy. Mater Des 2013;50:872–8. https://doi.org/10.1016/j.matdes.2013.03.105.
[80] Ji S, Huang R, Meng X, Zhang L, Huang Y. Enhancing friction stir weldability of 6061–T6 Al and AZ31B Mg alloys assisted by external non-rotational shoulder. J Mater Eng Perform 2017;26:2359–67. https://doi.org/10.1007/s11665-017-2640-8.
[81] Zhou L, Li GH, Zha GD, Shu FY, Liu HJ, Feng JC. Effect of rotation speed on microstructure and mechanical properties of bobbin tool friction stir welded AZ61 magnesium alloy. Sci Technol Weld Join 2018;23:596–605. https://doi.org/10.1080/13621718.2018.1432098.
[82] Padmanaban G, Balasubramanian V, Sarin Sundar JK. Influences of welding processes on microstructure, hardness, and tensile properties of AZ31B magnesium alloy. J Mater Eng Perform 2010;19:155–65. https://doi.org/10.1007/s11665-009-9389-7.
[83] Hou JC, Liu HJ, Zhao YQ. Influences of rotation speed on microstructures and mechanical properties of 6061–T6 aluminum alloy joints fabricated by self-reacting friction stir welding tool. Int J Adv Manuf Technol 2014;73:1073–9. https://doi.org/10.1007/s00170-014-5857-9.
[84] Wang FF, Li WY, Shen J, Hu SY, dos Santos JF. Effect of tool rotational speed on the microstructure and mechanical properties of bobbin tool friction stir welding of Al-Li alloy. Mater Des 2015;86:933–40. https://doi.org/10.1016/j.matdes.2015.07.096.
[85] Ion SE, Humphreys FJ, Whi SH. Dynamic recrystallisation and the development of microstructure during the high temperature deformation of magnesium. Acta Metall 1982;30:1909–19. https://doi.org/10.1016/0001-6160(82)90031-1.
[86] Park SHC, Sato YS, Kokawa H. Effect of micro-texture on fracture location in friction stir weld of Mg alloy AZ61 during tensile test. Scr Mater 2003;49:161–6. https://doi.org/10.1016/S1359-6462(03)00210-0.
[87] Esmaily M, Mortazavi N, Osikowicz W, Hindsefelt H, Svensson JE, Halvarsson M, et al. Corrosion behaviour of friction stir-welded AA6005-T6 using a bobbin tool. Corros Sci 2016;111:98–109. https://doi.org/10.1016/j.corsci.2016.04.046.
[88] Threadgill PL, Ahmed MMZ, Martin JP, Perrett JG, Wynne BP. The use of bobbin tools for friction stir welding of aluminium alloys. Mater Sci Forum 2010;638–642:1179–84. https://doi.org/10.4028/www.scientific.net/MSF.638-642.1179.
[89] Xu WF, Luo YX, Fu MW. Microstructure evolution in the conventional single side and bobbin tool friction stir welding of thick rolled 7085–T7452 aluminum alloy. Mater Charact 2018;138:48–55. https://doi.org/10.1016/j.matchar.2018.01.051.
[90] Sato YS, Kokawa H, Enomoto M, Jogan S. Microstructural evolution of 6063 aluminum during friction-stir welding. Metall Mater Trans A 1999;30:2429–37. https://doi.org/10.1007/s11661-999-0251-1.
[91] Esmaily M, Mortazavi N, Osikowicz W, Hindsefelt H, Svensson JE, Halvarsson M, et al. Bobbin and conventional friction stir welding of thick extruded AA6005-T6 profiles. Mater Des 2016;108:114–25. https://doi.org/10.1016/j.matdes.2016.06.089.
[92] Kainuma S, Katsuki H, Iwai I, Kumagai M. Evaluation of fatigue strength of friction stir butt-welded aluminum alloy joints inclined to applied cyclic stress. Int J Fatigue 2008;30:870–6. https://doi.org/10.1016/j.ijfatigue.2007.06.007.
[93] Zhou C, Yang X, Luan G. Effect of kissing bond on fatigue behavior of friction stir welds on Al 5083 alloy. J Mater Sci 2006;41:2771–7. https://doi.org/10.1007/s10853-006-6337-x.
[94] Wang FF, Li WY, Shen J, Wen Q, dos Santos JF. Improving weld formability by a novel dual-rotation bobbin tool friction stir welding. J Mater Sci Technol 2018;34:135–9. https://doi.org/10.1016/j.jmst.2017.11.001.
[95] Chen ZW, Pasang T, Qi Y. Shear flow and formation of Nugget zone during friction stir welding of aluminium alloy 5083-O. Mater Sci Eng A 2008;474:312–6. https://doi.org/10.1016/j.msea.2007.05.074.
[96] Yang C, Ni DR, Xue P, Xiao BL, Wang W, Wang KS, et al. A comparative research on bobbin tool and conventional friction stir welding of Al-Mg-Si alloy plates. Mater Charact 2018;145:20–8. https://doi.org/10.1016/j.matchar.2018.08.027.
[97] Zhao Y, Wang C, Dong C. Microstructural characteristics and mechanical properties of water cooling bobbin-tool friction stir welded 6063–T6 aluminum alloy. MATEC Web Conf 2018;206:03002. https://doi.org/10.1051/matecconf/201820603002.
[98] Dalder ENC, Pastrnak JW, Engel J, Forrest RS, Kokko E, Ternan KM, et al. Bobbin-tool friction-stir welding of thick-walled aluminum alloy pressure eessels. Weld J 2007:1–17.
[99] Warsinski K, West M, Freeman J, Curtis T. Investigation of lazy S feature in self-reacting tool friction stir welds. Frict. Stir Weld. Process. VI 2011:171–6. https://doi.org/10.1002/9781118062302.ch21.
[100] Cao X, Jahazi M. Effect of welding speed on the quality of friction stir welded butt joints of a magnesium alloy. Mater Des 2009;30:2033–42. https://doi.org/10.1016/j.matdes.2008.08.040.
[101] Skinner M, Edwards RL. Improvements to the FSW process using the self-reacting technology. Mater Sci Forum 2003;426–432:2849–54. https://doi.org/10.4028/www.scientific.net/MSF.426-432.2849.
[102] Oonne CD, Biallas G. Microstructure and mechanical properties of the aluminium alloy 6056 welded by friction stir welding techniques. Weld World 2006;50:98–106.
[103] Neumann T, Zettler R, Vilaça P, dos Santos JF, Quintino L. Analysis of self-reacting friction stir welds in a 2024-T351 alloy. Frict. Stir Weld. Process. IV, Orlando, Florida; 2007.
[104] Adriana M, Obregon T. Effect of process parameters on temperature distribution, microstructure, and mechanical properties of self-reacting friction stir welded aluminum alloy 6061-T651. The University of Texas; 2011.
[105] Okamoto K, Sato A, Park SHC, Hirano S. Microstructure and mechanical properties of FSWed aluminum extrusion with bobbin Tools. Mater Sci Forum 2012;706–709:990–5. https://doi.org/10.4028/www.scientific.net/MSF.706-709.990.
[106] Zhou L, Li GH, Liu CL, Wang J, Huang YX, Feng JC, et al. Microstructural characteristics and mechanical properties of Al–Mg–Si alloy self-reacting friction stir welded joints. Sci Technol Weld Join 2017;22:438–45. https://doi.org/10.1080/13621718.2016.1251733.
[107] Zhang J, Feng XS, Gao JS, Huang H, Ma ZQ, Guo LJ. Effects of welding parameters and post-heat treatment on mechanical properties of friction stir welded AA2195-T8 Al-Li alloy. J Mater Sci Technol 2018;34:219–27. https://doi.org/10.1016/j.jmst.2017.11.033.

[108] Shen Z, Yang X, Zhang Z, Cui L, Yin Y. Mechanical properties and failure mechanisms of friction stir spot welds of AA 6061–T4 sheets. Mater Des 2013;49:181–91. https://doi.org/10.1016/j.matdes.2013.01.066.
[109] Scialpi A, De Filippis LAC, Cavaliere P. Influence of shoulder geometry on microstructure and mechanical properties of friction stir welded 6082 aluminium alloy. Mater Des 2007;28:1124–9. https://doi.org/10.1016/j.matdes.2006.01.031.
[110] Mendes N, Loureiro A, Martins C, Neto P, Pires JN. Effect of friction stir welding parameters on morphology and strength of acrylonitrile butadiene styrene plate welds. Mater Des 2014;58:457–64. https://doi.org/10.1016/j.matdes.2014.02.036.
[111] Wang FF, Li WY, Shen J, Zhang ZH, Li JL, Dos Santos JF. Global and local mechanical properties and microstructure of bobbin tool friction-stir-welded Al-Li alloy. Sci Technol Weld Join 2016;21:479–83. https://doi.org/10.1080/13621718.2015.1132128.
[112] Huang YX, Wan L, Lv SX, Feng JC. Novel design of tool for joining hollow extrusion by friction stir welding. Sci Technol Weld Join 2013;18:239–46. https://doi.org/10.1179/1362171812Y.0000000096.
[113] Wan L, Huang Y, Wang Y, Lv S, Feng J. Friction stir welding of aluminium hollow extrusion: weld formation and mechanical properties. Mater Sci Technol 2015;31:1433–42. https://doi.org/10.1179/1743284714Y.0000000721.
[114] Wan L, Huang Y, Guo W, Lv S, Feng J. Mechanical properties and microstructure of 6082–T6 aluminum alloy joints by self-support friction stir welding. J Mater Sci Technol 2014;30:1243–50. https://doi.org/10.1016/j.jmst.2014.04.009.
[115] Wan L, Huang Y, Lv Z, Lv S, Feng J. Effect of self-support friction stir welding on microstructure and microhardness of 6082–T6 aluminum alloy joint. Mater Des 2014;55:197–203. https://doi.org/10.1016/j.matdes.2013.09.073.
[116] Balasubramanian V. Relationship between base metal properties and friction stir welding process parameters. Mater Sci Eng A 2008;480:397–403. https://doi.org/10.1016/j.msea.2007.07.048.
[117] Huang Y, Xie Y, Meng X, Lv Z, Cao J. Numerical design of high depth-to-width ratio friction stir welding. J Mater Process Technol 2018;252:233–41. https://doi.org/10.1016/j.jmatprotec.2017.09.029.
[118] Huang Y, Meng X, Wang Y, Xie Y, Zhou L. Joining of aluminum alloy and polymer via friction stir lap welding. J Mater Process Technol 2018;257:148–54. https://doi.org/10.1016/j.jmatprotec.2018.02.043.
[119] Huang Y, Wan L, Huang T, Lv Z, Zhou L, Feng J. The weld formation of self-support friction stir welds for aluminum hollow extrusion. Int J Adv Manuf Technol 2016;87:1067–75. https://doi.org/10.1007/s00170-016-8591-7.
[120] Edwards GA, Stiller K, Dunlop GL, Couper MJ. The precipitation sequence in Al-Mg-Si alloys. Acta Mater 1998;46:3893–904. https://doi.org/10.1016/S1359-6454(98)00059-7.
[121] Simar A, Bréchet Y, De Meester B, Denquin A, Gallais C, Pardoen T. Integrated modeling of friction stir welding of 6xxx series Al alloys: process, microstructure and properties. Prog Mater Sci 2012;57:95–183. https://doi.org/10.1016/j.pmatsci.2011.05.003.
[122] Dong P, Li H, Sun D, Gong W, Liu J. Effects of welding speed on the microstructure and hardness in friction stir welding joints of 6005A–T6 aluminum alloy. Mater Des 2013;45:524–31. https://doi.org/10.1016/j.matdes.2012.09.040.
[123] Huang YX, Wan L, Lv ZL, Lv SX, Zhou L, Feng JC. Microstructure and microhardness of aluminium alloy friction stir welds with heat treatment. Sci Technol Weld Join 2016;21:638–44. https://doi.org/10.1080/13621718.2016.1152748.
[124] Liu H, Hu Y, Wang H, Du S, Sekulic DP. Stationary shoulder supporting and tilting pin penetrating friction stir welding. J Mater Process Technol 2018;255:596–604. https://doi.org/10.1016/j.jmatprotec.2018.01.010.
[125] Hu Y, Liu H, Li S, Du S, Sekulic DP. Improving mechanical properties of a joint through tilt probe penetrating friction stir welding. Mater Sci Eng A 2018;731:107–18. https://doi.org/10.1016/j.msea.2018.06.036.
[126] Wang BB, Chen FF, Liu F, Wang WG, Xue P, Ma ZY. Enhanced mechanical properties of friction stir welded 5083Al-H19 joints with additional water cooling. J Mater Sci Technol 2017;33:1009–14. https://doi.org/10.1016/j.jmst.2017.01.016.
[127] Sree Sabari S, Malarvizhi S, Balasubramanian V. Characteristics of FSW and UWFSW joints of AA2519-T87 aluminium alloy: effect of tool rotation speed. J Manuf Process 2016;22:278–89. https://doi.org/10.1016/j.jmapro.2016.03.014.
[128] Lin SB, Zhao YH, Wu L. Integral and layered mechanical properties of friction stir welded joints of 2014 aluminium alloy. Mater Sci Technol 2006;22(8):995–8. https://doi.org/10.1179/174328406X102408.
[129] Sattari S, Bisadi H, Sajed M. Mechanical properties and temperature distributions of thin friction stir welded sheets of AA5083. Int J Mech Appl 2012;2:1–6. https://doi.org/10.5923/j.mechanics.20120201.01.
[130] Kumar M, Kailas SV, Narayanan RG. Influence of external weld flash on the in-plane plane-strain formability of friction stir welded sheets. J Strain Anal Eng Des 2013;48:376–85. https://doi.org/10.1177/0309324713488884.
[131] Ma YE, Staron P, Fischer T, Irving PE. Size effects on residual stress and fatigue crack growth in friction stir welded 2195–T8 aluminium – Part II: Modelling. Int J Fatigue 2011;33:1426–34. https://doi.org/10.1016/j.ijfatigue.2011.05.008.
[132] Ma YE, Staron P, Fischer T, Irving PE. Size effects on residual stress and fatigue crack growth in friction stir welded 2195–T8 aluminium – Part I: Experiments. Int J Fatigue 2011;33:1417–25. https://doi.org/10.1016/j.ijfatigue.2011.05.006.
[133] Ji S, Li Z, Wang Y, Ma L. Joint formation and mechanical properties of back heating assisted friction stir welded Ti–6Al–4V alloy. Mater Des 2017;113:37–46. https://doi.org/10.1016/j.matdes.2016.10.012.
[134] Huang Y, Meng X, Xie Y, Lv Z, Wan L, Cao J, et al. Friction spot welding of carbon fiber-reinforced polyetherimide laminate. Compos Struct 2018;189:627–34. https://doi.org/10.1016/j.compstruct.2018.02.004.
[135] Azarsa E, Mostafapour A. Experimental investigation on flexural behavior of friction stir welded high density polyethylene sheets. J Manuf Process 2014;16:149–55. https://doi.org/10.1016/j.jmapro.2013.12.003.
[136] Eslami S, Ramos T, Tavares PJ, Moreira PMGP. Shoulder design developments for FSW lap joints of dissimilar polymers. J Manuf Process 2015;20:15–23. https://doi.org/10.1016/j.jmapro.2015.09.013.
[137] Davies PS, Wynne BP, Rainforth WM, Thomas MJ, Threadgill PL. Development of Microstructure and crystallographic texture during stationary shoulder friction stir welding of Ti-6Al-4V. Metall Mater Trans A 2011;42:2278–89. https://doi.org/10.1007/s11661-011-0606-2.
[138] EADS. DELTAN FS® SYSTEM FOR FRICTION-STIR WELDING n.d. http://www.technology-licensing.com/etl/int/en/What-we-offer/Technologies-for-licensing/Metallics-and-related-manufacturing-technologies/Delta N-system-for- friction-stir-welding.html.
[139] Wu H, Chen YC, Strong D, Prangnell P. Stationary shoulder FSW for joining high strength aluminum alloys. J Mater Process Technol 2015;221:187–96. https://doi.org/10.1016/j.jmatprotec.2015.02.015.
[140] Russell MJ, Threadgill PL, Thomas MJ, Wynne BP. Static shoulder friction stir welding of Ti-6Al-4V: process and evaluation. In: Proc. 11th World Conf. 'Titanium,' Kyoto, Japan; 2007.
[141] Russell MJ, Blignault C, Horrex NL, Wiesner CS. Recent developments in the friction stir welding of titanium alloys. Weld World 2013;52:12–5. https://doi.org/10.1007/BF03266662.
[142] Brassington WDP, Colegrove PA. Alternative friction stir welding technology for titanium–6Al–4V propellant tanks within the space industry. Sci Technol Weld Join 2017;22:300–18. https://doi.org/10.1080/13621718.2016.1236002.
[143] Rai R, De A, Bhadeshia HKDH, DebRoy T. Review: friction stir welding tools. Sci Technol Weld Join 2011;16:325–42. https://doi.org/10.1179/1362171811Y.0000000023.
[144] Ji SD, Meng XC, Liu JG, Zhang LG, Gao SS. Formation and mechanical properties of stationary shoulder friction stir welded 6005A–T6 aluminum alloy. Mater Des 2014;62:113–7. https://doi.org/10.1016/j.matdes.2014.05.016.
[145] Li JQ, Liu HJ. Effects of tool rotation speed on microstructures and mechanical properties of AA2219-T6 welded by the external non-rotational shoulder assisted friction stir welding. Mater Des 2013;43:299–306. https://doi.org/10.1016/j.matdes.2012.07.011.
[146] Zafar A, Awang M, Khan SR, Emamian S. Investigating friction stir welding on thick Nylon 6 plates. Weld Res 2016;95:210–8.
[147] Barmouz M, Shahi P, Asadi P. Friction stir welding/processing of polymeric materials. Adv Frict Weld Process 2014:601–70. https://doi.org/10.1533/9780857094551.601.

[148] Mostafapour A, Taghizad Asad F. Investigations on joining of Nylon 6 plates via novel method of heat assisted friction stir welding to find the optimum process parameters. Sci Technol Weld Join 2016;21:660–9. https://doi.org/10.1080/13621718.2016.1169669.
[149] Li D, Yang X, Cui L, He F, Zhang X. Fatigue property of stationary shoulder friction stir welded additive and non-additive T joints. Sci Technol Weld Join 2015;20:650–4. https://doi.org/10.1179/1362171815Y.0000000045.
[150] Wei S, Martin J. New techniques: Robotic friction stir welding. In: 10th Int. Symp. Frict. Stir Weld., Beijing, China; 2014. p. 20–2.
[151] Maltin CA, Nolton LJ, Scott JL, Toumpis AI, Galloway AM. The potential adaptation of stationary shoulder friction stir welding technology to steel. Mater Des 2014;64:614–24. https://doi.org/10.1016/j.matdes.2014.08.017.
[152] Martin J, Stanhope C, Gascoyne S. Novel techniques for corner joints using friction stir welding. In: TMS Annu. Meet.; 2011. p. 177–86. https://doi.org/10.1002/9781118062302.ch22.
[153] Jesus JS, Costa JM, Loureiro A, Ferreira JM. Assessment of friction stir welding aluminium T-joints. J Mater Process Technol 2018;255:387–99. https://doi.org/10.1016/j.jmatprotec.2017.12.036.
[154] Feistauer EE, Bergmann LA, dos Santos JF. Effect of reverse material flow on the microstructure and performance of friction stir welded T-joints of an Al-Mg alloy. Mater Sci Eng A 2018;731:454–64. https://doi.org/10.1016/j.msea.2018.06.056.
[155] Texier D, Atmani F, Bocher P, Nadeau F, Chen J, Zedan Y, et al. Fatigue performances of FSW and GMAW aluminum alloys welded joints: competition between microstructural and structural-contact-fretting crack initiation. Int J Fatigue 2018;116:220–33. https://doi.org/10.1016/j.ijfatigue.2018.06.020.
[156] Li D, Yang X, Cui L, He F, Zhang X. Investigation of stationary shoulder friction stir welding of aluminum alloy 7075–T651. J Mater Process Technol 2015;222:391–8. https://doi.org/10.1016/j.jmatprotec.2015.03.036.
[157] Meng X, Jin Y, Ji S, Yan D. Improving friction stir weldability of Al/Mg alloys via ultrasonically diminishing pin adhesion. J Mater Sci Technol 2018;34:1817–22. https://doi.org/10.1016/j.jmst.2018.02.022.
[158] Liu Z, Meng X, Ji S, Li Z, Wang L. Improving tensile properties of Al/Mg joint by smashing intermetallic compounds via ultrasonic-assisted stationary shoulder friction stir welding. J Manuf Process 2018;31:552–9. https://doi.org/10.1016/j.jmapro.2017.12.022.
[159] Huang Y, Meng X, Xie Y, Li J, Wan L. Joining of carbon fiber reinforced thermoplastic and metal via friction stir welding with co-controlling shape and performance. Compos Part A Appl Sci Manuf 2018;112:328–36. https://doi.org/10.1016/j.compositesa.2018.06.027.
[160] Ji SD, Meng XC, Li ZW, Ma L, Gao SS. Experimental study of stationary shoulder friction stir welded 7N01-T4 aluminum alloy. J Mater Eng Perform 2016;25:1228–36. https://doi.org/10.1007/s11665-016-1954-2.
[161] Shah LH, Othman NH, Gerlich A. Review of research progress on aluminium–magnesium dissimilar friction stir welding. Sci Technol Weld Join 2017;1718:1–15. https://doi.org/10.1080/13621718.2017.1370193.
[162] Strand S. Effects of friction stir welding on polymer microstructure. Brigham Young University; 2004.
[163] Ji S, Li Z, Zhang L, Zhou Z, Chai P. Effect of lap configuration on magnesium to aluminum friction stir lap welding assisted by external stationary shoulder. Mater Des 2016;103:160–70. https://doi.org/10.1016/j.matdes.2016.04.066.
[164] Ji S, Meng X, Liu Z, Huang R, Li Z. Dissimilar friction stir welding of 6061 aluminum alloy and AZ31 magnesium alloy assisted with ultrasonic. Mater Lett 2017;201:173–6. https://doi.org/10.1016/j.matlet.2017.05.011.
[165] Meng X, Jin Y, Ji S, Yan D. Improving friction stir weldability of Al/Mg alloys via ultrasonically diminishing pin adhesion. J Mater Sci Technol 2018;34. https://doi.org/10.1016/j.jmst.2018.02.022.
[166] Meng X, Xu Z, Huang Y, Xie Y, Wang Y, Wan L, et al. Interface characteristic and tensile property of friction stir lap welding of dissimilar aircraft 2060–T8 and 2099–T83 Al–Li alloys. Int J Adv Manuf Technol 2018;94:1253–61. https://doi.org/10.1007/s00170-017-0996-4.
[167] Ji S, Li Z. Microstructure and mechanical properties of friction stir lap welded Mg/Al joint assisted by stationary shoulder. Met Mater Int 2017;23:1158–67. https://doi.org/10.1007/s12540-017-7065-2.
[168] Yue Y, Zhou Z, Ji S, Zhang J, Li Z. Effect of welding speed on joint feature and mechanical properties of friction stir lap welding assisted by external stationary shoulders. Int J Adv Manuf Technol 2017;89:1691–8. https://doi.org/10.1007/s00170-016-9240-x.
[169] Li Z, Yue Y, Ji S, Chai P, Zhou Z. Joint features and mechanical properties of friction stir lap welded alclad 2024 aluminum alloy assisted by external stationary shoulder. Mater Des 2016;90:238–47. https://doi.org/10.1016/j.matdes.2015.10.056.
[170] Wen Q, Li WY, Wang WB, Wang FF, Gao YJ, Patel V. Experimental and numerical investigations of bonding interface behavior in stationary shoulder friction stir lap welding. J Mater Sci Technol 2019;35:192–200. https://doi.org/10.1016/j.jmst.2018.09.028.
[171] Ahmed MMZ, Wynne BP, Rainforth WM, Threadgill PL. Through-thickness crystallographic texture of stationary shoulder friction stir welded aluminium. Scr Mater 2011;64:45–8. https://doi.org/10.1016/j.scriptamat.2010.08.060.
[172] Li D, Yang X, Cui L, He F, Shen H. Effect of welding parameters on microstructure and mechanical properties of AA6061-T6 butt welded joints by stationary shoulder friction stir welding. Mater Des 2014;64:251–60. https://doi.org/10.1016/j.matdes.2014.07.046.
[173] Sun T, Roy MJ, Strong D, Withers PJ, Prangnell PB. Comparison of residual stress distributions in conventional and stationary shoulder high-strength aluminum alloy friction stir welds. J Mater Process Tech 2017;242:92–100. https://doi.org/10.1016/j.jmatprotec.2016.11.015.
[174] Sun T, Tremsin AS, Roy MJ, Hofmann M, Prangnell PB, Withers PJ. Investigation of residual stress distribution and texture evolution in AA7050 stationary shoulder friction stir welded joints. Mater Sci Eng A 2018;712:531–8. https://doi.org/10.1016/j.msea.2017.12.019.
[175] Barbini A, Carstensen J, dos Santos JF. Influence of a non-rotating shoulder on heat generation, microstructure and mechanical properties of dissimilar AA2024/AA7050 FSW joints. J Mater Sci Technol 2017;34:119–27. https://doi.org/10.1016/j.jmst.2017.10.017.
[176] Regensburg A, Schürer R, Weigl M, Bergmann J. Influence of pin length and electrochemical platings on the mechanical strength and macroscopic defect formation in stationary shoulder friction stir welding of aluminium to copper. Metals (Basel) 2018;8:2–9. https://doi.org/10.3390/met8020085.
[177] Mostafapour Amir. A study on the role of processing parameters in joining polyethylene sheets via heat assisted friction stir welding: Investigating microstructure, tensile and flexural properties. Int J Phys Sci 2012;7.. https://doi.org/10.5897/IJPS11.1653.
[178] Kiss Z, Czigany T. Microscopic analysis of the morphology of seams in friction stir welded polypropylene. Express Polym Lett 2012;6:54–62. https://doi.org/10.3144/expresspolymlett.2012.6.
[179] Bagheri A, Azdast T, Doniavi A. An experimental study on mechanical properties of friction stir welded ABS sheets. Mater Des 2013;43:402–9. https://doi.org/10.1016/j.matdes.2012.06.059.
[180] Rahbarpour R, Azdast T, Rahbarpour H, Shishavan SM. Feasibility study of friction stir welding of wood–plastic composites. Sci Technol Weld Join 2014;19:673–81. https://doi.org/10.1179/1362171814Y.0000000233.
[181] Mendes N, Loureiro A, Martins C, Neto P, Pires JN. Morphology and strength of acrylonitrile butadiene styrene welds performed by robotic friction stir welding. Mater Des 2014;64:81–90. https://doi.org/10.1016/j.matdes.2014.07.047.
[182] Czigány T, Kiss Z. Friction stir welding of fiber reinforced polymer composites. In: 18th Int. Conf. Compos. Mater.; 2015.
[183] Eslami S, Mourão L, Viriato N, Tavares PJ, Moreira PMGP. Multi-axis force measurements of polymer friction stir welding. J Mater Process Technol 2018;256:51–6. https://doi.org/10.1016/j.jmatprotec.2018.01.044.
[184] Ji S, Li Z, Zhang L, Wang Y. Eliminating the tearing defect in Ti-6Al-4V alloy joint by back heating assisted friction stir welding. Mater Lett 2017;188:21–4. https://doi.org/10.1016/j.matlet.2016.10.032.
[185] Zhou L, Liu HJ, Liu QW. Effect of process parameters on stir zone microstructure in Ti-6Al-4V friction stir welds. J Mater Sci 2010;45:39–45. https://doi.org/10.1007/s10853-009-3881-1.
[186] Pilchak AL, Juhas MC, Williams JC. Microstructural changes due to friction stir processing of investment-cast Ti-6Al-4V. Metall Mater Trans A Phys Metall Mater Sci 2007;38:401–8. https://doi.org/10.1007/s11661-006-9061-x.
[187] Knipling KE, Fonda RW. Microstructural evolution in Ti-5111 friction stir welds. Metall Mater Trans A 2011;42:2312–22. https://doi.org/10.1007/s11661-011-0630-2.
[188] Avettand-Fènoël MN, Taillard R. Effect of a pre or postweld heat treatment on microstructure and mechanical properties of an AA2050 weld obtained by SSFSW. Mater Des 2016;89:348–61. https://doi.org/10.1016/j.matdes.2015.09.151.

[189] Ma ZY, Feng AH, Chen DL, Shen J. Recent advances in friction stir welding/processing of aluminum alloys: microstructural evolution and mechanical properties. Crit Rev Solid State Mater Sci 2017;8436:1–65. https://doi.org/10.1080/10408436.2017.1358145.
[190] Leng L, Zhang ZJ, Duan QQ, Zhang P, Zhang ZF. Improving the fatigue strength of 7075 alloy through aging. Mater Sci Eng A 2018;738:24–30. https://doi.org/10.1016/j.msea.2018.09.047.
[191] Ferragut R, Somoza A, Tolley A. Microstructural evolution of 7012 alloy during the early stages of artificial ageing. Acta Mater 1999;47:4355–64. https://doi.org/10.1016/S1359-6454(99)00315-8.
[192] Berg LK, Gjoønnes J, Hansen V, Li XZ, Knutson-Wedel M, Waterloo G, et al. GP-zones in Al-Zn-Mg alloys and their role in artificial aging. Acta Mater 2001;49:3443–51. https://doi.org/10.1016/S1359-6454(01)00251-8.
[193] Sun Z, Yang X, Li D, Cui L. The local strength and toughness for stationary shoulder friction stir weld on AA6061-T6 alloy. Mater Charact 2016;111:114–21. https://doi.org/10.1016/j.matchar.2015.11.020.
[194] Arici A, Sinmazçelýk T. Effects of double passes of the tool on friction stir welding of polyethylene. J Mater Sci 2005;40:3313–6. https://doi.org/10.1007/s10853-005-2709-x.
[195] Arici A, Selale S. Effects of tool tilt angle on tensile strength and fracture locations of friction stir welding of polyethylene. Sci Technol Weld Join 2007;12:536–9. https://doi.org/10.1179/174329307X173706.
[196] Huang Y, Meng X, Xie Y, Wan L, Lv Z, Cao J, et al. Friction stir welding/processing of polymers and polymer matrix composites. Compos Part A Appl Sci Manuf 2018;105:235–57. https://doi.org/10.1016/j.compositesa.2017.12.005.
[197] Gao J, Shen Y, Zhang J, Xu H. Submerged friction stir weld of polyethylene sheets. J Appl Polym Sci 2014;41059:1–8. https://doi.org/10.1002/app.41059.
[198] He X, Gu F, Ball A. A review of numerical analysis of friction stir welding. Prog Mater Sci 2014;65:1–66. https://doi.org/10.1016/j.pmatsci.2014.03.003.
[199] Chen G, Li H, Wang G, Guo Z, Zhang S, Dai Q, et al. Effects of pin thread on the in-process material flow behavior during friction stir welding: a computational fluid dynamics study. Int J Mach Tools Manuf 2018;124:12–21. https://doi.org/10.1016/j.ijmachtools.2017.09.002.
[200] Chen G, Ma Q, Zhang S, Wu J, Zhang G, Shi Q. Computational fluid dynamics simulation of friction stir welding: a comparative study on different frictional boundary conditions. J Mater Sci Technol 2017;34:128–34. https://doi.org/10.1016/j.jmst.2017.10.015.
[201] Li JQ, Liu HJ. Design of tool system for the external nonrotational shoulder assisted friction stir welding and its experimental validations on 2219–T6 aluminum alloy. Int J Adv Manuf Technol 2013;66:623–34. https://doi.org/10.1007/s00170-012-4353-3.
[202] Chu K, Wang X, Wang F, Li Y, Huang D, Liu H, et al. Largely enhanced thermal conductivity of graphene/copper composites with highly aligned graphene network. Carbon N Y 2018;127:102–12. https://doi.org/10.1016/j.carbon.2017.10.099.
[203] Li H, Dai S, Miao J, Wu X, Chandrasekharan N, Qiu H, et al. Enhanced thermal conductivity of graphene/polyimide hybrid film via a novel “molecular welding” strategy. Carbon N Y 2018;126:319–27. https://doi.org/10.1016/j.carbon.2017.10.044.
[204] Chung SH, Kim H, Jeong SW. Improved thermal conductivity of carbon-based thermal interface materials by high-magnetic-field alignment. Carbon N Y 2018;140:24–9. https://doi.org/10.1016/j.carbon.2018.08.029.
[205] Aydin M. Effects of welding parameters and pre-heating on the friction stir welding of UHMW-polyethylene. Polym Plast Technol Eng 2010;49:595–601. https://doi.org/10.1080/03602551003664503.
[206] Vijendra B, Sharma A. Induction heated tool assisted friction-stir welding (i-FSW): A novel hybrid process for joining of thermoplastics. J Manuf Process 2015;20:234–44. https://doi.org/10.1016/j.jmapro.2015.07.005.
[207] Liu Z, Ji S, Meng X. Joining of magnesium and aluminum alloys via ultrasonic assisted friction stir welding at low temperature. Int J Adv Manuf Technol 2018;97:4127–36. https://doi.org/10.1007/s00170-018-2255-8.
[208] Ji S, Li Z, Zhou Z, Zhang L. Microstructure and mechanical property differences between friction stir lap welded joints using rotating and stationary shoulders. Int J Adv Manuf Technol 2017;90:3045–53. https://doi.org/10.1007/s00170-016-9640-y.
[209] Jayaraman N, Prevéy P, Mahoney M. Fatigue life improvement of an aluminum alloy FSW with low plasticity burnishing. In: Proc. 132nd TMS Annu. Meet., San Diego, CA; 2003. p. 1–10.
[210] Huang Y, Wan L, Lv S, Zhang J, Fu G. In situ rolling friction stir welding for joining AA2219. Mater Des 2013;50:810–6. https://doi.org/10.1016/j.matdes.2013.03.088.
[211] Huang Y, Wan L, Lv S, Liu H, Feng J. Gradient micro-structured surface layer on aluminum alloy fabricated by in situ rolling friction stir welding. Mater Des 2013;52:821–7. https://doi.org/10.1016/j.matdes.2013.06.026.
[212] Huang YX, Wan L, Lv SX, Zhang Z, Liu HJ. New technique of *in situ* rolling friction stir welding. Sci Technol Weld Join 2012;17:636–42. https://doi.org/10.1179/1362171812Y.0000000056.
[213] Ji S, Meng X, Ma L, Lu H, Gao S. Vertical compensation friction stir welding assisted by external stationary shoulder. Mater Des 2015;68:72–9. https://doi.org/10.1016/j.matdes.2014.12.009.
[214] Zhang H, Wang M, Zhou W, Zhang X, Zhu Z, Yu T, et al. Microstructure-property characteristics of a novel non-weld-thinning friction stir welding process of aluminum alloys. Mater Des 2015;86:379–87. https://doi.org/10.1016/j.matdes.2015.06.106.
[215] Wang M, Zhang H, Yu T, Zhu Z, Zhang X, Yang G. Influence and affecting mechanism of tool pin geometrical configuration on weld formation during non-tilting friction stir welding. J Mech Eng 2017;53:63. https://doi.org/10.3901/JME.2017.18.057.
[216] Guan M, Wang Y, Huang Y, Liu X, Meng X, Xie Y, et al. Non-weld-thinning friction stir welding. Mater Lett 2019;255:126506https://doi.org/10.1016/j.matlet.2019.126506.
[217] Zhang HJ, Wang M, Zhu Z, Zhang X, Yu T, Yang GX. Improving the structure-property of aluminum alloy friction stir weld by using a non-shoulder-plunge welding tool. Int J Adv Manuf Technol 2016;87:1095–104. https://doi.org/10.1007/s00170-016-8599-z.
[218] Huang Y, Meng X, Xie Y, Li J, Si X, Fan Q. Improving mechanical properties of composite/metal friction stir lap welding joints via a taper-screwed pin with triple facets. J Mater Process Technol 2019;268:80–6. https://doi.org/10.1016/j.jmatprotec.2019.01.011.
[219] Xu W, Liu J, Luan G, Dong C. Temperature evolution, microstructure and mechanical properties of friction stir welded thick 2219-O aluminum alloy joints. Mater Des 2009;30:1886–93. https://doi.org/10.1016/j.matdes.2008.09.021.
[220] Çam G, Mistikoglu S. Recent developments in friction stir welding of Al-Alloys. J Mater Eng Perform 2014;23:1936–53. https://doi.org/10.1007/s11665-014-0968-x.
[221] Sandnes L, Grong Ø, Torgersen J, Welo T, Berto F. Exploring the hybrid metal extrusion and bonding process for butt welding of Al–Mg–Si alloys. 1067–1067 Int J Adv Manuf Technol 2018;98. https://doi.org/10.1007/s00170-018-2397-8.
[222] Li N, Li W, Yang X, Xu Y, Vairis A. Corrosion characteristics and wear performance of cold sprayed coatings of reinforced Al deposited onto friction stir welded AA2024-T3 joints. Surf Coat Technol 2018;349:1069–76. https://doi.org/10.1016/j.surfcoat.2018.06.058.
[223] Li N, Li WY, Yang XW, Feng Y, Vairis A. An investigation into the mechanism for enhanced mechanical properties in friction stir welded AA2024-T3 joints coated with cold spraying. Appl Surf Sci 2018;439:623–31. https://doi.org/10.1016/j.apsusc.2018.01.049.
[224] Huang Y, Han B, Lv S, Wan L, Liu H, Feng J. In-situ additive friction stir welding method for eliminating weld-thining. CN103157903A; 2013.
[225] Li W, Assadi H, Gaertner F, Yin S. A review of advanced composite and nanostructured coatings by solid-state cold spraying process. Crit Rev Solid State Mater Sci 2018;8436:1–48. https://doi.org/10.1080/10408436.2017.1410778.
[226] Ogura T, Saito Y, Nishida T, Nishida H, Yoshida T, Omichi N, et al. Partitioning evaluation of mechanical properties and the interfacial microstructure in a friction stir welded aluminum alloy/stainless steel lap joint. Scr Mater 2012;66:531–4. https://doi.org/10.1016/j.scriptamat.2011.12.035.
[227] Meng X, Gao S, Ma L, Li Z, Yue Y, Xiao H. Effects of rotational velocity on microstructures and mechanical properties of surface compensation friction stir welded 6005A–T6 aluminum alloy. Eng Rev 2016;36:107–13.
[228] Wen Q, Yue Y, Ji S, Li Z, Gao S. Effect of welding speeds on mechanical properties of level compensation friction stir welded 6061–T6 aluminum alloy. High Temp Mater Process 2016;35:375–9. https://doi.org/10.1515/htmp-2014-0220.
[229] Liu H, Fujii H, Maeda M, Nogi K. Heterogeneity of mechanical properties of friction stir welded joints of 1050–H24 aluminum alloy. J Mater Sci Technol 2003;22:441–4.

[230] Korayem AH, Chen SJ, Zhang QH, Li CY, Zhao XL, Duan WH. Failure of CFRP-to-steel double strap joint bonded using carbon nanotubes modified epoxy adhesive at moderately elevated temperatures. Compos Part B Eng 2016;94:95–101. https://doi.org/10.1016/j.compositesb.2016.03.042.
[231] Wang W, Lin S, H Z. Friction stir welding method for eliminating weld thinning by using additional T-plate, involves obtaining flat weld and completing friction stir welding of first to-be-welded plate and second to-be-welded plate using additional T-plate; 2018.
[232] Kuang B, Shen Y, Chen W, Yao X, Xu H, Gao J, et al. The dissimilar friction stir lap welding of 1A99 Al to pure Cu using Zn as filler metal with “pinless” tool configuration. Mater Des 2015;68:54–62. https://doi.org/10.1016/j.matdes.2014.12.008.
[233] Ji SD, Meng XC, Ma L, Gao SS. Effect of groove distribution in shoulder on formation, macrostructures, and mechanical properties of pinless friction stir welding of 6061-O aluminum alloy. Int J Adv Manuf Technol 2016;87:3051–8. https://doi.org/10.1007/s00170-016-8734-x.
[234] Yang XW, Fu T, Li WY. Friction stir spot welding: a review on joint macro- and microstructure, property, and process modelling. Adv Mater Sci Eng 2014;2014:1–11. https://doi.org/10.1155/2014/697170.
[235] Acerra F, Buffa G, Fratini L, Troiano G. On the FSW of AA2024-T4 and AA7075-T6 T-joints: an industrial case study. Int J Adv Manuf Technol 2010;48:1149–57. https://doi.org/10.1007/s00170-009-2344-9.
[236] Li B, Shen Y. A feasibility research on friction stir welding of a new-typed lap-butt joint of dissimilar Al alloys. Mater Des 2012;34:725–31. https://doi.org/10.1016/j.matdes.2011.05.033.
[237] TWI. Weld repair, reclamation and rectification n.d. https://www.twi-global.com/capabilities/joining-technologies/weld-repair-reclamation-and-rectification/.
[238] Feng C, Liang J, Gong C, Pai W, Liu S. Repair volume extraction method for damaged parts in remanufacturing repair. Int J Adv Manuf Technol 2018;98:1523–36. https://doi.org/10.1007/s00170-018-2300-7.
[239] Chai Q, Xiao Z, Lai K, Hung, Zhou G. Can carbon cap and trade mechanism be beneficial for remanufacturing? Int J Prod Econ 2018;203:311–21. https://doi.org/10.1016/j.ijpe.2018.07.004.
[240] Wu X. Research on design management based on green remanufacturing engineering. Syst Eng Procedia 2012;4:448–54. https://doi.org/10.1016/j.sepro.2012.01.009.
[241] Heidarzadeh A, Jabbari M, Esmaily M. Prediction of grain size and mechanical properties in friction stir welded pure copper joints using a thermal model. Int J Adv Manuf Technol 2015;77:1819–29. https://doi.org/10.1007/s00170-014-6543-7.
[242] Sharma V, Prakash U, Kumar BVM. Surface composites by friction stir processing: a review. J Mater Process Technol 2015;224:117–34. https://doi.org/10.1016/j.jmatprotec.2015.04.019.
[243] Ji S, Meng X, Zeng Y, Ma L, Gao S. New technique for eliminating keyhole by active-passive filling friction stir repairing. Mater Des 2016;97:175–82. https://doi.org/10.1016/j.matdes.2016.02.088.
[244] Teimurnezhad J, Pashazadeh H, Masumi A. Effect of shoulder plunge depth on the weld morphology, macrograph and microstructure of copper FSW joints. J Manuf Process 2016;22:254–9. https://doi.org/10.1016/j.jmapro.2016.04.001.
[245] Khan NZ, Siddiquee AN, Khan ZA, Shihab SK. Investigations on tunneling and kissing bond defects in FSW joints for dissimilar aluminum alloys. J Alloys Compd 2015;648:360–7. https://doi.org/10.1016/j.jallcom.2015.06.246.
[246] Zheng Q, Feng X, Shen Y, Huang G, Zhao P. Effect of plunge depth on microstructure and mechanical properties of FSW lap joint between aluminum alloy and nickel-base alloy. J Alloys Compd 2017;695:952–61. https://doi.org/10.1016/j.jallcom.2016.10.213.
[247] Zhou N, Song D, Qi W, Li X, Zou J, Attallah MM. Influence of the kissing bond on the mechanical properties and fracture behaviour of AA5083-H112 friction stir welds. Mater Sci Eng A 2018;719:12–20. https://doi.org/10.1016/j.msea.2018.02.011.
[248] Han B, Huang Y, Lv S, Wan L, Feng J, Fu G. AA7075 bit for repairing AA2219 keyhole by filling friction stir welding. Mater Des 2013;51:25–33. https://doi.org/10.1016/j.matdes.2013.03.089.
[249] Arbegast WJ. A flow-partitioned deformation zone model for defect formation during friction stir welding. Scr Mater 2008;58:372–6. https://doi.org/10.1016/j.scriptamat.2007.10.031.
[250] Tao Y, Zhang Z, Ni DR, Wang D, Xiao BL, Ma ZY. Influence of welding parameter on mechanical properties and fracture behavior of friction stir welded Al-Mg-Sc joints. Mater Sci Eng A 2014;612:236–45. https://doi.org/10.1016/j.msea.2014.06.051.
[251] Zeng KW, Su ZM, Luo SM, Lin PC, Dong MT, Tang T, et al. Removing approach for flashes of friction stir spot welds. J Mater Process Technol 2013;213:1725–33. https://doi.org/10.1016/j.jmatprotec.2013.03.019.
[252] Shultz EF, Cole EG, Smith CB, Zinn MR, Ferrier NJ, Pfefferkorn FE. Effect of compliance and travel angle on friction stir welding with gaps. J Manuf Sci Eng 2010;132:041010https://doi.org/10.1115/1.4001581.
[253] Wanjara P, Monsarrat B, Larose S. Gap tolerance allowance and robotic operational window for friction stir butt welding of AA6061. J Mater Process Technol 2013;213:631–40. https://doi.org/10.1016/j.jmatprotec.2012.10.010.
[254] Yang Y, Kalya P, Landers RG, Krishnamurthy K. Automatic gap detection in friction stir butt welding operations. Int J Mach Tools Manuf 2008;48:1161–9. https://doi.org/10.1016/j.ijmachtools.2008.01.007.
[255] Liu XC, Wu CS. Elimination of tunnel defect in ultrasonic vibration enhanced friction stir welding. Mater Des 2016;90:350–8. https://doi.org/10.1016/j.matdes.2015.10.131.
[256] Sahlot Pankaj, Jha Kaushal, Dey GK, Arora Amit. Quantitative wear analysis of H13 steel tool during friction stir welding of Cu-0.8%Cr-0.1%Zr alloy. Wear 2017;378-379:82–9. https://doi.org/10.1016/j.wear.2017.02.009.
[257] Sahlot P, Arora A. Numerical model for prediction of tool wear and worn-out pin profile during friction stir welding. Wear 2018;408–409:96–107. https://doi.org/10.1016/j.wear.2018.05.007.
[258] Salih OS, Ou H, Sun W, McCartney DG. A review of friction stir welding of aluminium matrix composites. Mater Des 2015;86:61–71. https://doi.org/10.1016/j.matdes.2015.07.071.
[259] Bist A, Saini JS, Sharma B. A review of tool wear prediction during friction stir welding of aluminium matrix composite. Trans Nonferrous Met Soc China 2016;26:2003–18. https://doi.org/10.1016/S1003-6326(16)64318-2.
[260] Zhang YN, Cao X, Larose S, Wanjara P. Review of tools for friction stir welding and processing. Can Metall Q 2012;51:250–61. https://doi.org/10.1179/1879139512Y.0000000015.
[261] Avettand-Fènoël MN, Simar A. A review about friction stir welding of metal matrix composites. Mater Charact 2016;120:1–17. https://doi.org/10.1016/j.matchar.2016.07.010.
[262] Ji S, Huang R, Zhang L, Meng X, Lv Z. Microstructure and mechanical properties of friction stir repaired Al–Cu casting alloy. Trans Indian Inst Met 2018;71:2057–65. https://doi.org/10.1007/s12666-018-1340-x.
[263] Li W, Diao G, Liang Z, Wang D. Repair welding of tunnel defect in friction stir weld of Al-Zn-Mg alloys.In: Int. Conf. Mech. Eng. Control Autom.; 2017. p. 202–7. https://doi.org/10.12783/dtetr/icmeca2017/11934.
[264] Gunter C, Miles MP, Liu FC, Nelson TW. Solid state crack repair by friction stir processing in 304L stainless steel. J Mater Sci Technol 2017;34:140–7. https://doi.org/10.1016/j.jmst.2017.10.023.
[265] Li Z, Han K, Liu C, Huang C, Chang Z, Wu H, et al. Repair welding of defects in 2219 Al alloy friction stir welded joints. J Aeronaut Mater 2016;36:26–32.
[266] Liu H, Zhang H. Repair welding process of friction stir welding groove defect. Trans Nonferrous Met Soc China 2009;19:563–7. https://doi.org/10.1016/S1003-6326(08)60313-1.
[267] Liu HJ, Zhang HJ. Study of hybrid welding repair process of friction stir welding grove defect. Sci Technol Weld Join 2012;17:169–73. https://doi.org/10.1179/136217111X13218932822646.
[268] Ji SD, Meng XC, Li ZW, Ma L, Gao SS. Investigation of vertical compensation friction stir-welded 7N01-T4 aluminum alloy. Int J Adv Manuf Technol 2016;84. https://doi.org/10.1007/s00170-015-7904-6.
[269] Abu-Okail M, Ata MH, Abu-oqail A, Essa GMF, Mahmoud TS, Hassab-Allah I. Production of tailor-welded blanks by vertical compensation friction stir welding technique. Mater Sci Technol 2018;34:2030–41. https://doi.org/10.1080/02670836.2018.1510070.

[270] Huang YX, Han B, Tian Y, Liu HJ, Lv SX, Feng JC, et al. New technique of filling friction stir welding. Sci Technol Weld Join 2011;16:497–501. https://doi.org/10.1179/1362171811Y.0000000032.
[271] Du B, Sun Z, Yang X, Cui L, Song J, Zhang Z. Characteristics of friction plug welding to 10mm thick AA2219-T87 sheet: weld formation, microstructure and mechanical property. Mater Sci Eng A 2016;654:21–9. https://doi.org/10.1016/j.msea.2015.12.019.
[272] Metz DF, Barkey ME. Fatigue behavior of friction plug welds in 2195 Al-Li alloy. Int J Fatigue 2012;43:178–87. https://doi.org/10.1016/j.ijfatigue.2012.04.002.
[273] Behmand SA, Mirsalehi SE, Omidvar H, Safarkhanian MA. Filling exit holes of friction stir welding lap joints using consumable pin tools. Sci Technol Weld Join 2015;20:330–6. https://doi.org/10.1179/1362171815Y.0000000018.
[274] Zhou L, Nakata K, Tsumura T, Fujii H, Ikeuchi K, Michishita Y, et al. Microstructure and mechanical properties of 316L stainless steel filling friction stir-welded joints. J Mater Eng Perform 2014;23:3718–26. https://doi.org/10.1007/s11665-014-1124-3.
[275] Zhou L, Liu D, Nakata K, Tsumura T, Fujii H, Ikeuchi K, et al. New technique of self-refilling friction stir welding to repair keyhole. Sci Technol Weld Join 2012;17:649–55. https://doi.org/10.1179/1362171812Y.0000000058.
[276] Xiong J, Yang X, Lin W, Liu K. Evaluation of inhomogeneity in tensile strength and fracture toughness of underwater wet friction taper plug welded joints for low-alloy pipeline steels. J Manuf Process 2018;32:280–7. https://doi.org/10.1016/j.jmapro.2018.02.016.
[277] Yin Y, Yang X, Cui L, Wang F, Li S. Material flow influence on the weld formation and mechanical performance in underwater friction taper plug welds for pipeline steel. Mater Des 2015;88:990–8. https://doi.org/10.1016/j.matdes.2015.09.123.
[278] Mukherjee S, Ghosh AK. Friction stir processing of direct metal deposited copper-nickel 70/30. Mater Sci Eng A 2011;528:3289–94. https://doi.org/10.1016/j.msea.2011.01.063.
[279] Ji SD, Meng XC, Huang RF, Ma L, Gao SS. Microstructures and mechanical properties of 7N01-T4 aluminum alloy joints by active-passive filling friction stir repairing. Mater Sci Eng A 2016;664:94–102. https://doi.org/10.1016/j.msea.2016.03.131.
[280] Huang R, Ji S, Meng X, Li Z. Drilling-filling friction stir repairing of AZ31B magnesium alloy. J Mater Process Technol 2018;255:765–72. https://doi.org/10.1016/j.jmatprotec.2018.01.019.
[281] Niu S, Wu B, Ma L, Lv Z, Yan D. Passive filling friction stir repairing AZ31-B magnesium alloy by external stationary shoulder. Int J Adv Manuf Technol 2018;97:2461–8. https://doi.org/10.1007/s00170-018-2130-7.
[282] Reimann M, Gartner T, Suhuddin U, Göbel J, Dos Santos JF. Keyhole closure using friction spot welding in aluminum alloy 6061–T6. J Mater Process Technol 2016;237:12–8. https://doi.org/10.1016/j.jmatprotec.2016.05.013.
[283] Reimann M, Goebel J, Gartner TM, dos Santos JF. Refilling termination hole in AA 2198–T851 by refill friction stir spot welding. J Mater Process Technol 2017;245:157–66. https://doi.org/10.1016/j.jmatprotec.2017.02.025.
[284] Reimann M, Goebel J, dos Santos JF. Microstructure and mechanical properties of keyhole repair welds in AA 7075–T651 using refill friction stir spot welding. Mater Des 2017;132:283–94. https://doi.org/10.1016/j.matdes.2017.07.013.
[285] Saeedy S, Besharati Givi MK. Experimental Investigation of Double Side Friction Stir Welding (FSW) on High Density Polyethylene Blanks. In: ASME 2010 10th Bienn. Conf. Eng. Syst. Des. Anal. vol. 4; 2010. p. 845–8. https://doi.org/10.1115/ESDA2010-25346.
[286] Cabibbo M, Forcellese A, El Mehtedi M, Simoncini M. Double side friction stir welding of AA6082 sheets: microstructure and nanoindentation characterization. Mater Sci Eng A 2014;590:209–17. https://doi.org/10.1016/j.msea.2013.10.031.
[287] Widener CA. High-rotational speed friction stir welding with a fixed shoulder. In: 6th Int. Syposium Frict. Stir Weld., Montreal, Canada; 2006. p. 1–45.
[288] Ji S, Meng X, Xing J, Ma L, Gao S. Vertical compensation friction stir welding of 6061–T6 aluminum alloy. High Temp Mater Process 2016;35:843–51. https://doi.org/10.1515/htmp-2015-0063.
[289] Park SK, Hong ST, Park JH, Park KY, Kwon YJ, Son HJ. Effect of material locations on properties of friction stir welding joints of dissimilar aluminium alloys. Sci Technol Weld Join 2010;15:331–6. https://doi.org/10.1179/136217110X12714217309696.
[290] Yoon TJ, Kang CY. Observations on metallurgical phenomena and formation of onion ring nugget during friction stir lap welding of dissimilar aluminum by a new 3D technique. Mater Lett 2015;142:253–7. https://doi.org/10.1016/j.matlet.2014.12.033.
[291] Yoon TJ, Yun JG, Kang CY. Formation mechanism of typical onion ring structures and void defects in friction stir lap welded dissimilar aluminum alloys. Mater Des 2016;90:568–78. https://doi.org/10.1016/j.matdes.2015.11.014.
[292] Krishnan KN. On the formation of onion rings in friction stir welds. Mater Sci Eng A 2002;327:246–51. https://doi.org/10.1016/S0921-5093(01)01474-5.
[293] Liu FC, Nelson TW. In-situ material flow pattern around probe during friction stir welding of austenitic stainless steel. Mater Des 2016;110:354–64. https://doi.org/10.1016/j.matdes.2016.07.147.
[294] Venkateswaran P, Reynolds AP. Factors affecting the properties of Friction Stir Welds between aluminum and magnesium alloys. Mater Sci Eng A 2012;545:26–37. https://doi.org/10.1016/j.msea.2012.02.069.
[295] Liu FC, Nelson TW. In-situ grain structure and texture evolution during friction stir welding of austenite stainless steel. Mater Des 2017;115:467–78. https://doi.org/10.1016/j.matdes.2016.11.066.
[296] McNelley TR, Swaminathan S, Su JQ. Recrystallization mechanisms during friction stir welding/processing of aluminum alloys. Scr Mater 2008;58:349–54. https://doi.org/10.1016/j.scriptamat.2007.09.064.
[297] Dolatkhah A, Golbabaei P, Besharati Givi MK, Molaiekiya F. Investigating effects of process parameters on microstructural and mechanical properties of Al5052/SiC metal matrix composite fabricated via friction stir processing. Mater Des 2012;37:458–64. https://doi.org/10.1016/j.matdes.2011.09.035.
[298] Izadi H, Sandstrom R, Gerlich AP. Grain growth behavior and Hall-Petch strengthening in friction stir processed Al 5059. Metall Mater Trans A Phys Metall Mater Sci 2014;45:5635–44. https://doi.org/10.1007/s11661-014-2492-x.
[299] Dunkerton S, Nicholas D, Sketchley P. Repairing defective metal workpiece-by friction welding with a metal plug. 9125978; 1991.
[300] Coletta ER, Cantrell MA, McCool A. Friction plug weld repair geometric innovations; 2017. https://NtrsNasaGov/SearchJsp?R=20000112928.
[301] Li Z, Cantrell M, Brown R, McCool A. Process development and microstrutural characterization plug welded 2195 and 2219 alloys; 2000. https://NtrsNasaGov/SearchJsp?R=20000089963.
[302] Hartley PJ. Frition plug weld repair geometric innovations; 2017. https://NtrsNasaGov/SearchJsp?R=20000093962.
[303] Metz DF, Weishaupt ER, Barkey ME, Fairbee BS. A microstructure and microhardness characterization of a friction plug weld in friction stir welded 2195 Al-Li. J Eng Mater Technol 2012;134:021005https://doi.org/10.1115/1.4006066.
[304] Metz DF, Barkey ME, Bradt RC, Hubner JP, Weaver ML, Jackson JE, et al. Experimental and numerical characterization of the fatigue and fracture properties of friction plug welds in 2195-T8 aluminum lithium alloy. The University of Alabama; 2013.
[305] Lange M, Schwenker S. Friction plug welding of 2024-T3 Aluminum. In: Proc. Aircr. Struct. Integr. Conf., San Antoni; 2014.
[306] Du B, Cui L, Yang X, Wang D, Sun Z. Weakening mechanism and tensile fracture behavior of AA 2219–T87 friction plug welds. Mater Sci Eng A 2017;693:129–35. https://doi.org/10.1016/j.msea.2017.03.093.
[307] Mission Success Bulletin, Lockheed Martin Space System Company. http://WwwMafetOrg/Msb/Msb083001Pdf; 2001. p. 1–6.
[308] Brooke SA, Bradford V. Friction pull plug welding in aluminum alloys; 2014. https://NtrsNasaGov/SearchJsp?R=20120014529.
[309] Gibson D, Meyer A, Vennemann O, dos Santos J, Blakemore GR. Engineering applications of friction stitch welding. In: Proc. Int. Conf. Offshore Mech. Arct. Eng.; 2001. p. 139–43.
[310] Costa Pereira da Cunha PH, Szabo R, Bergmann L, dos Santos J. Preliminary study on the application of friction welding in structural repairs; 1998.
[311] Pauly D. Process development on an experimental friction hydro pillar processing system. Int Rep: GKSS; 1999.
[312] Nicholas E. Friction hydro pillar processing. In: 11th Annu. North Am. Weld. Res. Conf.; 1995. p. 7–9.
[313] Hattingh D, Van Zyl C. Temperature distribution for a friction taper stud weld in thick walled 10CrMo910 steel. South African Inst Mech Eng 2012;28:37–45.
[314] Meyer A, Pauly D, dos Santos J, Pinheiro G, Roos A, Gibson D, et al. Considerations on robotic friction stitch welding for the repair of marine structures. In: Proc. Int. Conf. Offshore Mech. Arct. Eng., vol. 3; 2001. p. 145–51.
[315] Wu F, Yeh T, Henrique P, Pereira C, Rodrigo C, Lessa DL, et al. Evaluation of discontinuities in A36 steel repairs with friction hydro pillar processing using

different axial forces. ISIJ Int 2013;53:2269–71. https://doi.org/10.2355/isijinternational.53.2269.
[316] Hattingh DG, Bulbring DLH, Els-Botes A, James MN. Process parameter influence on performance of friction taper stud welds in AISI 4140 steel. Mater Des 2011;32:3421–30. https://doi.org/10.1016/j.matdes.2011.02.001.
[317] Meyer A. Friction hydro pillar processing: bonding mechanism and properties. na; 2003.
[318] Ambroziak A, Gul B. Investigations of underwater FHPP for welding steel overlap joints. Arch Civ Mech Eng 2007;7:67–76. https://doi.org/10.1016/S1644-9665(12)60212-X.
[319] Cui L, Yang X, Wang D, Hou X, Cao J, Xu W. Friction taper plug welding for S355 steel in underwater wet conditions: Welding performance, microstructures and mechanical properties. Mater Sci Eng A 2014;611:15–28. https://doi.org/10.1016/j.msea.2014.04.087.
[320] Chludzinski M, Paes MP, Bastian FL, Strohaecker TR. Fracture toughness of friction hydro-pillar processing welding in C-Mn steel. Mater Des 2012;33:340–4. https://doi.org/10.1016/j.matdes.2011.07.056.
[321] Cui L, Yang X, Wang D, Cao J, Xu W. Experimental study of friction taper plug welding for low alloy structure steel: Welding process, defects, microstructures and mechanical properties. Mater Des 2014;62:271–81. https://doi.org/10.1016/j.matdes.2014.05.026.
[322] Huang YX, Han B, Lv SX, Feng JC, Liu HJ, Leng JS, et al. Interface behaviours and mechanical properties of filling friction stir weld joining AA 2219. Sci Technol Weld Join 2012;17:225–30. https://doi.org/10.1179/1362171811Y.0000000100.
[323] Yan Yinfei, Shen Yifu, Guo Chao, Liu Wenming, Li Junping. Friction plug welding acrylonitrile butadiene styrene sheets: the investigation of welding process, joint morphology and mechanical property. Int J Mater Form 2019;12(5):845–55. https://doi.org/10.1007/s12289-018-1456-x.
[324] Zhang GF, Jiao WM, Zhang JX. Filling friction stir weld keyhole using pin free tool and T shaped filler bit. Sci Technol Weld Join 2014;19:98–104. https://doi.org/10.1179/1362171813Y.0000000161.
[325] Huang Y, Meng X, Xie Y, Li J, Wan L. New technique of friction-based filling stacking joining for metal and polymer. Compos Part B Eng 2019;163:217–23. https://doi.org/10.1016/j.compositesb.2018.11.050.
[326] Li W, Li J, Zhang Z, Gao D, Wang W, Dong C. Improving mechanical properties of pinless friction stir spot welded joints by eliminating hook defect. Mater Des 2014;62:247–54. https://doi.org/10.1016/j.matdes.2014.05.028.
[327] Liu Z, Cui H, Ji S, Xu M, Meng X. Improving joint features and mechanical properties of pinless fiction stir welding of alcald 2A12-T4 aluminum alloy. J Mater Sci Technol 2016;32. https://doi.org/10.1016/j.jmst.2016.07.003.
[328] Liu Z, Ji S, Meng X, Huang R. Improving joint formation and tensile properties of friction stir welded ultra-thin Al/Mg alloy sheets using a pinless tool assisted by a stationary shoulder. Int J Adv Manuf Technol 2017;93:2071–9. https://doi.org/10.1007/s00170-017-0682-6.
[329] Venukumar S, Yalagi SG, Muthukumaran S, Kailas SV. Static shear strength and fatigue life of refill friction stir spot welded AA 6061–T6 sheets. Sci Technol Weld Join 2014;19:214–23. https://doi.org/10.1179/1362171813Y.0000000181.
[330] Sajed M. Parametric study of two-stage refilled friction stir spot welding. J Manuf Process 2016;24:307–17. https://doi.org/10.1016/j.jmapro.2016.09.011.
[331] Schilling C, Dos Santos J. Method and device for linking at least two adjoining work pieces by friction. welding 2001.
[332] Shen Z, Ding Y, Gopkalo O, Diak B, Gerlich AP. Effects of tool design on the microstructure and mechanical properties of refill friction stir spot welding of dissimilar Al alloys. J Mater Process Technol 2018;252:751–9. https://doi.org/10.1016/j.jmatprotec.2017.10.034.
[333] Xu Z, Li Z, Ji S, Zhang L. Refill friction stir spot welding of 5083-O aluminum alloy. J Mater Sci Technol 2018;34:878–85. https://doi.org/10.1016/j.jmst.2017.02.011.
[334] Kubit A, Wydrzynski D, Trzepiecinski T. Refill friction stir spot welding of 7075–T6 aluminium alloy single-lap joints with polymer sealant interlayer. Compos Struct 2018;201:389–97. https://doi.org/10.1016/j.compstruct.2018.06.070.
[335] Cao JY, Wang M, Kong L, Zhao HX, Chai P. Microstructure, texture and mechanical properties during refill friction stir spot welding of 6061–T6 alloy. Mater Charact 2017;128:54–62. https://doi.org/10.1016/j.matchar.2017.03.023.
[336] Shen Z, Ding Y, Chen J, Gerlich AP. Comparison of fatigue behavior in Mg/Mg similar and Mg/steel dissimilar refill friction stir spot welds. Int J Fatigue 2016;92:78–86. https://doi.org/10.1016/j.ijfatigue.2016.06.033.
[337] Suhuddin U, Fischer V, Kroeff F, dos Santos JF. Microstructure and mechanical properties of friction spot welds of dissimilar AA5754 Al and AZ31 Mg alloys. Mater Sci Eng A 2014;590:384–9. https://doi.org/10.1016/j.msea.2013.10.057.
[338] Junior WS, Emmler T, Abetz C, Handge UA, dos Santos JF, Amancio-Filho ST, et al. Friction spot welding of PMMA with PMMA/silica and PMMA/silica-g-PMMA nanocomposites functionalized via ATRP. Polymer (Guildf) 2014;55:5146–59. https://doi.org/10.1016/j.polymer.2014.08.022.
[339] Gonçalves J, dos Santos JF, Canto LB, Amancio-Filho ST. Friction spot welding of carbon fiber-reinforced polyamide 66 laminate. Mater Lett 2015;159:506–9. https://doi.org/10.1016/j.matlet.2015.08.036.
[340] Goushegir SM, dos Santos JF, Amancio-Filho ST. Failure and fracture micro-mechanisms in metal-composite single lap joints produced by welding-based joining techniques. Compos Part A Appl Sci Manuf 2016;81:121–8. https://doi.org/10.1016/j.compositesa.2015.11.001.
[341] André NM, Goushegir SM, dos Santos JF, Canto LB, Amancio-Filho ST. Friction Spot Joining of aluminum alloy 2024–T3 and carbon-fiber-reinforced poly (phenylene sulfide) laminate with additional PPS film interlayer: Microstructure, mechanical strength and failure mechanisms. Compos Part B Eng 2016;94:197–208. https://doi.org/10.1016/j.compositesb.2016.03.011.
[342] Esteves JV, Goushegir SM, dos Santos JF, Canto LB, Hage E, Amancio-Filho ST. Friction spot joining of aluminum AA6181-T4 and carbon fiber-reinforced poly (phenylene sulfide): effects of process parameters on the microstructure and mechanical strength. Mater Des 2015;66:437–45. https://doi.org/10.1016/j.matdes.2014.06.070.
[343] Montag T, Wulfsberg JP, Hameister H, Marschner R. Influence of tool wear on quality criteria for refill friction stir spot welding (RFSSW) process. Procedia CIRP 2014;24:108–13. https://doi.org/10.1016/j.procir.2014.08.015.
[344] Ji S, Wang Y, Li Z, Yue Y, Chai P. Effect of tool geometry on material flow behavior of refill friction stir spot welding. Trans Indian Inst Met 2017;70:1417–30. https://doi.org/10.1007/s12666-016-0937-1.
[345] Fox SL. Refill friction stir spot weld repair of a fatigue crack. South Dakota School of Mines and Technology; 2010.
[346] Parra B, Saccon VT, de Alcântara NG, Rosendo T, dos Santos JF. An Investigation on friction spot welding in AA6181-T4 alloy. Tecnol Em Metal e Mater 2011;8:184–90. https://doi.org/10.4322/tmm.2011.029.
[347] Shi Y, Yue Y, Zhang L, Ji S, Wang Y. Refill friction stir spot welding of 2198–T8 aluminum alloy. Trans Indian Inst Met 2018;71:139–45. https://doi.org/10.1007/s12666-017-1146-2.
[348] Li Z, Ji S, Ma Y, Chai P, Yue Y, Gao S. Fracture mechanism of refill friction stir spot-welded 2024–T4 aluminum alloy. Int J Adv Manuf Technol 2016;86:1925–32. https://doi.org/10.1007/s00170-015-8276-7.
[349] Liu X, Qiao F, Guo L, Qiu X. Metallographic structure, mechanical properties, and process parameter optimization of 5A06 joints formed by ultrasonic-assisted refill friction stir spot welding. Int J Miner Metall Mater 2017;24:164–70. https://doi.org/10.1007/s12613-017-1391-8.



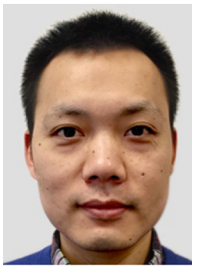
Xiangchen Meng received his Ph.D (2020) in Material Processing Engineering from Harbin Institute of Technology, China under the supervision of Prof. Yongxian Huang. He is currently a postdoctoral fellow in Mechanical Engineering at Harbin Institute of Technology. His research interests focus on welding of dissimilar materials and solid state repairing. To date, Dr Meng is an author of over 50 peer reviewed journal articles and over 5 invention patents, such as *Composites Part B, Composites Part A, Materials & Design, Materials Science and Engineering A*, etc, which have received a total citation of > 800, with an H index of 16.



Yongxian Huang is currently a Professor at the State Key Lab of Advanced Welding and Joining at Harbin Institute of Technology. He received his Ph.D. degree in Material Processing Engineering from Harbin Institute of Technology in 2008. He is the vice director of Department of Welding Science and Technology at Harbin Institute of Technology of China. He has been engaged in research on friction stir welding and processing, joining between polymer and metal, and green remanufacturing. To date, Dr Huang has published > 120 papers in the peer-reviewed international journals and > 60 invention patents, such as *Carbon, Corrosion Science, Composites Part B, Composites Part A, Materials & Design*, etc, which have received a total citation of > 1500, with an H index of 25.



Jian Cao is currently working as a professor at School of Materials Science & Engineering at Harbin Institute of Technology of China . He received his PhD degree from the Harbin Institute of Technology (HIT, 2007) under the supervision of Prof. Jicai Feng. He moved University of Manchester of UK in 2014 as an Academic Visitor. His interests focus on joining of dissimilar materials, analysis on the interface and surface of materials, and investigation on microstructure evolution and mechanical properties. By the middle of 2020, he has published > 150 papers in the peer-reviewed international journals and 20 invention patents , such as *Nature communication, Advanced Materials, Nanoscale, Advanced Energy Materials, International Journal of Hydrogen Energy, Comosite science and technology*, etc, which have received over 2000 citations with an H-index of 26 according to Google Scholar. Also, he has served as an editorial board member of *Acta Metallurgica Sinica (English Letters)*.



Junjun Shen graduated from the School of Materials Science and Engineering, Harbin Institute of Technology and got his Master degree in 2011. Currently, he serves as a Postdoctor and Research assistant at Institute of Materials Research of the Helmholtz-Zentrum Geesthacht at Germany. He has been engaged in research on bobbin tool friction stir welding and control of microstructural evolution and mechanical properties for a long time. To date, he has published more than 20 papers, which has received a total citation of > 500.



Jorge F. dos Santos is currently the Head of Department, Solid State Joining Processes" at Institute of Materials Research of the Helmholtz-Zentrum Geesthacht of Germany. He received his Ph.D. in Welding Technology from The Cranfield University in 1983. He is the *Chairman of Sub-Commission III-B "Friction Welding Processes" of the International Institute of Welding (IIW)* and also the *Chairman of Sub-Commission IX-NF "Weldability of Non-Ferrous Materials of the International Institute of Welding (IIW)*. His research interests include joining technology , friction based joining and processes , microstructural analysis and testing and assessment of welded joints. Prof dos Santos is an author of over 300 publications which have received more than 5000 citations with an H-index of 35 so far.